SYNTHESIS AND EVALUATION OF TETRAMETHOXY STILBENES RELATED TO COMBRETASTATIN A-4 AS POTENTIAL ANTICANCER AGENTS

BABATUNDE ADEGBULUGBE

MSc BY RESEARCH

UNIVERSITY OF SALFORD

SCHOOL OF SCIENCE, ENGINEERING AND ENVIRONMENT

2022

Table of contents

Acknowledgements

I would like to acknowledge the assistance and patience of Dr John Hadfield, Dr Al-Ameen Mohammed, Dr Muna Abubaker, Dr Jim Wilkinson, Kirit Amin and Lee Harman, all of whom without their assistance this project would not have been possible.

I would also like to acknowledge the support of all my family and friends.

Figures bibliography

Figure 1. Diagram Showing structure of tetramethoxy CA-4 derivative

Figure 2. Structures of CA-1 and CA- 4 [Diagram].

Figure 3. Cancer cells. (2020) [Diagram]. Retrieved 1 February 2022, from https://www.cancerresearchuk.org/about-cancer/what-is-cancer/how-cancer-starts/cancer-cells

Figure 4. Cis and trans combretastatin structures [Diagram].

Figure 5. Kounakis, K., & Tavernarakis, N. (2019). The cytoskeleton as a modulator of aging and neurodegeneration [Diagram] (figure 12.2), In P. Guest (Ed.), *Advances in experimental medicine and biology* (Vol. 1178, pp. 227-245). Cham: Springer.

Figure 6. Bowne-Anderson, H., Zanic, M., Kauer, M., & Howard, J. (2013). Microtubule dynamic instability: A new model with coupled GTP hydrolysis and multistep catastrophe [Diagram] (Figure 1). *Bioessays*, *35*(5), 452-461.

Figure 7. Steinmetz, M., & Prota, A. (2018). Microtubule-targeting agents: Strategies to hijack the cytoskeleton [Diagram] (Figure 1). *Trends In Cell Biology*, *28*(10), 776-792.

Figure 8. Forster, J., Harriss-Phillips, W., Douglass, M., & Bezak, E. (2017). A review of the development of tumour vasculature and its effects on the tumour microenvironment [Diagram] (Figure 1). *Hypoxia*, *Volume 5*, 21-32.

Figure 9. Brouhard, G., & Rice, L. (2014). The contribution of αβ-tubulin curvature to microtubule dynamics [Diagram] (Figure 1). *Journal Of Cell Biology*, *207*(3), 323-334. doi: 10.1083/jcb.201407095

Figure 10. Alberts, J., Johnson, A., Lewis, J., Raff, M., Roberts, K., & Walter, P. (2002). An overview of the cell cycle [Diagram](Figure 17.3). *Molecular biology of the cell* (4th ed.). New York: Garland Science.

Figure 11. Madu, C., Wang, S., Madu, C., & Lu, Y. (2020). Angiogenesis in breast cancer progression, diagnosis, and treatment [Diagram] (Figure 1). *Journal Of Cancer*, *11*(15), 4474-4494.

Figure 12. Cancer and carcinogens - Cell division - Edexcel - GCSE Combined Science Revision - Edexcel - BBC Bitesize. (2022) [Diagram]. Retrieved 1 February 2022, from https://www.bbc.co.uk/bitesize/guides/zpkx8mn/revision/4

Figure 13. Liekens, S., Schols, D., & Hatse, S. (2010). CXCL12-CXCR4 Axis in Angiogenesis, Metastasis and Stem Cell Mobilization [Diagram] (Figure 2). *Current Pharmaceutical Design*, *16*(35), 3903-3920. doi: 10.2174/138161210794455003

Figure 14. Diagram showing Ombrabulin structure.

Figure 15. Khan, Z., Iqbal, A., & Shahzad, S. (2017). Synthetic approaches toward stilbenes and their related structures [Diagram] (Figure 1). *Molecular Diversity*, *21*(2), 483-509.

Figure 16. Kumar, B., Sharma, P., Gupta, V., Khullar, M., Singh, S., Dogra, N., & Kumar, V. (2018). Synthesis and biological evaluation of pyrimidine bridged combretastatin derivatives as potential anticancer agents and mechanistic studies [Diagram] (Table 1). *Bioorganic Chemistry*, *78*, 130-140.

Figure 17. Tarade, D., Pandey, Sm., & McNulty, J. (2017). Review of cytotoxic CA4 analogues that do not target microtubules: Implications for CA4 development [Diagram] (Figure 1). *Mini-Reviews In Medicinal Chemistry*, *17*(999), 1-1.

Figure 18. Tarade, D., Pandey, Sm., & McNulty, J. (2017). Review of cytotoxic CA4 analogues that do not target microtubules: Implications for CA4 development [Diagram] (Figure 1). *Mini-Reviews In Medicinal Chemistry*, *17*(999), 1-1.

Figure 19. Tarade, D., Pandey, Sm., & McNulty, J. (2017). Review of cytotoxic CA4 analogues that do not target microtubules: Implications for CA4 development [Diagram] (Figure 1). *Mini-Reviews In Medicinal Chemistry*, *17*(999), 1-1.

Figure 20. Tarade, D., Pandey, Sm., & McNulty, J. (2017). Review of cytotoxic CA4 analogues that do not target microtubules: Implications for CA4 development [Diagram] (Figure 1). *Mini-Reviews In Medicinal Chemistry*, *17*(999), 1-1.

Figure 21. Akselsen, Ø., Odlo, K., Cheng, J., Maccari, G., Botta, M., & Hansen, T. (2012). Synthesis, biological evaluation and molecular modelling of 1, 2, 3-triazole analogs of combretastatin A-1 [Diagram] (Figure 1). *Bioorganic & Medicinal Chemistry*, *20*(1), 234-242.

Figure 22. Bukhari, S., Kumar, G., Revankar, H., & Qin, H. (2017). Development of combretastatins as potent tubulin polymerization inhibitors [Diagram] (Figure 12). *Bioorganic Chemistry*, *72*, 130-147.

Figure 23. Bukhari, S., Kumar, G., Revankar, H., & Qin, H. (2017). Development of combretastatins as potent tubulin polymerization inhibitors [Diagram] (Figure 12). *Bioorganic Chemistry*, *72*, 130-147.

Figure 24. Gaukroger, K., Hadfield, J., Lawrence, N., Nolan, S., & McGown, A. (2003). Structural requirements for the interaction of combretastatins with tubulin: How important is the trimethoxy unit? [Diagram] (Scheme 8). *Org. Biomol. Chem.*, *1*(17), 3033-3037.

Figure 25. Gaukroger, K., Hadfield, J., Lawrence, N., Nolan, S., & McGown, A. (2003). Structural requirements for the interaction of combretastatins with tubulin: How important is the trimethoxy unit? [Diagram] (Schemes 2, 3 and 5). *Org. Biomol. Chem.*, *1*(17), 3033-3037.

Figure 26. Bukhari, S., Kumar, G., Revankar, H., & Qin, H. (2017). Development of combretastatins as potent tubulin polymerization inhibitors [Diagram] (Figure 13). *Bioorganic Chemistry*, *72*, 130-147.

Figure 27. Bukhari, S., Kumar, G., Revankar, H., & Qin, H. (2017). Development of combretastatins as potent tubulin polymerization inhibitors [Diagram] (Figure 14). *Bioorganic Chemistry*, *72*, 130-147.

Figure 28. Bukhari, S., Kumar, G., Revankar, H., & Qin, H. (2017). Development of combretastatins as potent tubulin polymerization inhibitors [Diagram] (Figure 15). *Bioorganic Chemistry*, *72*, 130-147.

Figure 29. Cushman, M., Nagarathnam, D., Gopal, D., Chakraborti, A., Lin, C., & Hamel, E. (1991). Synthesis and evaluation of stilbene and dihydrostilbene derivatives as potential anticancer agents that inhibit tubulin polymerization [Diagram] (Scheme I). *Journal Of Medicinal Chemistry*, *34*(8), 2579-2588.

Figure 30. Gaukroger, K., Hadfield, J., Lawrence, N., Nolan, S., & McGown, A. (2003). Structural requirements for the interaction of combretastatins with tubulin: How important is the trimethoxy unit? [Diagram] (Scheme 1). *Org. Biomol. Chem.*, *1*(17), 3033-3037.

Figure 31. Bukhari, S., Kumar, G., Revankar, H., & Qin, H. (2017). Development of combretastatins as potent tubulin polymerization inhibitors [Diagram] (Figure 15). *Bioorganic Chemistry*, *72*, 130-147.

Figure 32. Zong, Y., Shea, C., Maffucci, K., & Ojima, I. (2017). Computational design and synthesis of novel fluoro-analogs of combretastatins A-4 and A-1 [Diagram] (Figure 5). *Journal Of Fluorine Chemistry*, *203*, 193-199.

Figure 33. Bukhari, S., Kumar, G., Revankar, H., & Qin, H. (2017). Development of combretastatins as potent tubulin polymerization inhibitors [Diagram] (Figure 18). *Bioorganic Chemistry*, *72*, 130-147.

Figure 34. Bukhari, S., Kumar, G., Revankar, H., & Qin, H. (2017). Development of combretastatins as potent tubulin polymerization inhibitors [Diagram] (Figure 18). *Bioorganic Chemistry*, *72*, 130-147.

Figure 35. Bukhari, S., Kumar, G., Revankar, H., & Qin, H. (2017). Development of combretastatins as potent tubulin polymerization inhibitors [Diagram] (Figure 18). *Bioorganic Chemistry*, *72*, 130-147.

Figure 36. Pérez-Pérez, M., Priego, E., Bueno, O., Martins, M., Canela, M., & Liekens, S. (2016). Blocking blood flow to solid tumours by destabilizing tubulin: An approach to targeting tumour growth [Diagram] (Figure 6). *Journal Of Medicinal Chemistry*, *59*(19), 8685-8711.

Figure 37. Bukhari, S., Kumar, G., Revankar, H., & Qin, H. (2017). Development of combretastatins as potent tubulin polymerization inhibitors [Diagram] (Figure 3). *Bioorganic Chemistry*, *72*, 130-147.

Figure 38. Bukhari, S., Kumar, G., Revankar, H., & Qin, H. (2017). Development of combretastatins as potent tubulin polymerization inhibitors [Diagram] (Figure 3). *Bioorganic Chemistry*, *72*, 130-147.

Figure 39. Bukhari, S., Kumar, G., Revankar, H., & Qin, H. (2017). Development of combretastatins as potent tubulin polymerization inhibitors [Diagram] (Figure 3). *Bioorganic Chemistry*, *72*, 130-147.

Figure 40. Bukhari, S., Kumar, G., Revankar, H., & Qin, H. (2017). Development of combretastatins as potent tubulin polymerization inhibitors [Diagram] (Figure 3). *Bioorganic Chemistry*, *72*, 130-147.

Figure 41. Bukhari, S., Kumar, G., Revankar, H., & Qin, H. (2017). Development of combretastatins as potent tubulin polymerization inhibitors [Diagram] (Figure 4). *Bioorganic Chemistry*, *72*, 130-147.

Figure 42. Seddigi, Z., Malik, M., Saraswati, A., Ahmed, S., Babalghith, A., Lamfon, H., & Kamal, A. (2017). Recent advances in combretastatin based derivatives and prodrugs as antimitotic agents [Diagram] (Figure 3). *Medchemcomm*, *8*(8), 1592-1603.

Figure 43. Seddigi, Z., Malik, M., Saraswati, A., Ahmed, S., Babalghith, A., Lamfon, H., & Kamal, A. (2017). Recent advances in combretastatin based derivatives and prodrugs as antimitotic agents [Diagram] (Figure 3). *Medchemcomm*, *8*(8), 1592-1603.

Figure 44. Bukhari, S., Kumar, G., Revankar, H., & Qin, H. (2017). Development of combretastatins as potent tubulin polymerization inhibitors [Diagram] (Figure 5). *Bioorganic Chemistry*, *72*, 130-147.

Figure 45. Seddigi, Z., Malik, M., Saraswati, A., Ahmed, S., Babalghith, A., Lamfon, H., & Kamal, A. (2017). Recent advances in combretastatin based derivatives and prodrugs as antimitotic agents [Diagram] (Figure 3). *Medchemcomm*, *8*(8), 1592-1603.

Figure 46. Seddigi, Z., Malik, M., Saraswati, A., Ahmed, S., Babalghith, A., Lamfon, H., & Kamal, A. (2017). Recent advances in combretastatin based derivatives and prodrugs as antimitotic agents [Diagram] (Figure 4). *Medchemcomm*, *8*(8), 1592-1603.

Figure 47. McLoughlin, E., & O'Boyle, N. (2020). Colchicine-binding site inhibitors from chemistry to clinic: A review [Diagram] (Figure 5). *Pharmaceuticals*, *13*(1), 8.

Figure 48. McLoughlin, E., & O'Boyle, N. (2020). Colchicine-binding site Inhibitors from chemistry to clinic: A review [Diagram] (Figure 4). *Pharmaceuticals*, *13*(1), 8.

Figure 49. Bukhari, S., Kumar, G., Revankar, H., & Qin, H. (2017). Development of combretastatins as potent tubulin polymerization inhibitors [Diagram] (Figure 6). *Bioorganic Chemistry*, *72*, 130-147.

Figure 50. Bukhari, S., Kumar, G., Revankar, H., & Qin, H. (2017). Development of combretastatins as potent tubulin polymerization inhibitors [Diagram] (Figure 6). *Bioorganic Chemistry*, *72*, 130-147.

Figure 51. Bukhari, S., Kumar, G., Revankar, H., & Qin, H. (2017). Development of combretastatins as potent tubulin polymerization inhibitors [Diagram] (Figure 9). *Bioorganic Chemistry*, *72*, 130-147.

Figure 52. McLoughlin, E., & O'Boyle, N. (2020). Colchicine-binding site inhibitors from chemistry to clinic: A review [Diagram] (Figure 4). *Pharmaceuticals*, *13*(1), 8.

Figure 53. Bukhari, S., Kumar, G., Revankar, H., & Qin, H. (2017). Development of combretastatins as potent tubulin polymerization inhibitors [Diagram] (Figure 11). *Bioorganic Chemistry*, *72*, 130-147.

Figure 54. Mabeta, P., & McGaw, L. (2018). *Studies in natural products chemistry* (pp. 53 - 67). Elsevier science.

Figure 55. Mabeta, P., & McGaw, L. (2018). *Studies in natural products chemistry* (pp. 53 - 67). Elsevier science.

Figure 56. Seddigi, Z., Malik, M., Saraswati, A., Ahmed, S., Babalghith, A., Lamfon, H., & Kamal, A. (2017). Recent advances in combretastatin based derivatives and prodrugs as antimitotic agents [Diagram] (Figure 9). *Medchemcomm*, *8*(8), 1592-1603.

Figure 57. Piekuś-Słomka, N., Mikstacka, R., Ronowicz, J., & Sobiak, S. (2019). Hybrid cis-stilbene molecules: Novel anticancer agents [Diagram] (Figure 4). *International Journal Of Molecular Sciences*, *20*(6), 1300.

Figure 58. Tangutur, A., Kumar, D., Krishna, K., & Kantevari, S. (2017). Microtubule targeting agents as cancer chemotherapeutics: An overview of molecular hybrids as stabilizing and destabilizing agents [Diagram] (Figure 6). *Current Topics In Medicinal Chemistry*, *17*(22).

Figure 59. McNulty, J., & McLeod, D. (2013). A scalable process for the synthesis of (E)-pterostilbene involving aqueous Wittig olefination chemistry [Diagram] (Scheme 1). *Tetrahedron Letters*, *54*(47), 6303-6306.

Figure 60. Likhtenshtein, G. (2010). (Figure 1.1). *Stilbenes*. Weinheim: Wiley-VCH.

Figure 61. Rameau, N., Russo, B., Mangematin, S., Pinel, C., & Djakovitch, L. (2018). Stilbene synthesis through decarboxylative cross-coupling of substituted cinnamic acids with aryl halides [Diagram] (Graphical abstract). *Applied Catalysis A: General*, *560*, 132-143.

List of abbreviations:

CA- 4 – Combretastatin A-4

CA-1 – Combretastatin A-1

DNA – Deoxyribonucleic acid

WHO – World health organization

UV – Ultraviolet

GTP – Guanosine triphosphate

GDP – Guanosine diphosphate

CBS – Colchicine binding site

AI – Angiogenesis inhibitor

VDA – Vascular disrupting agent

mTOR – Mammalian target of rapamycin

VEGF – Vascular endothelial growth factor

VEGFR – Vascular endothelial growth factor receptor

EC – Endothelial cell

CA- 4P – Combretastatin A-4 phosphate

HIF- 1α – Hypoxia inducible factor – 1alpha

HUVEC – Human umbilical vein endothelial cell

G2/ M - Growth 2/mitosis

CDC 2 – Cell division control 2

P13K – Phosphatidylinositol 3- kinase

Akt – Ak strain transforming

GSK-3 – Glycogen synthase kinase- 3

RhoA/ ROCK – Ras homolog family member A / Rho- associated protein kinases

MAPS – Metalloproteinases

VE – Vascular endothelial

CTGF – Connective tissue growth factor

MAPK / ERK – Mitogen–activated protein kinase / extracellular–signal–regulated kinase

CXCR4 – C-X-C chemokine receptor type 4

CXCL12 – C-X-C motif chemokine ligand 12

ROS – Reactive oxygen species

COX-2 enzyme – Cyclo-oxygenase enzyme 2

DPPH – 2, 2-diphenyl-1-picrylhydrazyl

SOD – Superoxide dismutase

GR – Glutathione reductase

MRP – Multidrug resistance proteins

BCRP – Breast cancer resistance protein

MDR – Multidrug resistant

BafA1 – Bafilomycin A1

3-MA – 3-methyl adenine

Atg - Autophagy-related genes

AMD – Age related macular degeneration

Wnt – Wingless/Integrated

MCL-1 – Myeloid-cell leukaemia 1

HCC – Hepatocellular carcinoma

GSH – Glutathione

CA-1P – Combretastatin A-1 phosphate

CDDP – Cis-diaminedichloroplatinum

EPR – Enhanced permeability and retention effect

PEG – Polyethylene glycol

PLA – Polylactic acid

CRGDyK – Cyclic-RGD penta-peptides

NCI – National cancer institute

IsoCa-4 – Isocombretastatin A-4

TLC – Thin layer chromatography

S_N2 – Nucleophilic substitution 2

NMR – Nuclear magnetic resonance

R_f – Retention factor

MTT assay – 3-(4, 5-dimethylthiazol-2-yl)-2, 5-diphenyl-2H-terazolium bromide assay

EDTA – Ethylenediamine tetraacetic acid

RPMI – Roswell park memorial institute

DMSO – Dimethyl sulfoxide

IR – Infrared

DCM – Dichloromethane

Str – Stretch

Ar – Aromatic

Al – Aliphatic

Amu – Atomic mass unit

Abstract

It has been found that in many cases, the current drugs used for cancer treatment result in reoccurrence of the tumour and severe side effects. Drugs from natural sources display less toxicity (Ali et al., 2012). Combretastatins are known to have cytotoxic activity against cancer cells with minimal side effects (Kretzschmann & Fürst, 2013). Derivatives with improved activity and less detrimental side effects are required.

The different activities of different combretastatins and their derivatives is due to differences in the binding of the compounds to the Colchicine binding site (CBS) in the protein tubulin (Jin et al., 2011). It was thought to investigate whether addition of a further methoxy group to the A ring improved the binding of combretastatin derivatives to the CBS

Studies of the structure- activity relationship of combretastatins suggest that methoxy groups on the A ring are essential for activity against cancer cells. The purpose of this project was to synthesize a range of combretastatins, via Wittig reactions, with a tetramethoxy unit instead of a trimethoxy unit as the A ring, as shown in figure 1 and to test these for activity against cancer cell lines. The activity of these compounds was found and compared to that of the anti-cancer drug Cisplatin, that of combretastatin A4 and the activities of corresponding trimethoxy CA4 analogues.

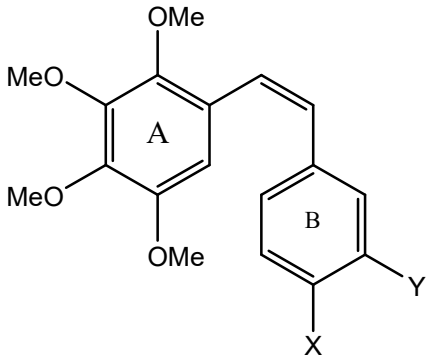

Figure 1. Diagram Showing structure of tetramethoxy CA-4 derivative

The combretastatin structure is relatively simple and easily manipulated and it has been found that making changes to the double bond and or substituents on the rings changes the activities and properties of compounds, hence the investigation into the effects of having a tetramethoxy A ring unit.

Combretastains are easily synthesized using the Wittig reaction, in this case using water as the solvent. In this project, a range of 10 benzaldehydes with different substituents were each reacted with a tetramethoxy phosphonium salt. The phosphonium salt was synthesized via a sequence of synthetic steps, starting from commercially available materials. Very few tetramethoxy combretastatins have been synthesized and even fewer have been tested for their cytotoxic activity.

Synthesis of the combretastatins resulted in formation of both *E* and *Z* isomers for each compound. It was attempted to separate the isomers in each case and to purify the compounds using flash column chromatography. Separation of the isomers proved to be very difficult but separation of the product from leftover starting materials and impurity products was possible.

The cytotoxicities of the synthesized stilbenes against two human cancer cell lines were obtained using an MTT assay.

Not much testing has been done with modifications to the trimethoxy motif of CA-4 (Bukhari, Kumar, Revankar & Qin, 2017). In this project it was found in all cases, where the activities of both trimethoxy and tetramethoxy combretastatin derivatives against the same cell line were known, that tetramethoxy analogues are less active than trimethoxy analogues and that some of the compounds synthesized were more active than Cisplatin.

1 Introduction

1.1 Background information

Plants of the *combretum* species have been used for many years in traditional medicine in Asia and Africa (Cragg, Kingston & Newman, 2011). One of this species, the African willow tree, *Combretum caffrum* (Pettit et al., 1995), grows in South Africa (Mabeta & McGaw, 2018). Its bark contains many compounds, among them the group known as combretastatins (Pettit et al., 1995), produced by plants to deal with infection by microbes and unfavourable environment (Sherbet, 2017) and these compounds have been shown to be able to inhibit tumour growth (Pettit et al., 1995). Pettit and co were the first to isolate these compounds in the 1980's (Mikstacka, Stefański & Różański, 2013). Two of the combretastatins, known as combretastatin A-1 (CA-1) and combretastatin A-4 (CA-4) attracted a lot of interest from chemists due to the fact that they were very potent (McLoughlin & O'Boyle, 2020) against a large range of cancer cell lines (Bukhari, Kumar, Revankar & Qin, 2017). Their structures are shown in figure 2.

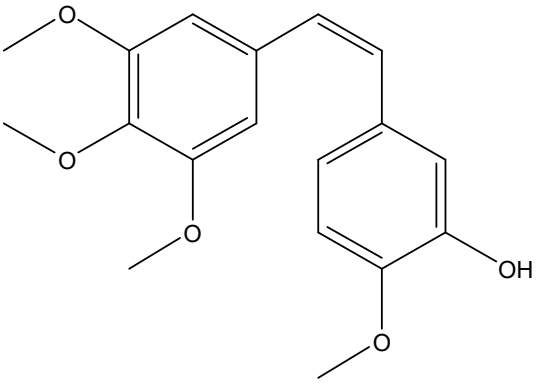

CA-4

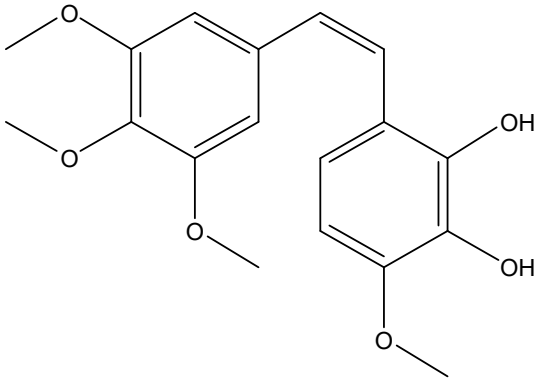

CA-1

Figure 2. Diagram showing structures of CA-1 and CA-4

These compounds have a mechanism of action involving interaction with the cellular protein tubulin in tumour cells instead of with tumour cell DNA (Pettit et al., 1995).

Paclitaxel, also known as taxol, was first isolated from the Pacific yew tree (Bukhari, Kumar, Revankar & Qin, 2017). It has been used in cancer treatment since the 1990's. It was the first drug compound discovered with a mechanism of action involving promotion of microtubule formation. It brought a lot of interest into other drugs with a similar mechanism of action, such as the combretastatins (Mikstacka, Stefański & Różański, 2013). The currently used anti-cancer drugs vinblastine and vincristine both interact with tubulin (Bukhari, Kumar, Revankar & Qin, 2017) Natural compounds and their derivatives have emerged in the last 50 years (Kinghorn, Chin & Swanson, 2009) as a strategy for new cancer treatments and many of the anti- cancer drugs in clinical use come from this source (Kingston, 2009).

The drugs in use currently in cancer treatment suffer from several drawbacks. They usually display toxicity towards normal, healthy cells. They frequently come up against multi- drug resistance (Faustino, Francisco, Isca & Duarte, 2019), metastasis is a problem (Mabeta & McGaw, 2018) and another issue is the high cost (Garbicz et al., 2018). Combretastatins don't have these problems (Karatoprak et al., 2020).

Human colon cancer (Mabeta & McGaw, 2018) and murine lymphatic leukaemia cancer (Mikstacka, Stefański & Różański, 2013) were the first to be tested with CA-4, followed by a range of other cancer cell lines and it was found that CA-4 was highly active against many of them (Bukhari, Kumar, Revankar & Qin, 2017).

CA-4 is a lead compound, which is a compound with a desirable property, such as activity, which is used as a basis for further modifications with the aim of improving certain properties such as cytotoxic activity, aqueous solubility, or geometric isomerism. and because of its simple structure, it is easy to produce derivatives (Bukhari, Kumar, Revankar & Qin, 2017). The different derivatives differ regarding these mentioned properties (Jung et al., 2009) Many CA-4 derivatives have been synthesized and tested against cancer cell lines in labs around the world, but only a handful such as CA4P (Fosbretabulin), AVE8062 (Ombrabulin) and CA1P (Oxi4503) have progressed to clinical trials (Seddigi et al., 2017).

1.2 Cancer

The growth of the population, the increase in age within it, coupled with lifestyle changes (Caul, 2021), such as the food we eat and the environment we live in (Shi et al., 2016), mean that incidence of cancer is on the rise (Caul, 2021). In 2014 it was predicted by the WHO that number of cancer cases per year will rise to 13 million (Shi et al., 2016).

The term cancer is used to describe a group of similar diseases ("Cancer", 2022). Normally cells grow and then divide, with the production of new cells which replace the old ones. When cancer occurs, some cells in the body ignore the signals that facilitate normal cell division and death of damaged or old cells. Cells then start to divide uncontrollably, often forming tumours which can then invade surrounding tissues. Cancer can occur in almost any part of the human body. The diagram in figure 3 depicts a tumour.

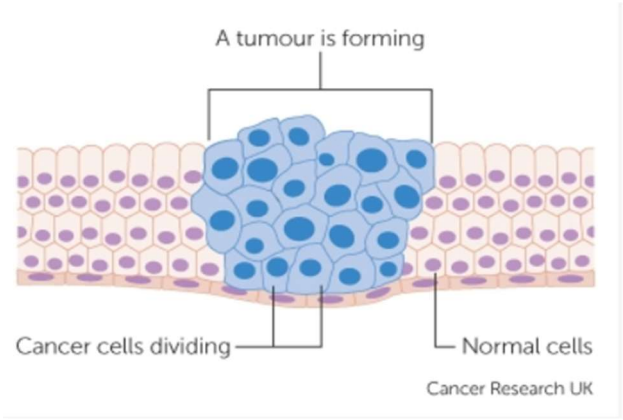

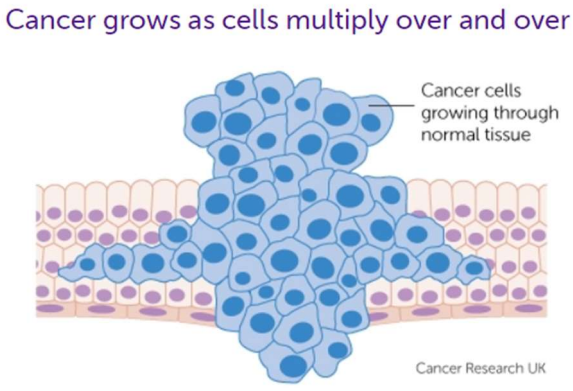

Figure 3. Diagram depicting a tumour ("Cancer cells", 2020).

Over 200 different types of cancer exist which can affect humans. In certain cases, cancer which forms in one part of the body spreads to other parts in a process called metastasis ("What Is Cancer?", 2022). The interference of tumours with surrounding tissues can affect normal functioning of organs ("How can cancer kill you? | Dying with cancer | Cancer Research UK", 2021). The underlying cause of cancer is genetic changes, alterations to the genes controlling growth and division of cells. These changes can either be inherited or because of exposure to certain conditions such as tobacco smoke or UV-rays. The forms of cancer are labelled according to the region of the body where they originated from ("What Is Cancer?", 2022).

The 3 main methods of cancer treatment are surgery, chemotherapy, or radiotherapy. The drugs used can target either DNA, proteins, or the endocrine system. Drugs targeting proteins are effective whilst having low cytotoxicity to normal cells. This is due to their selectivity for cancer cells over normal ones (Karatoprak et al., 2020).

1.3 Structure of combretastatins

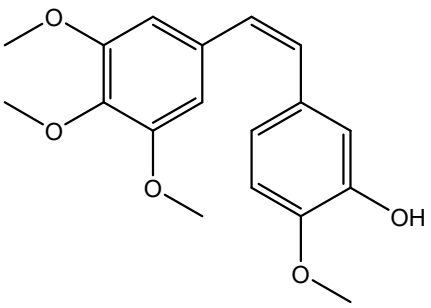

Cis combretastatin A-4

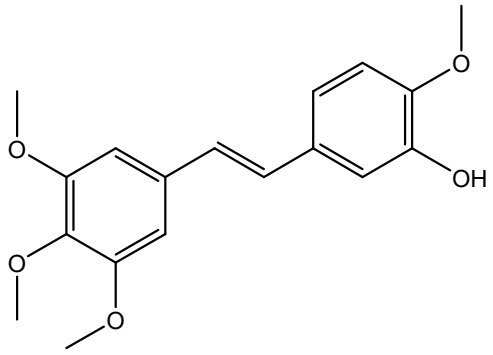

Trans combretastatin A-4

Figure 4. Diagram showing cis and trans combretastatin A-4 structures

Combretastatins have benzene rings attached at each end of an ethylene bridge. They can therefore be *cis* or *trans* in structure, as illustrated ion figure 4. The positions on the bridge or rings can be substituted by various groups. The simple combretastatins are small, only having a mass of 300-400 amu. The advantages of having small molecules as drugs include increased permeability into cells, increased stability, increased tolerance, and less immunogenicity (Sherbet, 2017).

1.4 Structure-activity relationship

Only the *cis* conformation of combretastatins has significant anti- cancer activity, the *trans* form has little or none (McLoughlin & O'Boyle, 2020). This is because the *cis* conformation holds the benzene rings at the optimal distance apart and dihedral angle for binding to its target, the tubulin protein within cells. The active *cis* form readily isomerizes to the more stable, inactive *trans* form within the environment of the body (Bukhari, Kumar, Revankar & Qin, 2017).

It was initially thought that the trimethoxy unit A ring of combretastatins was essential for activity, recent studies have shown that only one of the methoxy units is involved with binding to tubulin (McLoughlin & O'Boyle, 2020), the meta methoxy groups are replaceable (Zong, Shea, Maffucci & Ojima, 2017).

Regarding the B ring of CA-4, its methoxy group is important for activity but the OH group is not and is readily replaced without affecting activity (Bukhari, Kumar, Revankar & Qin, 2017).

1.5 Mode of action of combretastatins

CA-4 has a multi- pronged mechanism of action against tumours. It attacks tumour cells both directly, being cytotoxic to them and indirectly by shutting down tumour vasculature which supplies tumours with oxygen and nutrients which tumours need to survive. Both effects arise due to the interaction of CA-4 with tubulin (Mabeta & McGaw, 2018). Much is still unknown regarding the precise mechanisms of combretastatins activity against cancer cells (Pérez-Pérez et al., 2016).

1.6 Tubulin

Tubulin is a protein, found in all animal cells (Seddigi et al., 2017). There are two types of interest to us, known as α and β tubulin. They are very similar in structure but there are some differences (Bukhari, Kumar, Revankar & Qin, 2017), there is around 40% similarity in their constituent amino acids. Each tubulin monomer has a mass of around 50 KDa (McLoughlin & O'Boyle, 2020). The overall structure is the same for both, consisting of helices surrounding a beta sheet core (Downing & Nogales, 1998). Each tubulin monomer consists of three domains, which are the N-terminal, intermediate and C-terminal domains. Differences in the C-terminal domain are responsible for different tubulin isotypes. α- tubulin has six isotype forms, β- tubulin has seven (Pérez-Pérez et al., 2016). The C- terminal tubulin domain also associates with microtubule associated proteins (Nogales, 2012). α and β tubulin undergo polymerisation within cells, forming structures known as microtubules (Bukhari, Kumar, Revankar & Qin, 2017). To do this, first they polymerize head to tail, forming protofilaments. Thirteen protofilaments then associate laterally to form the hollow, cylindrical structures known as microtubules illustrated in figure 5.

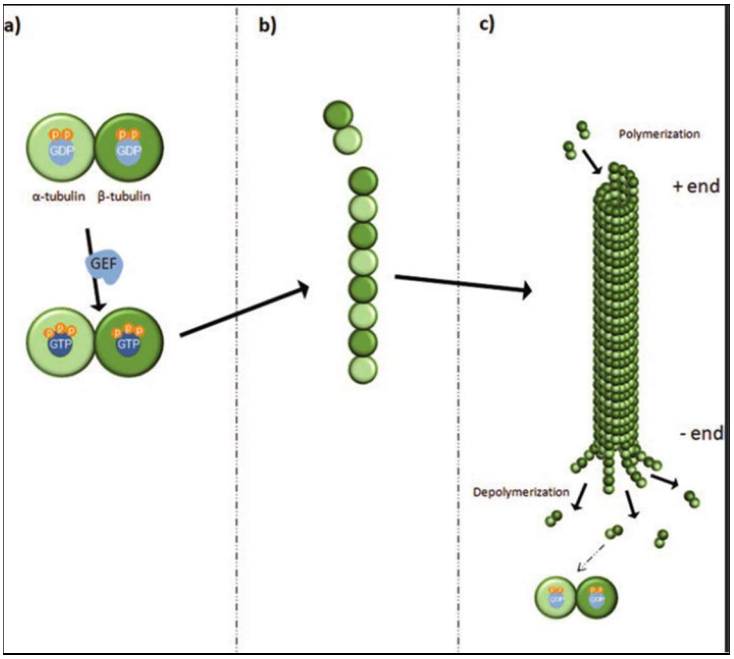

Figure 5. Diagram showing microtubule formation (Kounakis & Tavernarakis, 2019).

Microtubule structure possesses polarity, with a positive end comprised of β- tubulin units and a negative end comprised of α- tubulin units (Seddigi et al., 2017). This polarity plays a key role in their biological function (Kaur, Kaur, Gill, Soni & Bariwal, 2014). The tubulin dimer is stable, unlike the monomers (Downing & Nogales, 1998). The structure of the tubulin dimer was first obtained using electron crystallography by Nogales and co in 1998 and the atomic structure has been improved to 3.5 angstrom resolution (Pérez-Pérez et al., 2016). α and β units both have a site where they bind to guanosine triphosphate (GTP). GTP binds reversibly to β-tubulin at what is known as the exchangeable site and GTP binds irreversibly to α- tubulin at what is known as the non- exchangeable site. The exchangeable site is located on the surface of the dimer while the non- exchangeable is buried within (Kaur, Kaur, Gill, Soni & Bariwal, 2014). Microtubules are key cell organelles and have many roles, including in cell replication, signalling pathways, shape of cells and intracellular transport (Mikstacka, Stefański & Różański, 2013).

1.6.1 Mechanism of microtubule polymerization/ depolymerization

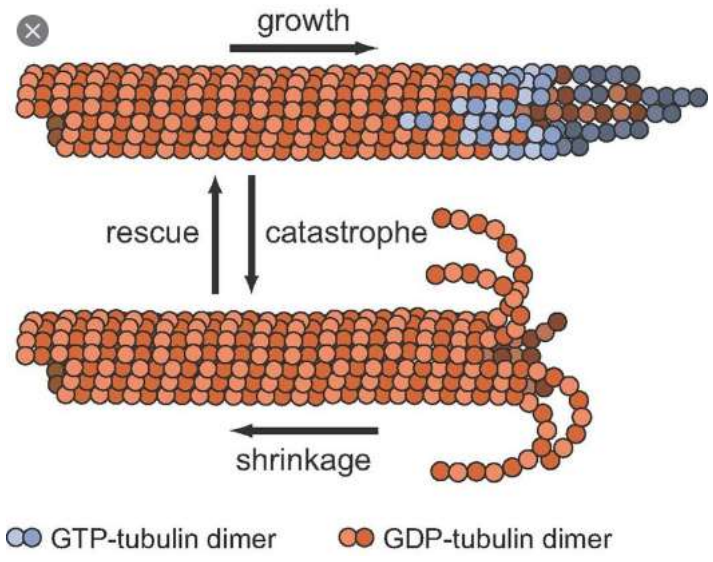

Figure 6. Diagram showing tubulin/ microtubule interaction (Bowne- Anderson, Zanic, Kauer & Howard, 2013).

There is a dynamic balance within the cell between tubulin and the microtubules it polymerizes to form. Guanosine triphosphate (GTP) binds to tubulin at both the α and β subunits,

irreversibly at the α subunit but reversibly at the β subunit. The GTP bound tubulin then adds on to the positive end of the microtubule, lengthening it.

During this polymerisation process, the GTP is hydrolysed to guanosine diphosphate (GDP). GDP bound tubulin does not bind well to tubulin and so it breaks off, shortening the microtubule. The length of the microtubule thus depends on the relative rates of GTP bound tubulin adding on and GDP bound tubulin breaking off. A relatively faster rate of GTP bound tubulin adding on lengthens the microtubule while a relatively faster rate of the GDP bound tubulin breaking off shortens the microtubule (McLoughlin & O'Boyle, 2020). A tubulin- GDP unit can only detach from the microtubule tip, not from the middle. Since tubulin only adds on to the microtubule in the GTP bound state, there exists a tubulin-GTP cap, protecting the microtubule from depolymerisation. When the GTP to GDP hydrolysis process catches up to the tip, the cap is lost and rapid depolymerisation occurs, this process is known as 'catastrophe'. The addition of another GTP- tubulin cap is termed as 'rescue' (Kaur, Kaur, Gill, Soni & Bariwal, 2014). The polymerisation process is what causes GTP hydrolysis, therefore the α/ β unit activates itself and it is not activated by another protein (Downing & Nogales, 1998) Anything that affects this polymerization/ depolymerisation balance has a drastic effect on microtubules and therefore the cellular processes they play a part in (Kingston, 2009). A single GTP- tubulin unit on each protofilament is enough to maintain microtubule stability (Downing & Nogales, 1998). The process is illustrated in figure 6.

1.6.2 Microtubules and cell shape

Microtubules form a large part of the cell cytoskeleton (Cooper, 2000) and are present as rigid filaments (Matis, 2020). They play a role in determining the shape of cells (Cooper, 2000). The shapes of cells have a role in their properties and functions (Haupt & Minc, 2018). Of particular interest is the role of cell shape in the function of endothelial cells which line the walls of tumour vasculature (McLoughlin & O'Boyle, 2020).

1.6.3 Microtubules and cell replication

During cell replication, microtubules are involved in the separation of chromosomes into daughter cells. Microtubules make up the mitotic spindle which reaches out from the

centrosomes of daughter cells, connecting to the kinetochores of chromosomes and pulling them apart into individual cells. Microtubules can do this due to the ongoing dynamic balance between polymerization of tubulin to form microtubules and depolymerisation of microtubules forming tubulin. This allows for shortening or lengthening of microtubules as required by the cell. Microtubules lengthen when reaching out from cell centrosomes to attach to chromosomes and subsequently shorten when pulling the attached chromosomes into the daughter cells (Kingston, 2009).

1.6.4 Microtubules and signalling pathways

Microtubules have an important role in signalling pathways within the cell, including those involved in inducing cell apoptosis. For example, microtubules interact with proteins involved in mitogen activated protein kinase (MAPK) signalling such as p38, extracellular regulated kinases (ERK) and c- Jun N terminal kinases (JNK). Drugs that interact with microtubules can therefore activate these pathways (Parker, Kavallaris & McCarroll, 2014).

Tubulin is now an important target for anti-cancer drugs (Mikstacka, Stefański & Różański, 2013). The α/ β- tubulin unit has many sites for drugs to bind (Sherbet, 2017).

1.6.5 Tubulin binding sites

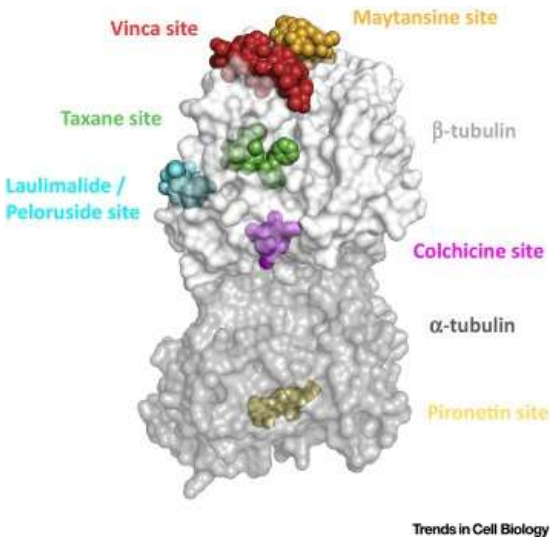

Figure 7. Diagram showing tubulin binding sites (Steinmetz & Prota, 2021).

Using crystallography and computational methods, twenty-seven possible sites for binding have thus far been identified (Mühlethaler et al., 2021). Some of these are illustrated in figure 7. The three most well-known sites are the colchicine, taxane and vinca sites (Nakamura, Kajita, Matsumoto & Hashimoto, 2013).

The colchicine site is located where the α and β units meet (Kaur, Kaur, Gill, Soni & Bariwal, 2014). It is mainly a deep, hydrophobic pocket with two adjunct regions (Pérez-Pérez et al., 2016). The colchicine site is surrounded mainly by β- tubulin residues (Gaspari, Prota, Bargsten, Cavalli & Steinmetz, 2017). The compounds in this study, combretastatin A-4 derivatives all bind at the colchicine binding site (CBS). It is assumed that the different compounds have different anti- cancer activities due to different interactions with the (CBS) and therefore different degrees of binding to tubulin (Pérez-Pérez et al., 2016). It has been found that compounds that bind to the (CBS) usually contain a trimethoxy unit in their structure (Li et al., 2018). The taxane site is situated inside the microtubule lumen, within a hydrophobic pocket, in- between protofilaments. The vinca site is situated at the exchangeable site of β-tubulin (Kaur, Kaur, Gill, Soni & Bariwal, 2014). Drugs binding to tubulin can act by either stabilizing microtubules or by destabilizing them (McLoughlin & O'Boyle, 2020). Drugs binding to the colchicine and vinca sites are microtubule destabilizers, drugs binding to the taxane site microtubule stabilizers (Kaur, Kaur, Gill, Soni & Bariwal, 2014).

Like CA-4, the drugs vincristine and vinblastine are microtubule destabilizers; however, they bind not to the colchicine but rather to the vinca site (Bukhari, Kumar, Revankar & Qin, 2017). The drugs docetaxel and paclitaxel are microtubule stabilizers, and they bind to the taxane site (Sherbet, 2017). All the tubulin interacting drugs currently on the market bind to either the vinca or taxane sites. These drugs have high potency, but they also have several disadvantages. They frequently run into multi- drug resistance, they have high lipophilicity, which makes it necessary to solubilise them with surfactants, and these surfactants can cause an adverse reaction in patients and thirdly they require intravenous administration, because of their poor aqueous solubility. Tubulin interacting drugs which bind to the colchicine site do not have these problems. This is because they have comparatively higher solubility in water, meaning that they can be administered orally and, they are poor substrates of P-gp efflux pumps which are one of the major causes of multidrug resistance (Li et al., 2018).

1.7 Tumour vasculature

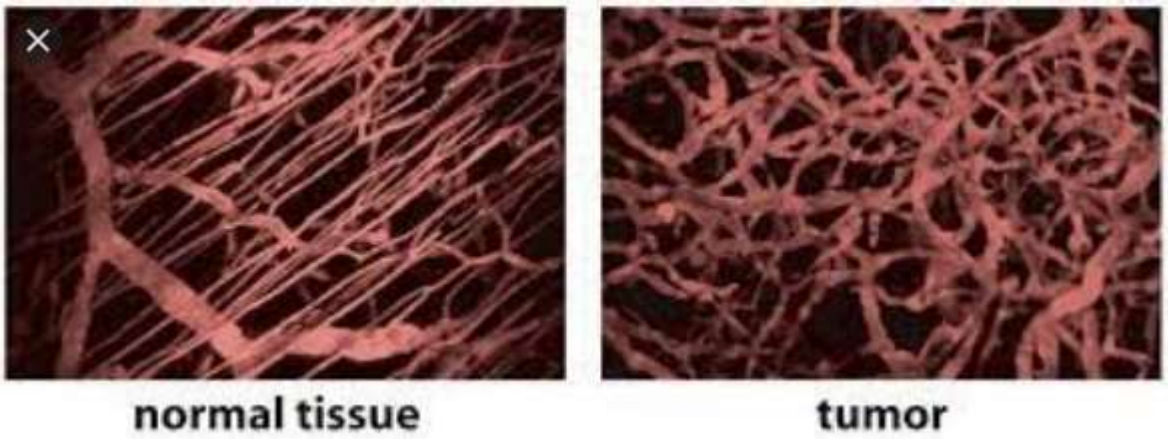

Figure 8. Diagram showing differences between normal and tumour vasculature (Forster, Harriss-Phillips, Douglass & Bezak, 2017).

As mentioned in the previous section regarding modes of action of combretastatins, CA-4 and its derivatives target tumour vasculature. Tumours require a steady supply of blood and oxygen to survive (Lippert, 2007) and for metastasis to occur (Mabeta & McGaw, 2018). Solid tumours cannot grow larger than $2mm^3$ in size without the support of a vascular network (Seddigi et al., 2017). Smaller tumours can get the blood and oxygen they require by the process of diffusion from the normal tissues surrounding the tumour (Kretzschmann & Fürst, 2013). Tumours acquire this necessary vasculature by a process known as angiogenesis, which is the formation of new blood vessels (Garbicz et al., 2018). Tumour vasculature is different from normal vasculature in several ways. Tumour vasculature has more twists and turns, the distribution of vessels is more uneven throughout the tumour, the diameter of vessels is non- uniform, there is more branching, there are many blind-ended vessels, the flow of blood is slower, vessels are enlarged and not fully developed, there is a decreased amount of smooth muscle cells in the vessels as well as the connections between endothelial cells and pericytes of tumour vessels being poor. The poor connections between tumour vessel cells result in increased permeability and interstitial fluid pressure within vessels. As in all blood vessels, tumour blood vessels are lined with endothelial cells; however, the endothelial cells in tumour blood vessels proliferate at a faster rate (Kretzschmann & Fürst, 2013). A picture showing the obvious difference between normal and tumour vessels is shown in figure 8. These differences between normal and tumour vasculature mean that certain drugs can be selective in their action against tumour

vasculature instead of normal blood vessels (Sherbet, 2017). Drugs which target tumour vasculature are a recent development in cancer treatment (Mabeta & McGaw, 2018).

Drugs affecting tumour vasculature are of two kinds, angiogenesis inhibitors (AIs), which target formation of new blood vessels or vascular disrupting agents (VDAs), which target existing vasculature. The main action of CA-4 and derivatives is as VDAs.

1.8 Angiogenesis inhibitors and vascular disrupting agents

AIs have been around for a long time, VDA's are more recent (Kretzschmann & Fürst, 2013). The effect of VDAs is on the interior, central region of the tumour, where it shuts down the tumour vasculature, cutting off the supply of oxygen and blood resulting in central tumour necrosis. This tumour central region is typically resistant to existing conventional therapies. There is an issue though with VDAs which is what is known as the 'viable rim'. VDA's do not affect vasculature at the periphery of the tumour, as this vasculature is normal and thus remains unaffected, this means that a region of tumour cells is left behind, which can support neovascularisation and therefore tumour regrowth (Grisham, Ky, Tewari, Chaplin & Walker, 2018). The precise mechanism by which VDAs act on tumour vasculature is not known at present (Kretzschmann & Fürst, 2013).

AIs act on tumour neovasculature, on the outer, peripheral regions of a tumour. They are also effective against small tumours (McKeage, 2011). The use of AIs has been an emerging strategy over the past few years. Compounds have been developed that target proangiogenic pathways such as the mTOR pathway and the vascular endothelial growth factor/ vascular endothelial growth factor receptor pathway (VEGF/ VEGFR pathway) (Siemann, 2011).

AIs and VDAs both act by targeting endothelial cells (ECs) of tumour vasculature. The endothelial cells are cells that line the inner surface of blood vessels. Differences between VDAs and AIs include, AIs inhibit growth and proliferation of ECs while VDAS are cytotoxic to the ECs, AIs are effective when tumours are still small compared to VDAs which are effective with large tumours, AIs should be administered chronically while VDAs should have acute administration (Pérez-Pérez et al., 2016) and as has been mentioned already, they affect different regions of the tumour.

The use of either VDAs or AIs alone is disadvantageous as, acting alone, neither type of agent affects the entirety of the tumour vasculature (Hori, 2011). AIs have already seen introduction into the clinic but without much success (Kretzschmann & Fürst, 2013) AIs and VDAs are complementary to each other regarding the areas of the tumour they affect and used together the viable rim problem of using VDAs as single agents is no longer a problem. It is for this reason that they have been entered into clinical trials as a combination therapy an example of which is the combination of bevacizumab and CA-4P (Grisham, Ky, Tewari, Chaplin & Walker, 2018). Imaging techniques have been used to show that the effect of VDAs is restricted to tumour and not normal vasculature (Pérez-Pérez et al., 2016).

The abnormality of tumour vasculature presents challenges to chemo and radio therapy, such as regional hypoxia, however the clear distinction between tumour and normal vasculature means that tumour vasculature is still an attractive target for drug therapies (Siemann, 2011).

1.8.1 Limitations of vascular disrupting agents

Aside from the viable rim issue of VDAs, the other major issue regarding VDA treatment is that of tumour regrowth brought about by hypoxia. The administration of a VDA destroys tumour vessels in the interior, causing the condition of hypoxia. The onset of hypoxia causes the HIF-1α protein to be activated, which starts the development of new blood vessels. Also, because of HIF-1α activation is an increase in the expression of proangiogenic cytokines and activation of genes responsible for angiogenesis. Tumours have many strategies for dealing with the adverse conditions brought about by exposure to VDAs, such as they can use different angiogenic pathways, they can utilise the process of autophagy and they can recruit endothelial progenitor cells amongst other strategies. All these strategies result in drug resistance and regrowth of tumours (Smolarczyk, Czapla, Jarosz-Biej, Czerwinski & Cichoń, 2021).

1.9 The effect of CA-4

1.9.1 Effect of CA-4 on microtubules

Unpolymerized tubulin takes a curved shape, when it polymerizes to form microtubules that curved shape becomes straight. The curved to straight transition is a requirement for microtubule formation (McLoughlin & O'Boyle, 2020). The tubulin units transition between

being curved and being straight but prefer being curved unless forced out of it. Side interactions between the protofilaments keep the units in the straight conformation. When the curved and straight conformations of tubulin are compared, certain structural differences are observed. In the curved conformation helix H7 is axially displaced and there is some rotation between domains (Amos, 2011).

Upon the binding of CA-4 to tubulin, the A ring with its methoxy groups is buried within a hydrophobic cavity of the colchicine site with β-tubulin residues all around it (Gaspari, Prota, Bargsten, Cavalli & Steinmetz, 2017) where it forms hydrogen bonds with various residues (Li et al., 2018). The B ring is sandwiched between β- tubulin residues and there are hydrophobic interactions between the B ring and residues of both α and β- tubulin units. Hydrogen bonds are formed between the hydroxyl group on the B ring and various α- tubulin residues. CA-4 and thus its derivatives are not able to bind to tubulin while the tubulin units are incorporated into microtubules, binding can only occur with tubulin in the free state. The binding of the compounds to tubulin causes conformational changes only to the colchicine binding site, not to the entire tubulin structure (Gaspari, Prota, Bargsten, Cavalli & Steinmetz, 2017). When CA-4 binds to tubulin, the tubulin units are constrained in the curved conformation (McLoughlin & O'Boyle, 2020), the drug prevents the βT7 loop from taking on the conformation it must be in for tubulin to be straight (Gaspari, Prota, Bargsten, Cavalli & Steinmetz, 2017), interactions between protofilaments are lost resulting in disassembly of microtubules (McLoughlin & O'Boyle, 2020).

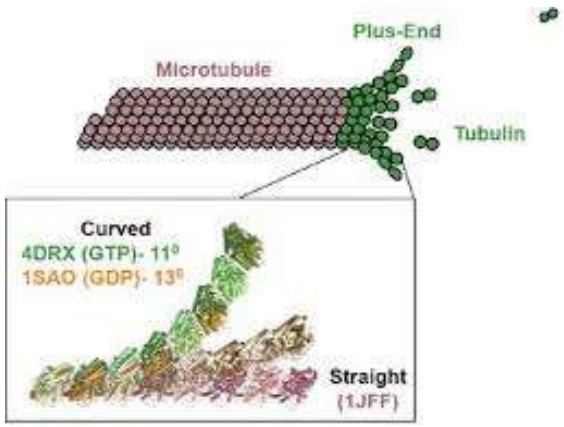

Figure 9. Diagram showing curved/ straight tubulin (Brouhard & Rice, 2014).

The curved to straight tubulin transition is illustrated in figure 9. The drug therefore hinders the formation of microtubules (McLoughlin & O'Boyle, 2020) which is of importance for reasons already outlined.

1.9.2 CA-4 and tumour vasculature

As has been outlined, the interaction of CA-4 with tubulin affects microtubule formation, which in turn affects cell shape as microtubules form part of the cell cytoskeleton. There are several ways in which CA-4 affects tumour vasculature.

CA-4 affects the shape of the endothelial cells which line the tumour vasculature blood vessels, and it is selective in targeting these instead of normal endothelial cells and vasculature for reasons still not completely clear (McLoughlin & O'Boyle, 2020). The change in shape results in loss of contacts between endothelial cells and the endothelial cells also detach from the blood vessel substratum, these conditions combine resulting in the exposure of the blood vessel basal lamina. This exposure causes clotting factors and blood platelets to be activated. The activation results in the coagulation of blood within the vessels which in turn increases vascular resistance, which affects the blood supply of the tumour

CA-4 causes vasoconstriction of the tumour vessels, caused by muscle cells on the tumour vessel interior. Like blood coagulation within vessels, this also increases vascular resistance (Mabeta & McGaw, 2018).

The change in cell shape of tumour vessel endothelial cells after CA-4 treatment causes adherens junctions between the cells to be disrupted, which results in the vessels becoming more permeable to external agents (Kretzschmann & Fürst, 2013).

These factors all combine causing tumour vasculature shutdown, resulting in necrosis in the centre of the tumour (Mabeta & McGaw, 2018).

It was found however that the changes to the shape of endothelial cells brought about by CA-4 are only temporary and that after removal of the drug, the endothelial cells regain their normal shape after twenty-four hours.

It was found in *in vitro* studies that the CA-4 prodrug, CA-4-P (Combretastatin A4- phosphate) disrupted microtubule dynamics in human umbilical vein endothelial cells (HUVECS),

completely depolymerising microtubules. It did this with concentrations between 0.1 and 1.0 μM of the drug, with initial effects seen after administration of just nM of the drug. It was found during *in vitro* studies, using mice with human tumour xenografts that tumour vasculature was rapidly shut down with first effects seen after just ten minutes of CA-4-P administration (Kretzschmann & Fürst, 2013).

The selectivity of CA-4P for tumour over normal vasculature was investigated *in vitro* using a rat cancer model. It was found that after administration of 100mg/kg of CA4P, there was one hundred times less blood flow to the tumour after six hours, with this effect lasting twenty-four hours. Of vital importance was the fact that blood flow to the healthy organs showed little or no reduction.

CA4P is more effective when administration is in small, repeat doses as opposed to one single, large dose. At small doses, CA4P doesn't exhibit direct cytotoxicity towards tumour cells however it is still able to shut down tumour vasculature (Mabeta & McGaw, 2018). The discovery that CA-4 caused vascular shutdown at ten percent of the maximum tolerated dose is what caused much interest in the applications of CA-4 and its derivatives as an anti-cancer drug (Bukhari, Kumar, Revankar & Qin, 2017).

Following administration of one dose of CA- 4, the flow of blood to a tumour returns to pre-administration levels after twenty-four hours (Greene, Meegan & Zisterer, 2015).

1.9.3 CA-4 and cancer cell proliferation

As has been previously stated, the binding of CA-4 to tubulin affects the dynamic tubulin/ microtubule balance, the extent to which it does this changes with dosage and with different cell lines (Mabeta & McGaw, 2018). This situation affects the formation of normal mitotic spindle within the tumour cells. There are mitotic checkpoints within the cell that oversee normal microtubule dynamics and anything abnormal occurring means that progression into the next phase of the cell cycle is halted (Sherbet, 2017). CA-4 therefore interrupts the G2/M transition, which is the progression of cells from the G2 growth phase into mitosis (Jackman, 2011). This in turn results in mitotic catastrophe followed by cell apoptosis. The rapidly dividing cancer cells are more affected by CA-4 than normal cells are (Mabeta & McGaw, 2018). A picture showing the stages of the cell cycle is shown in figure 10.

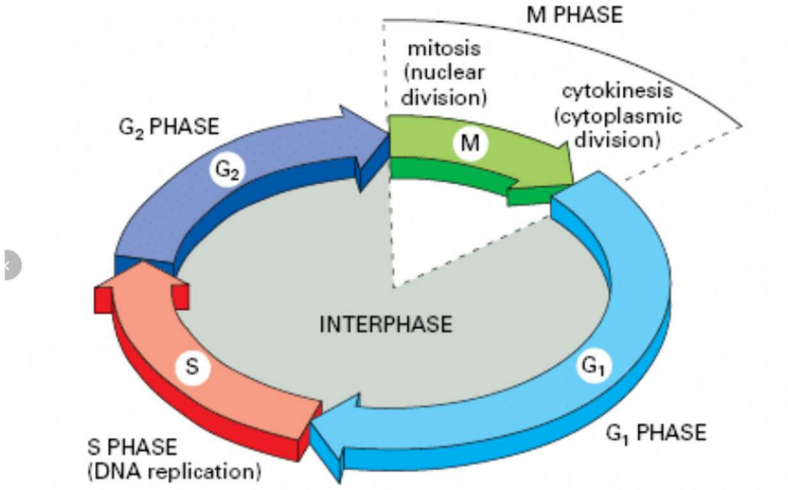

Figure 10. Diagram showing stages of the cell cycle (Alberts et al., 2002).

At the same time as cell cycle arrest occurring, signalling pathways that lead to tumour cell apoptosis are activated (Sherbet, 2017), by a mechanism yet to be fully understood (Mikstacka, Stefański & Różański, 2013).

CA-4 is cytotoxic against a range of human cancer cell lines, as well as those that are multi-drug resistant (Mikstacka, Stefański & Różański, 2013).

CA-4 can also cause tumour cells to go into mitosis early or cause an abnormal mitosis, both of which lead to mitotic catastrophe and cell apoptosis (Sherbet, 2017).

The major mitotic checkpoint for the G2/M transition involves the M phase promoting factor complex. This complex is made up of subunits of the proteins cdc2 and cyclinB1. For the transition to occur, this complex must be activated. CA-4 treatment results in decreased levels of the proteins cdc2 and cyclinB1, as well as of the protein cdc25c which is another protein involved in activation of the complex. Other such complexes exist within cells (Duan et al., 2016).

1.9.4 CA-4 and cell proliferation signalling pathways

CA-4 influences various signalling pathways within tumour cells, through its interaction with tubulin. The pathway that is affected the most is the PI3K/ Akt/ mTOR pathway. This pathway is of vital importance in processes of the cells such as cell metabolism, growth, and survival

(Sherbet, 2017). It is found that in many tumour cells there is increased activation of this pathway, resulting in excessive growth and multiplication of tumour cells (Khan, Yap, Yan & Cunningham, 2013). CA-4 administration causes a decrease in the expression of the proteins involved in this pathway, PI3K and Akt, thus suppressing the pathway (Liang et al., 2016). The Akt protein also activates the mTOR pathway, which in turn activates the tumour cell survival signalling pathway, NK- kB. The combination of allosteric inhibition of PI3K and mTOR with the administration of CA-4 shows promise as a cancer treatment.

The GSK- 3β pathway also brings about apoptosis in tumour cells. This pathway also involves Akt, Akt causes its inactivation. CA-4 affects the GSK- 3β pathway both directly, bringing about cell apoptosis through this route and indirectly by inhibiting Akt inactivation of the pathway.

CA-4 activates the RhoA/ ROCK pathway, which is involved in the regulation of other signalling pathways such as the already mentioned Akt/ mTOR pathway (Sherbet, 2017).

CA-4 causes activation of the caspase 3 pathway (Sherbet, 2017). This pathway involves proteases which break down cellular components, including cellular proteins, bringing about apoptosis (Seervi & Xue, 2015).

1.9.5 CA-4 and angiogenesis

As has been mentioned already, tumours require a blood supply if they are to grow beyond a certain size and they obtain the vasculature required for this in a process called angiogenesis. In angiogenesis, new blood vessels sprout from the ones that already exist. The process of angiogenesis is regulated by a balance of antiangiogenic factors and proangiogenic factors. The process of angiogenesis is illustrated in figure 11 . The process of angiogenesis involves many steps such as endothelial cell proliferation, the breaking down of the extracellular matrix, endothelial cell migration and finally vessel formation. Any of these several steps can act as a target for drugs that inhibit angiogenesis. The importance of neovascularisation in tumour progression is evident in the link between increased expression of the proangiogenic factor, VEGF, and a poor prognosis in many human cancers (Griggs, Metcalfe & Hesketh, 2001).

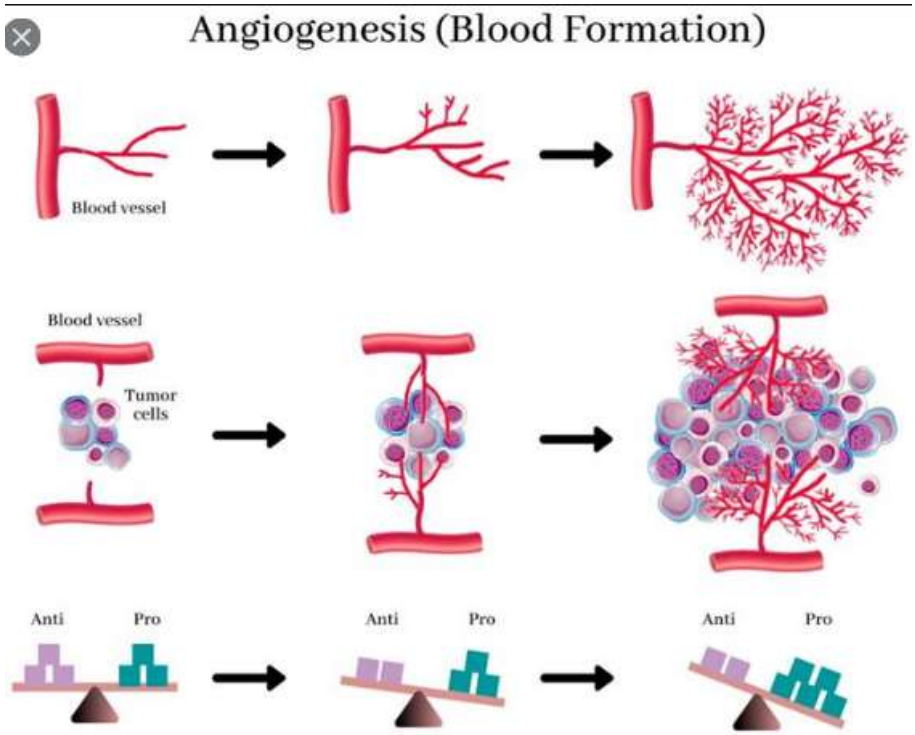

Figure 11. Picture illustrating angiogenesis (Madu, Wang, Madu & Lu, 2020).

While CA-4 acts principally as a vascular disrupting agent, it also has antiangiogenic properties (Pérez-Pérez et al., 2016).

Angiogenesis will occur in a tumour when there is a tumour induced overabundance of proangiogenic factors, such as metalloproteinases (MAPS) and VEGF, over antiangiogenic factors such as thrombospondin and angiostatin (Griggs, Metcalfe & Hesketh, 2001). It is known that there are as many as thirty different factors that promote angiogenesis, the best and most important of which is VEGF. Studies have shown that VEGF affects each of the multiple steps in the process of angiogenesis (Su et al., 2016). The fact that CA-4 suppresses proangiogenic signalling is borne out by the fact that its administration results in repression of VEGF/ VEGFR2 signalling (Sherbet, 2017).

The migration of endothelial cells, which is one of the steps in angiogenesis is thought to involve several pathways, the vascular endothelial (VE)-cadherin/ β- catenin pathway and the connective tissue growth factor (CTGF) pathway, both of which are pathways CA-4 interacts with (Pérez-Pérez et al., 2016). The VE- cadherin/ β- catenin pathway is a proangiogenic pathway, which CA-4 inhibits by inhibiting phosphorylation of VE- cadherin (Greene, Meegan

& Zisterer, 2015). The CTGF pathway is an antiangiogenic pathway which CA-4 up regulates. The up regulation of this pathway depends on ROCK signalling and its effect was increased by the presence of MAPK/ Erk inhibitors, providing a reason for why combretastatin activity is increased by the presence of kinase inhibitors.

In mice models with tumours, using a ROCK inhibitor it was proved that activation of Rho/ ROCK is critical for the effects of CA4P on tumour vasculature (Pérez-Pérez et al., 2016).

The action of CA-4 and its derivatives in inhibiting angiogenesis has not at present been thoroughly researched (Nik et al., 2019).

1.9.6 CA-4 and metastasis

Metastasis is the process by which tumour cells, originating in one part of the body, known as the primary site, migrate to other parts of the body. This is illustrated in figure 12. The process of angiogenesis in tumours increases the possibility of metastasis happening. Due to this, when angiogenesis is being targeted, metastasis is also being targeted (Nik et al., 2019). Likewise, targeting tumour cell proliferation targets the process of metastasis. There are two ways in which combretastatins directly affect metastasis. Firstly, they inhibit the process of angiogenesis in the small metastases preventing their development and secondly, they inhibit the migration of tumour cells from the primary site to other regions of the body (Greene, Meegan & Zisterer, 2015). In cancer treatments, action against tumour cell proliferation and action against the process of metastases should be carried out concurrently.

In tumours, the relationship between the cell receptor CXCR4 and its ligand CXCL12 is very important in cancer metastasis. Tumour cells undergo migration to parts of the body where there is a high expression of CXCL12. Control of the CXCR4/ CXCL12 interaction therefore provides some control over metastasis. This process is illustrated in figure 13

Jiang et al carried out a study where a CA-4P/ nanoparticle combination was administered to a 4T1 cancer mouse model. The issue of metastasis was addressed by also administering plerixafor, a CXCR4 antagonist.

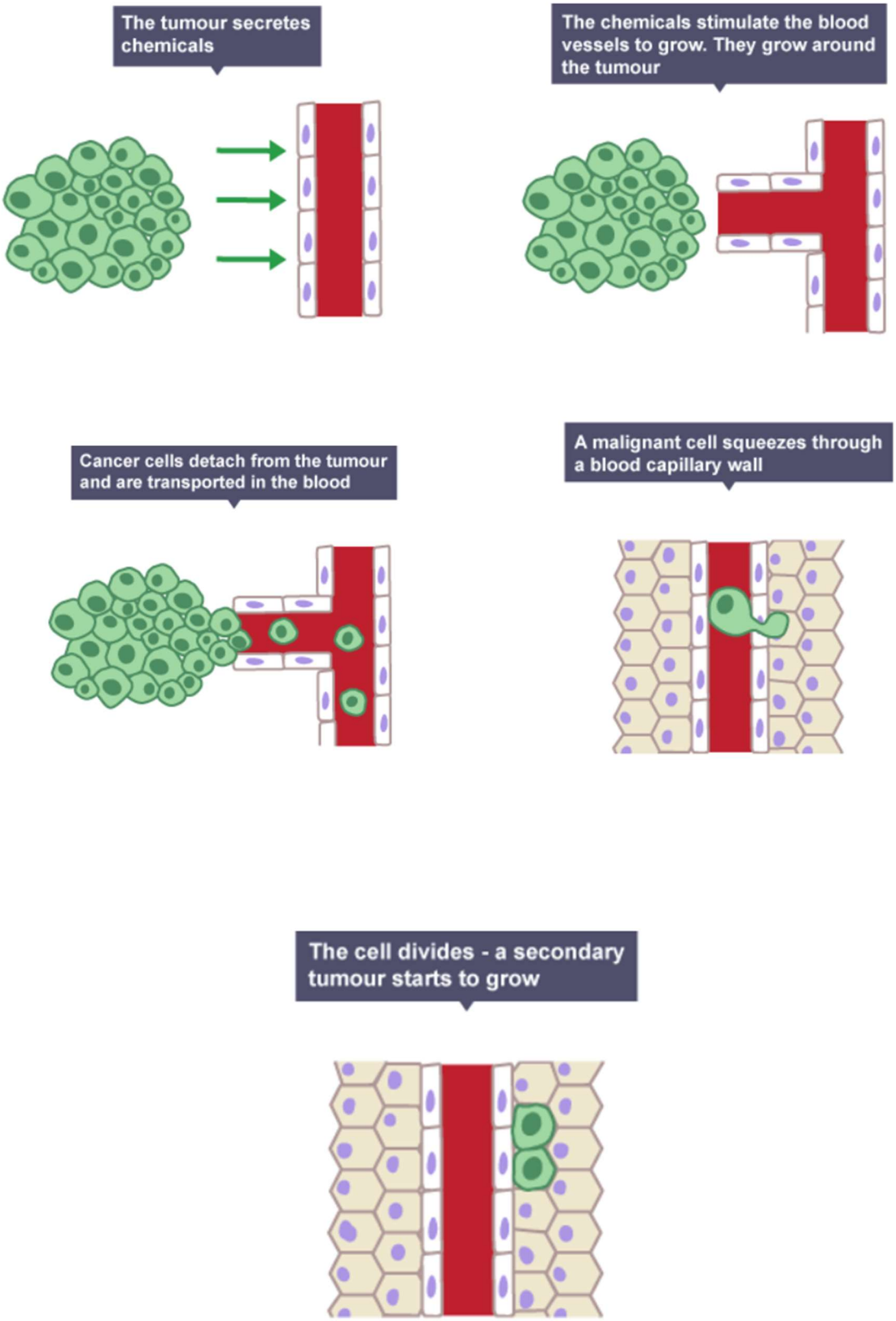

Figure 12. Diagram showing metastatic process ("Cancer and carcinogens - Cell division - Edexcel - GCSE Combined Science Revision - Edexcel - BBC Bitesize", 2022).

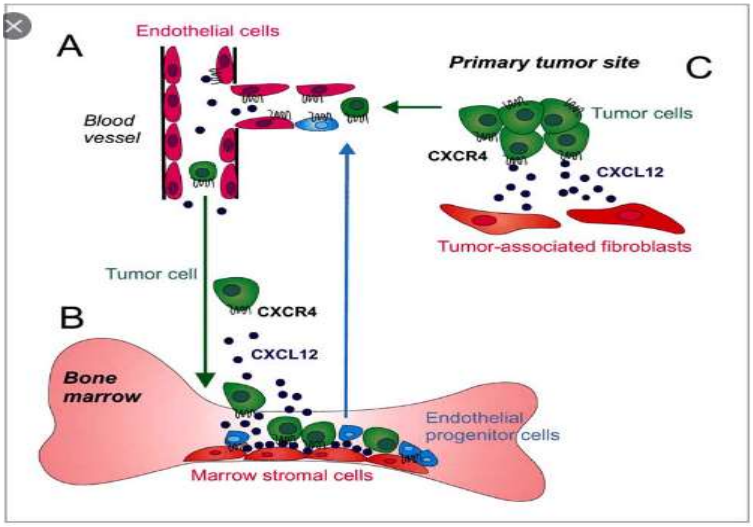

Figure 13. Diagram showing CXCR4/ CXCL12 interaction (Liekens, Schols & Hatse, 2010).

Increased anti- tumour activity was observed as well as inhibition of the cancer metastasis (Jiang et al., 2019).

As has been mentioned, inhibiting tumour cell proliferation inhibits metastasis as well. This was evident in studies involving gastric and tumour cancer, where CA-4 administration, which inhibited the PI3K/ Akt pathway also inhibited metastasis in these tumours.

To elaborate on what was mentioned regarding effect of CA-4 on small metastases, The CA-4 prodrug, Ombrabulin, structure shown in figure 14, was administered to a mouse model with the LY80 Yoshida cell line and the shutdown of blood flow to small metastases, which inhibited metastasis, was observed (Pérez-Pérez et al., 2016).

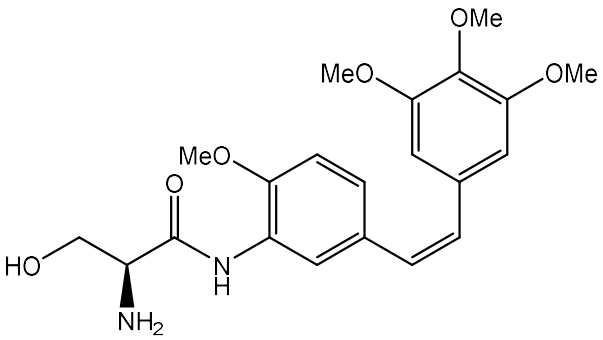

Figure 14. Diagram showing Ombrabulin structure

1.9.7 Antioxidant activity of CA-4

An increase in the human body of what are known as reactive oxygen species (ROS), such as H_2O_2, HO and O_2^- (Ray, Huang & Tsuji, 2012), cause an increase in the occurrence of compounds such as COX-2 enzyme and prostaglandins, which are known to play a role in cancer development (Sirerol et al., 2016). Antioxidant activity is the ability to react with and neutralize reactive oxygen species. Synthesized stilbenes as a group tend to have similar activities. This means that the similarity in structures of all synthesized stilbenes means that they show many similar biological properties. The fact that the stilbene resveratrol has known antioxidant activity is what therefore prompted interest in investigating the antioxidant activity of CA-4. The structure of resveratrol is shown in figure 15. The neutralisation of reactive oxygen species is termed as scavenging (Karatoprak et al., 2020) . Compounds can scavenge ROS via either hydrogen atom donation or electron transfer (Yin et al., 2009). CA-4 was found to have a high scavenging ability against DPPH (2, 2-diphenyl-1-picryhydrazyl) radicals whereas many other CA-4 analogues do not (Karatoprak et al., 2020) This is because the hydroxyl group, present on CA-4 facilitates scavenging due to the fact it is a good source of hydride, which acts as a reducing agent during removal of radicals (Kwak, Joo, Gansukh, Mistry & Keum, 2019). The DPPH assay is commonly used in evaluating the scavenging ability of chemical compounds (Pyrzynska & Pękal, 2013).

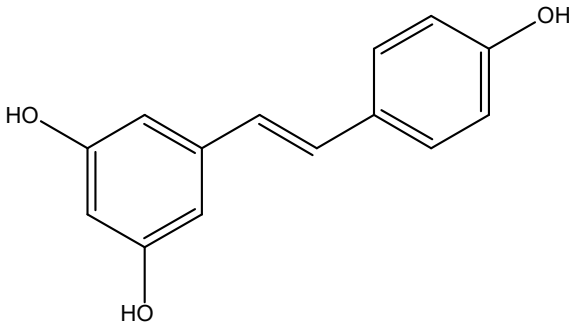

Figure 15. Diagram showing structure of resveratrol (Khan, Iqbal & Shahzad, 2017).

Several combretastatin derivatives incorporating a pyrimidine bridge, to maintain the combretastatin *cis* conformation, were synthesized and then tested for activity against human lung cancer and breast cancer cell lines. Many of the derivatives showed significant activity,

with micromolar IC_{50} values. The structures of the two derivatives with the highest activities are shown in figure 16. When these analogues were analysed biologically it was shown that the anti- cancer activity of these compounds could be due to their ability to inhibit the action of antioxidant enzymes, which results in increased ROS levels, which triggers apoptosis in cancer cells. This was supported by the fact that when a DPPH assay was carried out, the derivatives showed no direct antioxidant properties of their own.

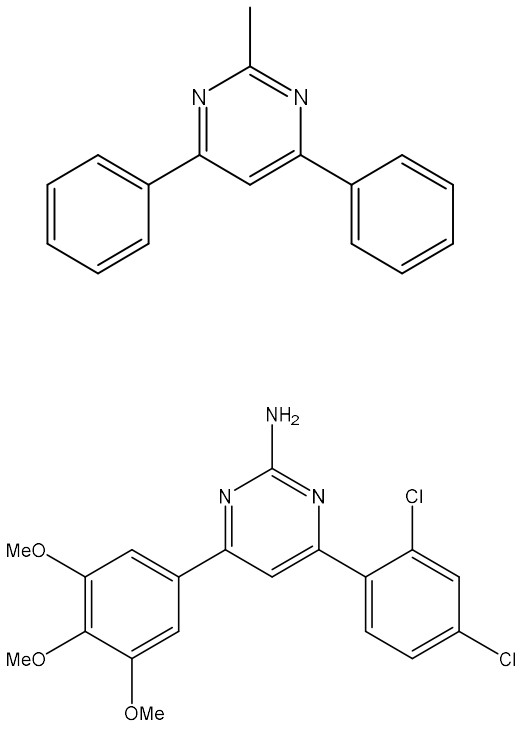

Figure 16. Diagram showing structures of combretastatin derivatives with pyrimidine bridge (Kumar et al., 2018).

A study was carried out to verify this hypothesis. The major three enzymes within all animal cells responsible for antioxidant activity are superoxide dismutase (SOD), glutathione reductase (GR) and catalase. The effect of the two derivatives on these enzymes *in vitro* was investigated. It was found that they caused a decrease in levels of glutathione reductase and catalase and no change in levels of SOD, which supports the theory (Kumar et al., 2018).

All this leads to the conclusion that having antioxidant activity is one of several mechanisms of action of combretastatins against cancer cells (Karatoprak et al., 2020).

1.9.8 CA-4 and multidrug resistance

Many of the anticancer drugs in current clinical use, such as paclitaxel, vinblastine and vincristine, all drugs which bind to tubulin at the taxane or vinca sites on tubulin, have the issue of multidrug resistance (MDR), despite being highly potent. MDR describes the resistance of cancer cells to a wide range of anticancer drugs, even though these drugs have different structures and mechanisms of action (Li et al., 2017) The use of any of these drugs in treatment of tumours results in tumour cells with an over expression of the genes responsible for multidrug resistance. One of the results of this over expression is the increased expression of P-glycoprotein efflux pumps within tumour cells. These pump large amounts of the administered drug out of tumour cells before they can carry out their action. There exist other such drug efflux pumps within cells such as the MRP1, MRP2 (McLoughlin & O'Boyle, 2020) and breast cancer resistance protein (BCRP) drug efflux pumps. CA-4 and derivatives, which bind to the colchicine binding site, do not encounter these problems (Li et al., 2018).

Another issue which contributes to the occurrence of multidrug resistance is the occurrence of tubulin isotypes in cancer cells. Tubulin isotypes show differences in the carboxy- terminal region of tubulin units. Each α tubulin unit and β tubulin unit comprises of several different tubulin isotypes. Different tissues show different expressions of these isotypes. Treatment of tubulin with CA-4 can result in changes in isotype expression as a resistance mechanism and therefore changes binding ability of the drug to the tubulin, affecting anticancer activity. This altered expression of tubulin isotypes therefore causes multidrug resistance. For example, it was found that in a human lung cancer line resistant to CA-4, there was increased βI tubulin isotype expression and a decrease in βIII tubulin isotype expression. Such a situation occurs in many MDR resistant cell lines (Kumbhar, Bhandare, Panda & Kunwar, 2019).

1.9.9 CA-4 analogues that don't target microtubules

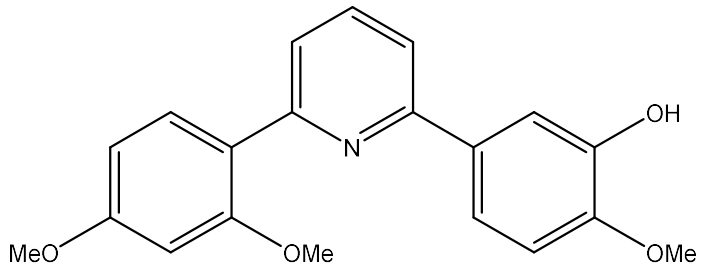

Figure 17. Diagram showing non- microtubule targeting compound (Tarade, Pandey & McNulty, 2017).

It has been found that there are several CA-4 analogues which have a mechanism of action against tumour cells which does not involve, as so many others do, the targeting of tubulin or microtubules. Such compounds show anti- cancer activity even though they do not cause inhibition of the polymerization of tubulin. This means that structure- activity relationship studies into this group of CA-4 analogues must be carried out. Some of these compounds are discussed. These compounds had high activity against tumour cells, despite not been very effective at inhibiting tubulin polymerisation. The compound shown in figure 17 showed some tubulin polymerization inhibition at 10μM. However, it showed high cytotoxicity against human lung cancer (A549), MDA- MB 231 and Hela ovarian cancer cell lines, with IC_{50} values of 44 nM, 4.6 nM, and 1.4 nM respectively.

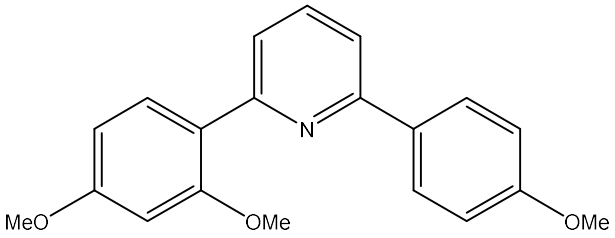

Figure 18. Diagram showing non- microtubule targeting compound (Tarade, Pandey & McNulty, 2017).

The compound shown in figure 18 did not show any inhibition of tubulin polymerisation at 10 μM but displayed high cytotoxicity towards the human lung cancer (A549), MDA- MB 231 and Hela ovarian cancer cell lines, with IC_{50} values of 89 nM, 3.1 nM, and 3.8 nM respectively. Neither of the pyridine analogues just mentioned possess the two-carbon long link essential for binding to tubulin, added proof that they have an alternative target.

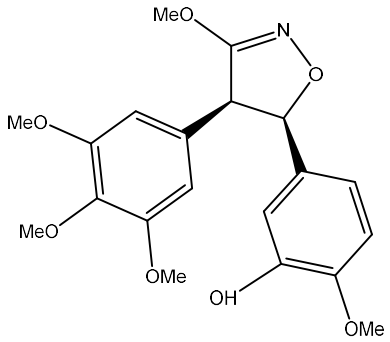

Figure 19. Diagram showing structure of non- microtubule targeting isooxazoline analogue (Tarade, Pandey & McNulty, 2017).

The CA-4 analogue shown in figure 19, with an isoxazoline ring replacing the cis double bond showed an IC_{50} in tubulin polymerisation inhibition of 9.9 μM and an IC_{50} of 0.1 μM when tested against the human leukaemia cell line, HL60.

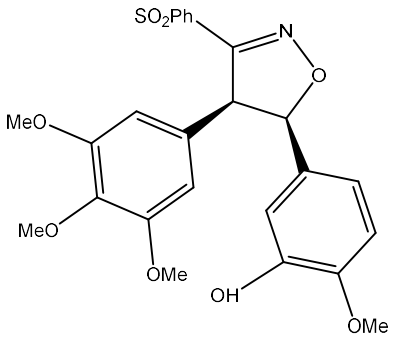

Figure 20. Diagram showing structure of second non- microtubule targeting isoxazoline analogue (Tarade, Pandey & McNulty, 2017).

The compound shown in figure 20 showed poor inhibition of tubulin polymerisation even at concentrations of 40 μM but displayed an IC_{50} of 0.9 μM against the HL60 cell line.

These findings support the assumption that both isoxazoline analogues depicted in figures 19 and 20, have a target in the cell that is not tubulin. More evidence to support that is the fact that both compounds arrest the cancer cell cycle in the G2 phase and not the G2/ M transition as tubulin targeting compounds do and secondly that the death of the cancer cells treated with these compounds involves an extrinsic apoptotic as opposed to an intrinsic apoptotic pathway, which is followed by tubulin targeting agents.

It is now therefore thought that CA-4 itself might also have targets within cells other than tubulin. It could have multiple targets. Some of these could be other proteins within the cell. It is possible that the existence of these targets is hidden by the obvious and major targeting of tubulin by agents. As an example of this, it has been found that the anticancer drug Paclitaxel, as well as interacting with tubulin, also binds to Bcl-2, which is an anti-apoptotic protein. Also, to be taken away from these findings is the fact that just because a CA-4 derivative does not show significant inhibition of tubulin polymerisation does not mean it cannot display high cytotoxicity against cancer cells (Tarade, Pandey & McNulty, 2017).

1.9.10 CA-4 and autophagy

Autophagy is the process by which lysosomes within cells break down old or defective cell components. It is how cells maintain their integrity. It is triggered by cells being exposed to stresses. The administration of pharmaceutical agents or the hypoxia they cause in some cases can trigger autophagy as a defence mechanism. Cancer brings about aberrations in the autophagic process.

When it comes to cancer in cells, autophagy acts in two different, conflicting ways. It both suppresses tumours by preventing formation of defective cells by breaking down of cell organelles like defective proteins and it promotes tumour growth by acting as a survival mechanism in tumour cells after drug administration by acting as an energy source for cancer cell metabolism. The role that autophagy plays during drug treatment of a tumour seems to depend on the specific drug, the type of tumour and the stage the tumour is at. There is still a lot of ongoing debate on the issue. Recent findings seem to suggest however that autophagy serves as a resistance mechanism in tumour cells after drug administration.

It was shown in a study by Li et al (2014) that CA-4 caused autophagy to occur in a wide range of cancer cell lines.

Bafilomycin A1 (BafA1) and 3- methyl adenine (3-MA) both inhibit the process of autophagy in cells. It was shown that when used together with CA-4 in treatment of SMMC- 7721 and SGC- 7901 cell lines the amount of apoptosis brought on by CA-4 was increased. This supports the theory that autophagy is a survival mechanism, employed by tumour cells. A similar increase in tumour cell death occurred when CA-4 administration was coupled with inhibition of the autophagy genes, Beclin- 1 and Atg. Autophagy inhibitors are therefore a possible strategy for improving the effectiveness of CA-4 (Li et al., 2014).

1.9.11 CA-4 and macular degeneration

Wet age- related macular degeneration (AMD) is the leading cause of loss of vision or blindness in the world, with currently up to 30 million sufferers. It is predicted that in the next 25 years, the number of cases will triple due to an ageing population.

During wet AMD, neovascularisation occurs behind the retina, this is termed as choroidal neovascularisation. Liquid leaking from the newly formed vessels causes damage to photoreceptors within the macula resulting in vision distortion.

Cancer and macular degeneration have some similarities. The growth of tumours, followed by metastasis and wet age- related macular degeneration (AMD) both involve the abnormal growth of blood vessels, hence the possible usefulness of CA-4P in treating wet AMD. Tests have been carried out regarding this possible use of the drug. CA-4P was proven effective at prevention of choroidal neovascularisation and it also caused choroidal neovascularisation already present to regress in a mouse model. Phase I and II clinical trials have been carried out in treating wet AMD sufferers with CA-4P, but findings seem to suggest that the safety and effectiveness of CA-4P in this setting rule it out as a replacement for existing drugs used in treating the disease (Ibrahim et al., 2013).

1.9.12 Side effects of CA-4

All vascular disrupting agents have an effect on the cardiovascular system (Kretzschmann & Fürst, 2013), such as issues with heart rate and blood pressure, which are closely monitored. These side effects can be treated.

In a study carried out by Oncotelic into CA-4P toxicity in animals, it was found that CA-4P had side effects on organs in the gastrointestinal tract. Effects that regulated dosage of drug administered were formation of ulcers and haemorrhaging (Kretzschmann & Fürst, 2013).

CA-4 treatment has side effects that are minimal and passing, such as vomiting, nausea and hypertension

It is hoped that CA-4 derivatives can be synthesized which don't have these issues (Mabeta & McGaw, 2018).

1.10 Combretastatin A-1

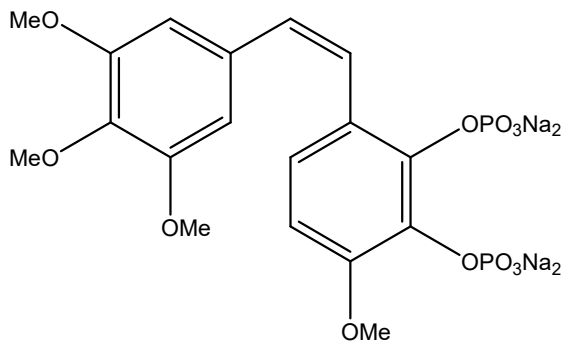

Figure 21. Diagram showing structure of CA-1P (Akselsen et al., 2012).

Combretastatin A-1 (CA-1), like combretastatin A-4 is a natural compound found in the African bush willow tree, *Combretum caffrum* (Pettit et al., 1995). Its structure is shown in figure 2. Both CA-1 and its prodrug CA-1P, structure shown in figure 21, exhibit cytotoxicity towards a wide range of cancers found in humans.

Like CA-4, CA-1 is a vascular disrupting agent and is in fact even a better one (Akselsen et al., 2012). CA-1 also binds to tubulin at the colchicine site, and it also inhibits polymerisation of tubulin (Mao et al., 2016). After being administered, CA-1P undergoes dephosphorylation to

the active form, CA-1. While it has the same mechanisms of action against tumour cells that CA-4 has, that is, as a vascular disrupting agent, CA-1 has an additional mechanism. CA-1 is oxidized by enzymes found to be present in increased amounts in certain types of tumours. It is oxidized to an ortho- quinone form. In a direct action, these quinones break down DNA and proteins within tumour cells. This is because quinones have high instability, they are strong oxidants as well as being strong electrophiles. (Cheynier, Schneider, Salmon & Fulcrand, 2010) They react with proteins such as GSH, which are nucleophiles via a 1,4- Michael addition and with the bases in DNA via a 1,2- and/ or 1,4- Michael addition. (Obach & Kalgutkar, 2010) The quinones also cause an increase in the production of reactive oxygen species tumour cells, resulting in the condition of oxidative stress and bringing about tumour cell death via this mechanism (Devi & Mehendale, 2014).

Hepatocellular carcinoma (HCC) is one of the major contributors to cancer deaths. New and effective treatments are required for it. It has been discovered that CA-1P has extremely high activity against this cancer *in vitro* and *in vivo.* This is for several reasons. CA-1P is a tubulin polymerization inhibitor, it causes AKT to be inactivated. This affects many signalling pathways in the cancer cell. GSK-3β, which is a proapoptotic protein is activated, the Wnt/ β-catenin pathway, which is a pathway promoting tumour cell survival is inhibited and Mcl-1 which is an anti-apoptotic protein is degraded. As well as showing high activity against the HCC tumour cells themselves, CA-1P also causes apoptosis in tumour-associated macrophages, which inhibit the activity of the immune system against the tumour cells. This means that CA-1P could have potential clinical applications for HCC treatment (Mao et al., 2016).

1.11 Modifications to CA-4

The aims of synthesizing CA-4 analogues include to increase potency compared to CA-4 and to make improvements to its properties (Bukhari, Kumar, Revankar & Qin, 2017), such as addressing issues with aqueous solubility and the occurrence of *cis* to *trans* isomerism (McLoughlin & O'Boyle, 2020).

Side effects to the cardiovascular and nervous systems, which limit the dosage of drug that can be administered, are also an issue (Duan et al., 2016).

Another aim is to synthesize CA-4 derivatives which are more selective in their targeting of tumour vasculature over normal vasculature (Bukhari, Kumar, Revankar & Qin, 2017).

1.11.1 Modifications to the A- ring

Several naturally derived compounds which affect tubulin polymerisation possess a trimethoxy A- ring unit. In synthesizing CA-4 derivatives, many modifications to the *cis* double bond linking the rings and to the B- ring have been carried out, but there have been very few modifications carried out to the A- ring.

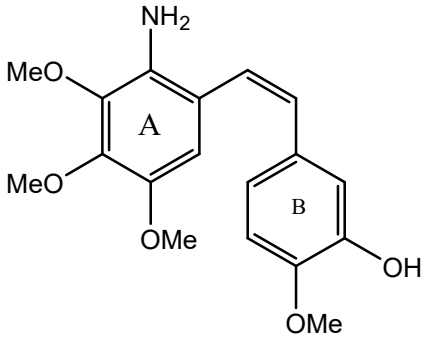

Figure 22. Diagram showing structure of amino CA-4 derivative (Bukhari, Kumar, Revankar & Qin, 2017).

The compound shown in fig. 22, with an amino group substituent in the 2- position but keeping the trimethoxy structure was synthesized and tested for cytotoxicity against a range of cancer cell lines and it was found to have activity comparable to CA-4.

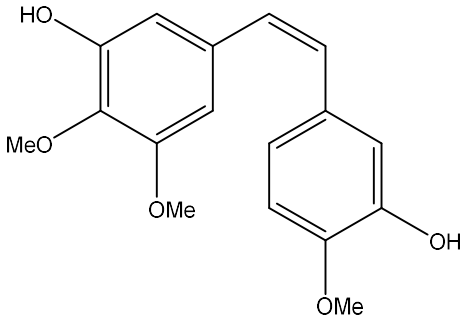

Figure 23. Diagram showing structure of hydroxyl substituted A-ring CA-4 derivative (Bukhari, Kumar, Revankar & Qin, 2017).

Replacing a meta positioned methoxy group with a hydroxyl group, as shown in figure 23, deleting methoxy groups or substituting the methoxy groups with larger groups resulted in compounds with less cytotoxicity (Bukhari, Kumar, Revankar & Qin, 2017).

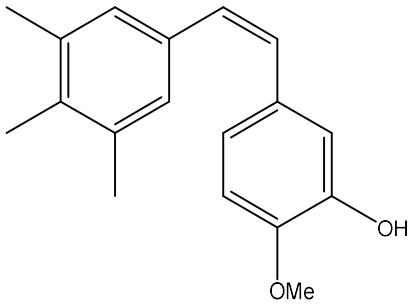

Figure 24. Diagram showing structure of trimethyl substituted A- ring (Gaukroger, Hadfield, Lawrence, Nolan & McGown, 2003).

The compound depicted in figure 24, with methyl groups substituting the methoxy groups on the A- ring of CA-4, was synthesized by Gaukroger et al (2003). On testing, the compound showed diminished cytotoxicity to cancer cells but an increase in ability to bind to tubulin. This case demonstrated that compounds with A- ring substituents other than methoxy groups interact with tubulin.

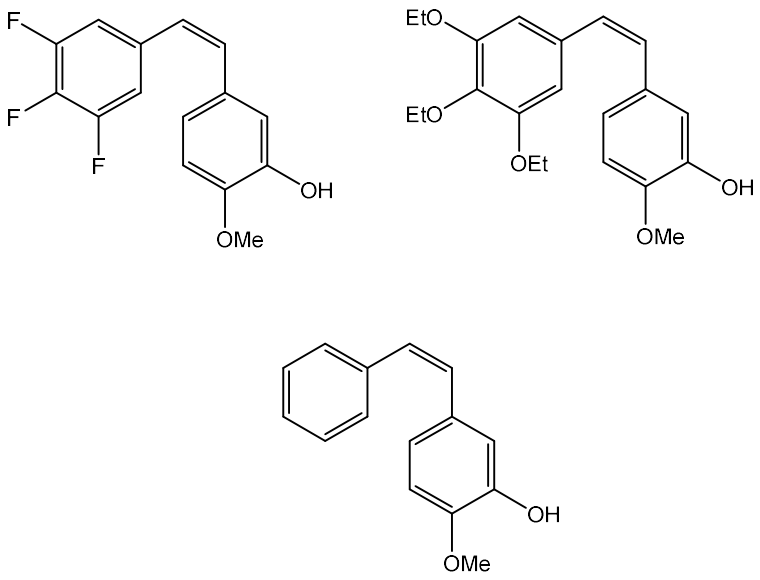

Figure 25. A- ring modified compounds (Gaukroger, Hadfield, Lawrence, Nolan & McGown, 2003).

Gaukroger et al (2003) also synthesized the compounds shown in figure 25. These compounds were tested for ability to bind to tubulin, compared to CA-4. CA-4 possessed an IC_{50} in tubulin polymerisation inhibition of 0.175 μM, the triethoxy compound 0.5 μM, the trifluoro compound 4.5 μM and the compound with an unsubstituted A- ring 2.5 μM (Gaukroger, Hadfield, Lawrence, Nolan & McGown, 2003).

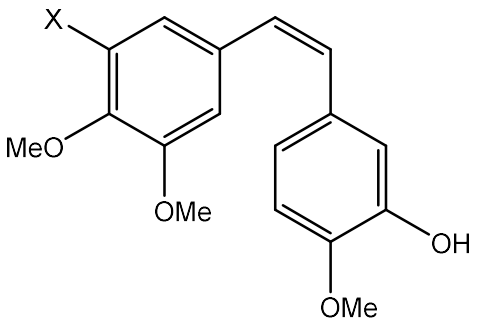

X = F, Cl, Br

Figure 26. Compound with halo- substituted A- ring (Bukhari, Kumar, Revankar & Qin, 2017).

The compounds shown in figure 26 were synthesized by Pettit et al., (2005), in which halogen atoms replace one of the methoxy groups in the *meta* position. The reason for choosing this substitution is that studies have shown that only one of the the methoxy groups on the A-ring is essential for binding of the compound to tubulin (McLoughlin & O'Boyle, 2020), both methoxy groups in the *meta* position are replaceable (Zong, Shea, Maffucci & Ojima, 2017). The chloro and bromo derivatives showed less cytotoxic and tubulin polymerization inhibition activity than CA-4, while the fluoro compound showed activity similar to CA-4.

In the compounds shown in figure 27, the three methoxy groups on the A- ring were substituted with five and six membered rings. The substitution of the trimethoxy group with a homocyclic ring resulted in compounds with diminished cytotoxicity. Compound A exhibited less cytotoxicity compared to CA-4. The substitution of the trimethoxy group with a heterocyclic ring however resulted in compounds with cytotoxicity towards certain cell lines. Compound B, which is either a benzo[β] thiophene (X= O) or a benzofuran (X= S), which were synthesized by Simoni et al, both showed cytotoxicity to H-460 and BMEC cancer cell lines and both inhibit tubulin polymerisation better than CA-4 (Bukhari, Kumar, Revankar & Qin, 2017).

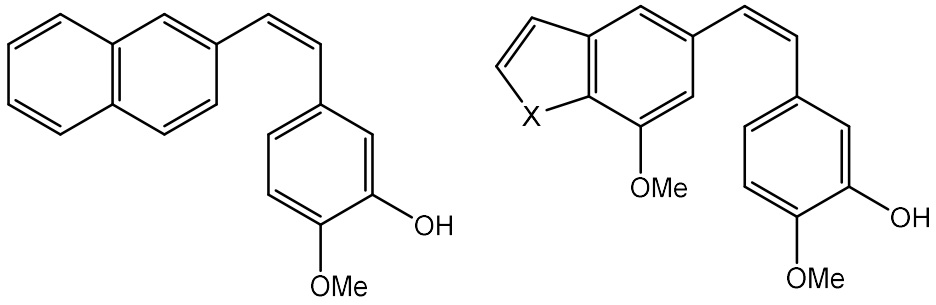

A B

Figure 27. Compounds with 5/6 membered rings replacing trimethoxy motif (Bukhari, Kumar, Revankar & Qin, 2017).

It was discovered that in most cases, making substitutions at the A- ring of CA- 4 structure resulted in compounds with less cytotoxicity compared to CA-4. There are exceptions however, such as substitutions to the trimethoxy A- ring involving halogen atoms or groups. Cytotoxicity is more favourable when the halogen atoms or groups are smaller in size (Greene, Meegan & Zisterer, 2015).

1.11.2 Modifications to the B- ring

There are two main groups into which modifications to the CA-4 B- ring can be divided, either substitutions can be made to the ring, or the ring can be replaced entirely with a heterocyclic or homocyclic structure. Much of the research that has been done to this point has been regarding substituting the hydroxyl group with other groups. The two pro drugs of CA-4, CA-4P and AVE8062, both have the hydroxyl group of CA-4 replaced with other groups.

The compound shown in figure 28 was synthesized by Oshumi et al (1999). It showed more solubility in water than CA-4 due to the fact that the NH_2 group will spend some time protonated, resulting in a more polar group, similar inhibition of tubulin polymerisation and was three times more cytotoxic against tumours in a mouse model (Bukhari, Kumar, Revankar & Qin, 2017).

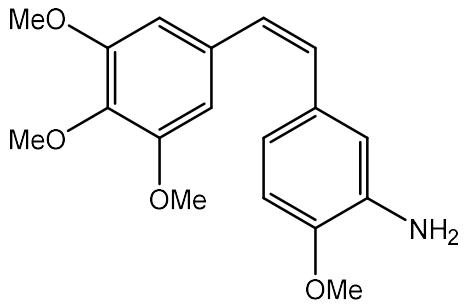

Figure 28. Compound with amino/ OH substitution (Bukhari, Kumar, Revankar & Qin, 2017).

The compound shown in figure 29 inhibited tubulin polymerization at a similar level to CA-4. The compound had increased cytotoxicity compared to CA-4 against certain cell lines, such as the MCF- 7 breast cancer and HT- 29 colon cancer cell lines. It had diminished cytotoxicity compared to CA-4 against other cell lines, such as the SKMEL- 5, A-549 and MLM cancer cell lines. With this compound, changing the position of the B- ring methoxy group from the 4' to either the 2' or 3' or substitution of the methoxy group with other groups resulted in a huge loss of activity (Cushman et al., 1991).

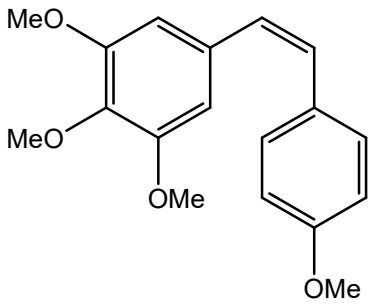

Figure 29. CA-4 with OH replaced by proton (Cushman et al., 1991).

The compound in figure 30 is simply CA-4 without the B- ring methoxy group. It does not show any inhibition of tubulin polymerization and has much less cytotoxicity than CA-4 (Gaukroger, Hadfield, Lawrence, Nolan & McGown, 2003).

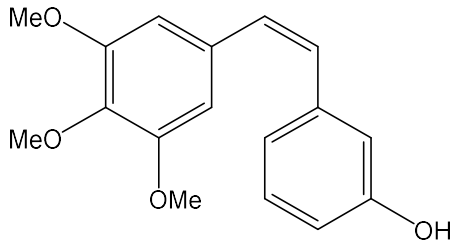

Figure 30. CA-4 compound without B- ring methoxy (Gaukroger, Hadfield, Lawrence, Nolan & McGown, 2003).

The activity of the compounds shown in figures 29 and 30, and the results of the change in position of the methoxy group in fig.29 corroborate the findings summarised in the discussion of the structure activity relationship of CA-4, that the methoxy group and its position on the B-ring are important for activity (Cushman et al., 1991).

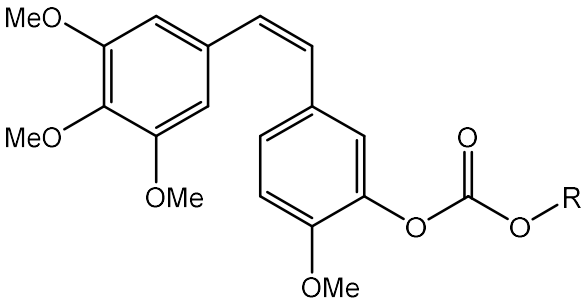

Figure 31. CA- 4 derivative with ether/ OH substitution (Bukhari, Kumar, Revankar & Qin, 2017).

The compounds shown in figure 31, where R is either a methyl, ethyl, n- propyl or n- butyl group were synthesized by Simoni et al (2008) and tested for anti- cancer activity against K562, MDA-MB- 231, A549 and MCF- 7 human cancer cell lines, amongst others. Several of the compounds had exceptional activity against these cell lines, with IC_{50} values in the nanomolar range. The compounds in figure 31 stopped the cell cycle at the G2/M transition and inhibited tubulin polymerization in a manner similar to CA-4 (Bukhari, Kumar, Revankar & Qin, 2017).

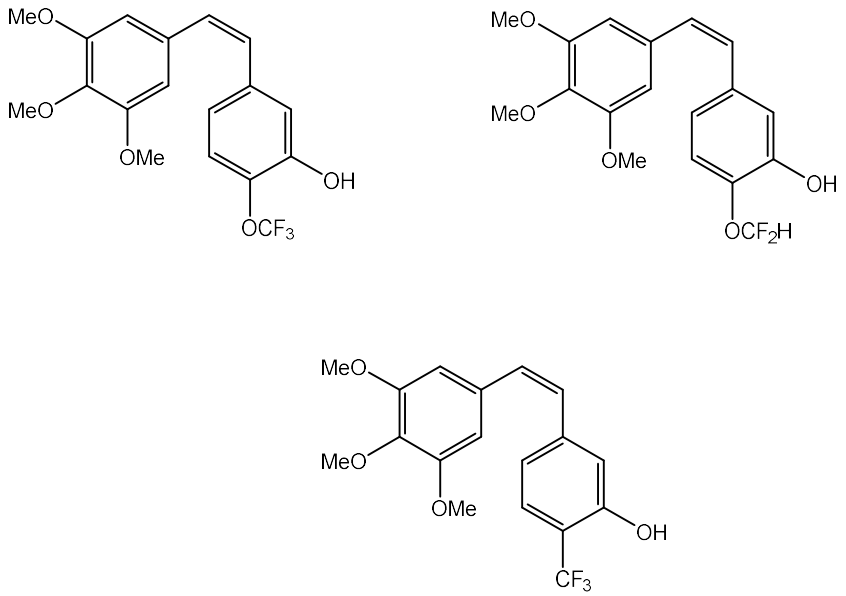

Figure 32. Compounds with methoxy/halogen group substitutions (Zong, Shea, Maffucci & Ojima, 2017).

The compounds shown in figure 32 were designed by Zong et al (2017). These and other similar compounds were then analysed computationally using the process of docking analysis to investigate their interaction with tubulin. It was found that many of these compounds interacted with tubulin better than CA-4 does. These compounds were therefore synthesized in the lab and tested against various cancer cell lines. They were shown to exhibit high potency, including against multi- drug resistant cell lines (Zong, Shea, Maffucci & Ojima, 2017).

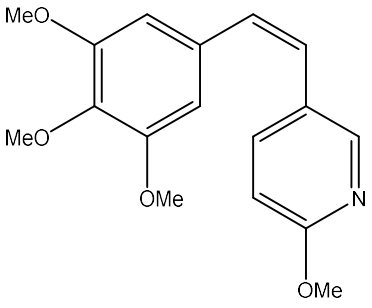

Figure 33. CA-4 B- ring replaced by pyridine (Bukhari, Kumar, Revankar & Qin, 2017).

The modifications to the B- ring discussed so far all involve substitutions to the ring; however, CA-4 analogues have also been synthesized where the B- ring is replaced entirely. When the B- ring was replaced by heterocyclic rings such as pyrimidine, pyridazine or pyridine (as in figure 33), the result was compounds highly active against the Colon 26 cancer cell line. The 2- methoxy pyridine compound shown in figure 33 had increased solubility in water compared to CA-4 and demonstrated nM range cytotoxicity.

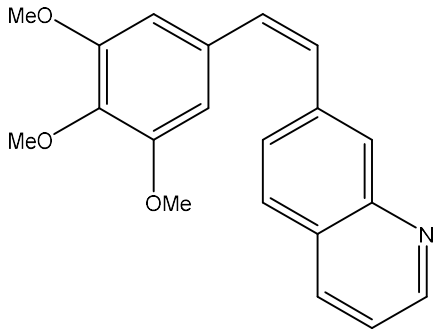

Figure 34. CA-4 derivative with quinoline B- ring (Bukhari, Kumar, Revankar & Qin, 2017).

The compound shown in figure 34, with a quinolone structure B- ring showed a huge loss in cytotoxicity compared to CA-4 but it was a potent tubulin polymerisation inhibitor.

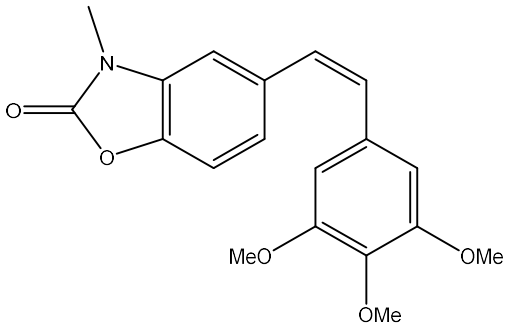

Figure 35. CA-4 derivative with benzoxazolone B- ring (Bukhari, Kumar, Revankar & Qin, 2017).

Derivatives were synthesized where the CA- 4 B- ring was replaced by a benzoxazolone structure. The compound shown in figure 35 proved to have the highest cytotoxicity with IC_{50} of 0.25 μM, 0.19 μM, 0.28 μM and 0.73 μM against HT- 29, HepG2, EA.hy926 and K562 cancer cell lines respectively. The HT- 29 cell line is resistant to most combretastatins. The compound in figure 35 is so active against resistant cultures because it is a bioisostere of CA-4. Bioisosteres exhibit similar biological properties as the parent compound but can have an increase in certain properties, for instance cytotoxic activity (Dick & Cocklin, 2020), in this case resulting in cytotoxic activity against resistant strains (Bukhari, Kumar, Revankar & Qin, 2017).

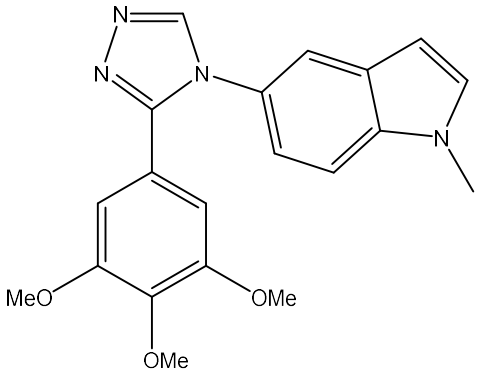

Figure 36. CA- 4 derivative with indole B- ring (Pérez-Pérez et al., 2016).

The compound shown in figure 36, with an indole as the B- ring and a triazole ring as the bridge, to restrain the structure of the compound in the *cis* conformation, was synthesized and tested. It showed cytotoxicity towards multi- drug resistant colon cancers as well as prostate cancer (Pérez-Pérez et al., 2016).

There has been a considerable amount of study into modifications to the B- ring structure of CA-4. It has been shown that in most cases, these modifications result in a loss of activity compared to CA-4. There are however some exceptions, such as replacing the hydroxyl group with an amino group or deletion of the hydroxyl group (Karatoprak et al., 2020). Studies so far have also shown that B- ring modifications are more successful than A- ring modifications regarding making improvements to the potency of CA-4 (Greene, Meegan & Zisterer, 2015).

1.11.3 Changes to the double bond

All the combretastatins have both a *cis* and a *trans* form. The activity of the *cis* isomer can be ten thousand times greater than that of the *trans* form (Gaukroger, Hadfield, Hepworth & Lawrence, 2001). With the combretastatin compounds, the *cis* to *trans* isomeric change easily occurs when the *cis* isomer is exposed to conditions of light, heat or acidic media (Bukhari, Kumar, Revankar & Qin, 2017). The solution to the problem of this unwanted isomerism is to either modify the double bond joining the rings or replace the linking double bond entirely with a ring system. Both solutions retain the compound in the important *cis* conformation. These alterations to the double bond can change potency, stability and solubility in water, although changes to potency do not usually occur unless changes to the double bond are accompanied with changes to the B- ring.

1.11.3.1 Modifications to the double bond

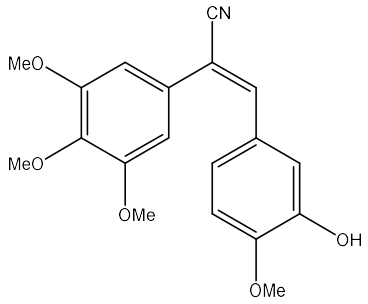

Figure 37. CA- 4 derivative with cyano group modification (Bukhari, Kumar, Revankar & Qin, 2017).

The compound shown in figure 37, with a cyano group attached to the double bond at the position closer to the trimethoxy ring displayed cytotoxicity similar to CA-4; however, an ethyl or methyl group at the same position resulted in a huge loss of activity, although inhibition of tubulin polymerisation was still significant (Bukhari, Kumar, Revankar & Qin, 2017).

The compound shown in figure 38, with an acryl amide group substituent on the double bond was synthesized with the aim of both stabilizing the compound in the *cis* conformation and also to improve on the solubility of the parent compound CA- 4 in water. The presence of the acryl

amide group in the position shown resulted in a loss of both cytotoxicity and of tubulin polymerisation inhibition.

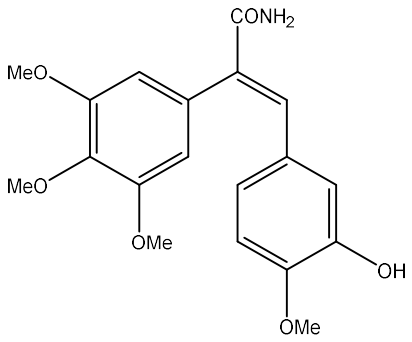

Figure 38. CA-4 derivative with acryl amide modified linkage (Bukhari, Kumar, Revankar & Qin, 2017).

The compound shown in figure 39, a difluorostilbene is said to inhibit tubulin polymerisation on a level similar to or better than CA- 4 (Bukhari, Kumar, Revankar & Qin, 2017).

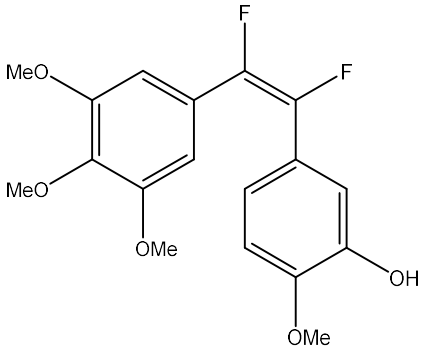

Figure 39. CA- 4 derivative with fluorine substituents on double bond (Bukhari, Kumar, Revankar & Qin, 2017).

Piperlongumine CA- 4 derivatives were synthesized by Srivenugopal et al (2016). The structure shown in figure 40 was the lead compound and it showed high activity against the SKBR- 3 breast cancer cell line. It was found to increase levels of reactive oxygen species in tumour

cells and was also found to activate the p53 tumour suppressor gene (Bukhari, Kumar, Revankar & Qin, 2017).

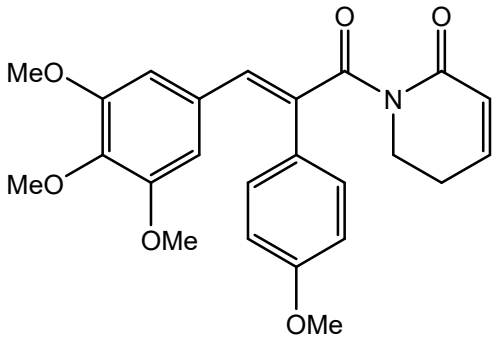

Figure 40. Piperlongumine CA- 4 derivative (Bukhari, Kumar, Revankar & Qin, 2017).

1.11.3.2 Replacing the *cis* double bond with ring systems

Many studies have taken place where the *cis* bond linking the rings in combretastatins has been replaced by a wide variety of heterocyclic rings such as furanones, β- lactam, triazoles and imidazoles. The presence of the ring locks the compound in the *cis* conformation and no isomerisation to the *trans* isomer can occur (Bukhari, Kumar, Revankar & Qin, 2017). The ring added is often chosen so as to improve the solubility of the compound in water (Li et al., 2018), a heterocyclic ring possessing electron lone pairs imparts improved solubility (McLoughlin & O'Boyle, 2020), but the choice of ring can also increase the potency of a compound (Pérez-Pérez et al., 2016). A five membered heterocyclic ring is the most often used (Li et al., 2018).

1.11.3.2.1 5- Membered heterocyclic rings

Nam et al., (2002) synthesized many CA- 4 derivatives where the *cis* bond was replaced with cyclopentenones and furanones and other 5- membered heterocyclic rings. Of the compounds synthesized the compound shown in figure 41, with the furanone ring, displayed the highest cytotoxicity, having an average IC_{50} of 4.4 nM against MCF- 7, SK- MEL- 2 and A549 cancer cell lines (Bukhari, Kumar, Revankar & Qin, 2017).

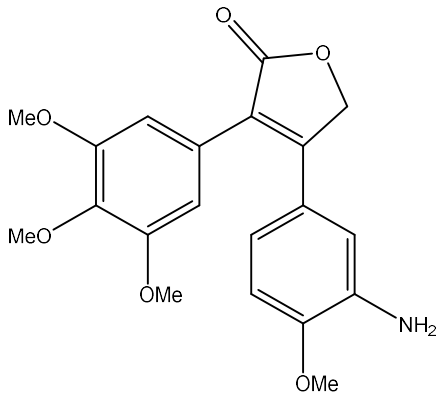

Figure 41. CA- 4 derivative with furanone ring (Bukhari, Kumar, Revankar & Qin, 2017).

Derivatives were synthesized by Romagoli et al., (2016), where the *cis* bond in CA- 4 was replaced with an imidazole ring, as well as having some additional changes to the B- ring. Of the derivatives synthesized, the compound shown in figure 42 had the highest cytotoxicity, with IC_{50} values in the range of 0.4 – 3.8 nM against seven cancer cell lines. It also inhibited tubulin polymerization, with an IC_{50} of 0.87 µM (Seddigi et al., 2017).

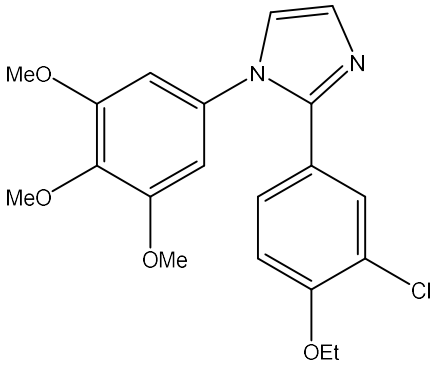

Figure 42. CA- 4 derivative with an imidazole ring (Seddigi et al., 2017).

Recently, there has been much interest in CA- 4 derivatives where the *cis* bond is replaced with a triazole ring. Madadi et al., (2015) synthesized many of these compounds, with the compound shown in figure 43 showing the highest cytotoxicity, with GI_{50} values of below 10 nM against most of the 60 cancer cell lines tested against (Seddigi et al., 2017).

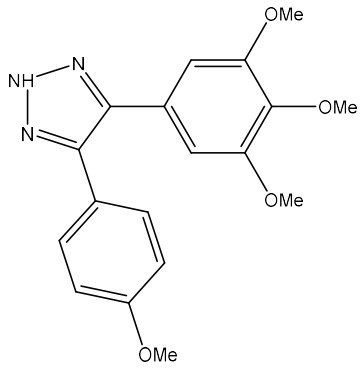

Figure 43. CA- 4 derivative with triazole ring (Seddigi et al., 2017).

1.11.3.2.2 6- Membered heterocyclic rings

A six- membered pyridine ring has also been used to restrict combretastatin derivatives in the *cis* conformation

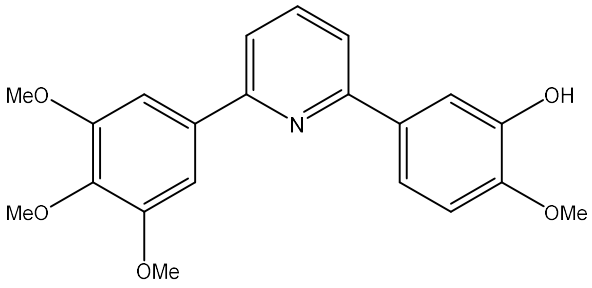

Figure 44. CA- 4 derivative with pyridine linker (Bukhari, Kumar, Revankar & Qin, 2017).

Most of such compounds displayed significant cytotoxic action against cancer cells and inhibited tubulin polymerization. The compound shown in figure 44 displayed antiproliferative activity, caused cell cycle arrest, inhibited angiogenesis and affected vasculature in tumour cells, in a manner identical to CA- 4. It is worth mentioning that this activity is based on the orientation of the A and B ring to each other. There is significant activity when the link joining the rings is three atoms long, i.e., the rings are meta to each other, however when the distance between the rings is increased to four atoms i.e., the rings are para to each other, there is a dramatic loss of activity (Bukhari, Kumar, Revankar & Qin, 2017).

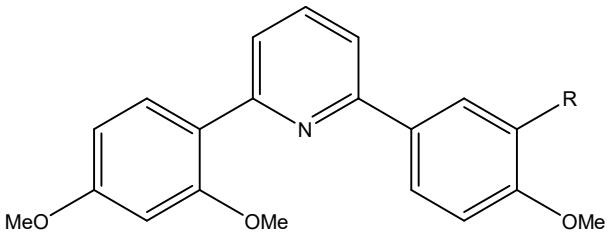

Figure 45. Second CA-4 derivative with pyridine linker (Seddigi et al., 2017).

A similar group of compounds was synthesized by Zheng et al., (2014), all including a pyridine ring. The most potent of these is shown in figure 45, where the R group is a hydrogen atom or a hydroxyl group. These compounds had IC_{50} values of below 0.09 μM against a range of cancer cell lines. The mechanism of action of these compounds was also found to be identical to that of CA- 4 (Seddigi et al., 2017).

1.11.3.2.3 β- Lactam rings

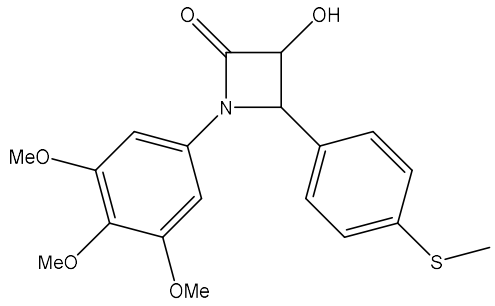

Figure 46. CA- 4 derivative with β- lactam ring linker (Seddigi et al., 2017).

Malebari et al., (2017) synthesized CA- 4 analogues incorporating a β- lactam ring. These compounds were found to be active against the drug resistant HT- 29 colon cancer cell line. The compound shown in figure 46 showed the greatest inhibition of tumour growth, having an IC_{50} of 15 nM. The mechanism of action of this compound was similar to that of CA- 4 (Seddigi et al., 2017).

The compound shown in figure 47 was very active against the drug resistant HT- 29 cell line, with an IC_{50} value of 12 nM, compared to CA- 4's value against this cell line of 4.17 µM (McLoughlin & O'Boyle, 2020).

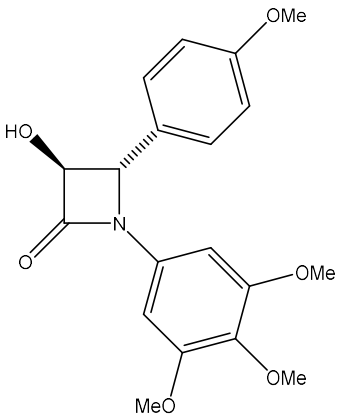

Figure 47. Second CA- 4 derivative with β- lactam ring linker (McLoughlin & O'Boyle, 2020).

It was found that using three- membered rings or six- membered rings to replace the *cis* double bond resulted in analogues with drastically less activity than CA-4. It is thought that these structures inhibit the binding of the compounds to tubulin's colchicine site (McLoughlin & O'Boyle, 2020).

1.11.3.3 Chalcone CA- 4 derivatives

CA-4 chalcone derivatives are compounds where the *cis* double bond of the combretastatin is replaced with a *cis* double bond in conjugation with a carbonyl group. Ducki et al., (2007, 2009) synthesized a range of chalcones incorporating the substitution pattern of the rings of CA- 4. These compounds all had activities greater than CA- 4 in vitro against K562 leukaemia cell line. Compounds A, B and C, shown in figure 48 had IC_{50} values of 4.3, 0.21 and 1.5 nM against the K562 cell line, which showed that the introduction of either an- alkyl group or alkoxy group to the basic chalcone structure increased potency. All three compounds were shown to bind to the colchicine site on tubulin and affect tumour vasculature, similarly to CA-4 (McLoughlin & O'Boyle, 2020).

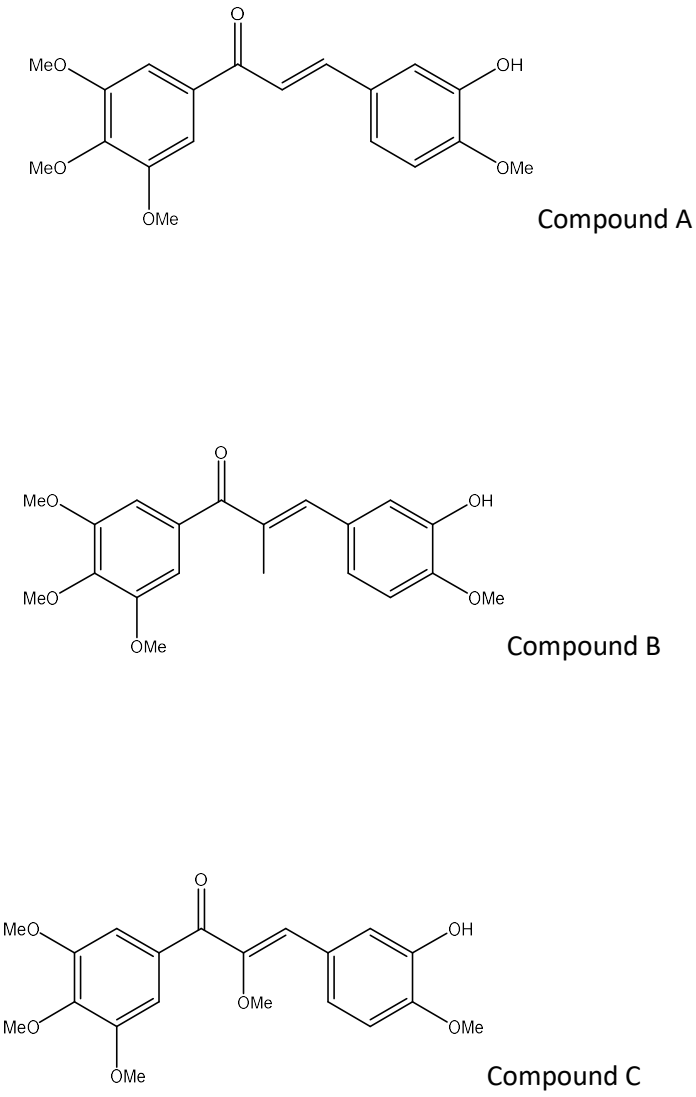

Figure 48. CA- 4 chalcone derivatives (McLoughlin & O'Boyle, 2020).

1.11.3.4 Phenstatins

Instead of the *cis* double bond, CA- 4 derivatives can incorporate a keto group. In CA- 4, this produces a compound known as phenstatin, structure shown in figure 49 (Bukhari, Kumar, Revankar & Qin, 2017).

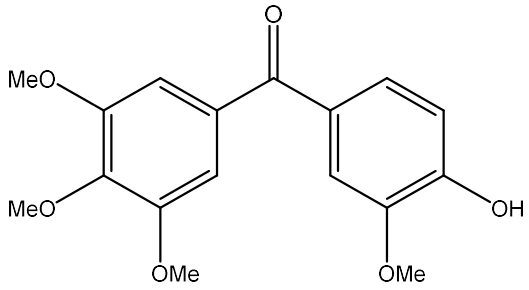

Figure 49. Structure of phenstatin (Bukhari, Kumar, Revankar & Qin, 2017).

This compound retains the activity of CA- 4 *in vivo*, without having the problem issue of the unwanted *cis* to *trans* isomerism (McLoughlin & O'Boyle, 2020).

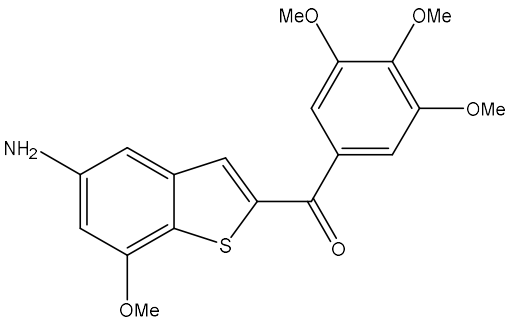

Figure 50. Phenstatin analogue with benzothiophene B- ring (Bukhari, Kumar, Revankar & Qin, 2017).

Many analogues of phenstatins have been synthesized, with modifications to the B- ring, such as replacement with a benzothiophene, such as in figure 50. These analogues exhibit cytotoxicity similar to CA- 4 against many cancer cell lines in humans, with IC_{50} values ranging from 2.6 to 18 nM (Bukhari, Kumar, Revankar & Qin, 2017).

1.11.3.5 Isocombretastatins

In the compound known as isocombretastatin A- 4, the *cis* double bond of CA- 4 is replaced with a 1, 1- ethylene bridge, as shown in figure 51, retaining the compounds *cis* conformation.

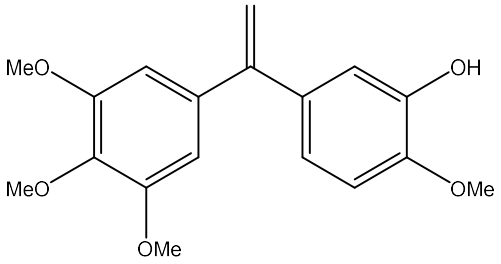

Figure 51. Isocombretastatin A- 4 (Bukhari, Kumar, Revankar & Qin, 2017).

The compound shown in figure 51 inhibited cancer cell proliferation, showed inhibition of tubulin polymerization and brought on G_2/ M phase cell cycle arrest, all in a manner similar to CA- 4 (Bukhari, Kumar, Revankar & Qin, 2017). The compound had activity on a level similar to CA- 4 against many cancer cell lines, with IC_{50} values ranging from two to five nM (McLoughlin & O'Boyle, 2020).

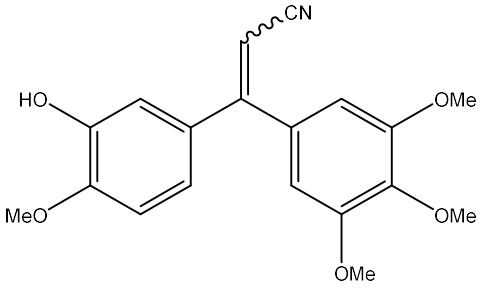

Figure 52. Isocombretastatin A- 4 with acrylonitrile substituent (McLoughlin & O'Boyle, 2020).

The compound shown in figure 52, an acrylonitrile analogue of isocombretastatin CA- 4 displayed an IC_{50} value of 3.0 nM, compared to CA- 4's IC_{50} of 2.3 nM; against the HCT116 colorectal cancer cell line (McLoughlin & O'Boyle, 2020).

1.11.3.6 Sulphur and selenium linkers

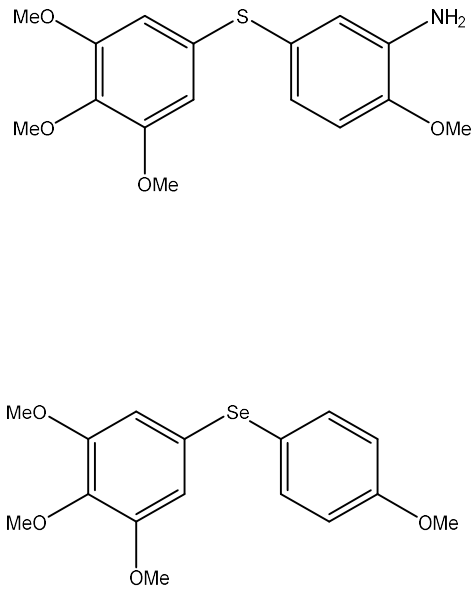

Figure 53. CA- 4 derivative with sulphur and selenium linker (Bukhari, Kumar, Revankar & Qin, 2017).

Lima et al., (2013) carried out syntheses where the CA- 4 derivative *cis* double bond was replaced by either a sulphur atom or a selenium atom, as shown in figure 53. These compounds showed greater activity than CA- 4 against a breast cancer cell line. The selenide showed significant inhibition of cancer cell proliferation in HT- 29, PC- 3 and 786 cancer cell lines, with an average IC_{50} value of 12 nM (Bukhari, Kumar, Revankar & Qin, 2017).

1.12 Prodrugs

Aside from the problem of unwanted isomerism the other major issue with the use CA- 4 and its derivatives in clinical treatment is the lack of solubility of the compounds in water, which means that when the drug is administered, a large amount of it does not reach the site of action. CA- 4 is active against many cancer cell lines *in vitro*, but not *in vivo*, due to this issue. To deal with this problem prodrugs are used. A prodrug is a compound which to start with, upon administration is inactive, but is metabolised *in vivo* into its active form (McLoughlin & O'Boyle, 2020).

1.12.1 Combretastatin- A4 phosphate (CA- 4P)

CA- 4P is a phosphorylated form of CA-4, with improved solubility in water, its structure is shown in figure 54.

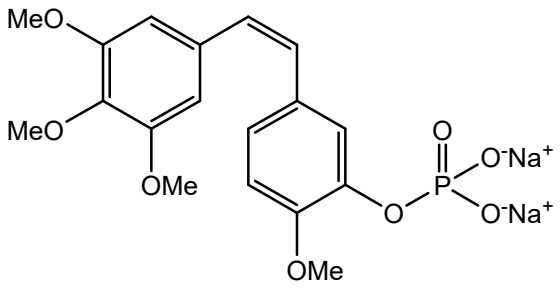

Figure 54. Structure of CA- 4P (Mabeta & McGaw, 2018).

After administration CA- 4P is converted by phosphatases at the site of action into the active form, CA- 4. The CA- 4 then enters the tumour cells (Mabeta & McGaw, 2018). The CA - 4P to CA- 4 conversion happens at a much faster rate in the tumour environment compared to elsewhere in the body (Greene, Meegan & Zisterer, 2015), this is because phosphatases, the enzymes responsible for phosphate hydrolysis are overexpressed in many tumours (Wang et al., 2008) Studies have indicated that CA- 4P and CA- 4 show similar activities against all cell lines they were tested against, in situations where they don't exhibit similar activities it is possibly due to the time it takes for the prodrug to active form conversion (Semenov et al., 2010).

Drawbacks to the use of CA- 4P include that the concentration of the drug in the blood diminishes at a fast rate following administration, compounds have thus been searched for which circumvent this problem and it has been found that CA- 4 phosphate diesters fulfil the criteria (Karatoprak et al., 2020). Another problem with this prodrug is the already discussed issue of *cis* to *trans* isomerisation, which also occurs with this compound (McLoughlin & O'Boyle, 2020). Also, the drug does not work well with oral administration (Pérez-Pérez et al., 2016).

1.12.2 AVE 8062 (Ombrabulin)

AVE 8062 is another CA – 4 prodrug, its structure is shown in figure 55. It also has increased solubility in water compared to CA- 4. It shuts down tumour vasculature to a greater extent

than CA- 4 (Mabeta & McGaw, 2018). CA- 4P and AVE8062 have different mechanisms of action for the shutting down of tumour vasculature, AVE 8062 induces zero pressure in the blood vessels feeding the tumours and brings about an increase in arteriole resistance, both leading to tumour cell death. It is converted *in vivo* into amino CA- 4 by aminopeptidases (Hori, 2011).

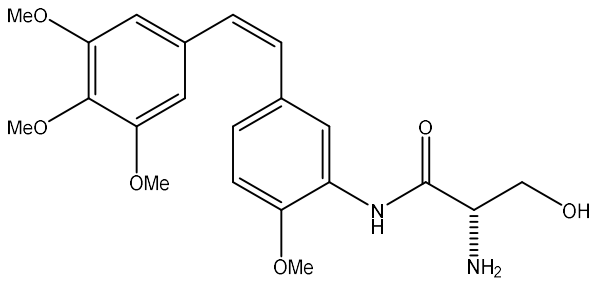

Figure 55. Structure of AVE8062 (Mabeta & McGaw, 2018).

Many other different prodrugs have been synthesized.

1.12.3 β- Galactosyl derivatives

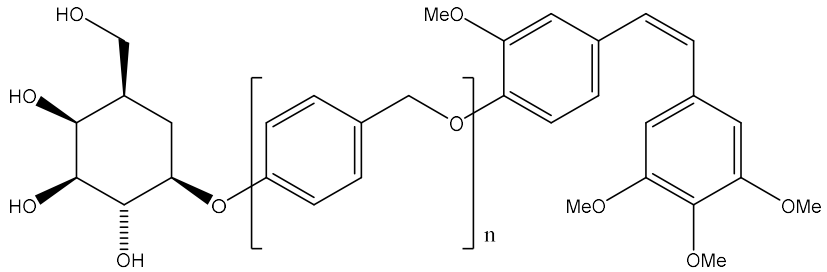

Figure 56. CA-4-β- galactosyl derivative prodrugs (Seddigi et al., 2017).

B- Galactosyl derivatives of CA- 4 were synthesized by Suzuki et al., (2017), where n = 0 and n = 1, as shown in figure 56. They were investigated for the treatment of ovarian cancer. Both compounds solved the problem of bioavailability as they had high aqueous solubility. They

also had the advantage of not showing toxicity to normal cells. Both compounds are prodrugs. There is increased presence of the enzyme β- galactosidase in the ovarian cancer cell environment and this enzyme has the effect of cleaving off the β- galactose portions of the prodrugs, releasing CA- 4. The compound where n= 1 had an EC_{50} of 2.47 nM against the OVCAR3 ovarian cancer cell line and an EC_{50} of 2.67 nM against the OVK18 ovarian cancer cell line. These values were similar to or better than those obtained for CA-4 (Seddigi et al., 2017).

1.12.4 Glutathione activated prodrugs

Prodrugs based on activation by glutathione (GSH) are currently receiving a lot of study. It is known that there is 30 times more glutathione in cancer cells than in normal cells. A prodrug was synthesized by Kong et al., (2017) which takes advantage of that fact and therefore ensuring delivery of the drug just to the intended site of action i.e., the tumour environment. The compound synthesized had a disulphide bond, which is cleaved by GSH, releasing CA- 4. However, this compound was evaluated in treating MDA- MB- 231 cancer cells, with disappointing results (Seddigi et al., 2017).

1.12.5 Light activated prodrugs

A new method of utilising prodrugs was developed by Nkepang et al., (2014) Folate receptors are over expressed in many different cancer types. A prodrug was made comprising of folic acid, which seeks them out. Also, part of the prodrug was a photosynthesizer and CA- 4. The prodrug was activated by light at the site of action, cleaving the linker in the compound and releasing CA- 4 (Seddigi et al., 2017).

1.13 CA- 4 derivatives and clinical trials

The three CA- 4 derivatives that have progressed furthest in clinical trials are CA- 4P (named as fosbretabulin), AVE8062 (named Ombrabulin) and CA-1P (named Oxi4503).

1.13.1 Fosbretabulin

Fosbretabulin, structure shown in figure 54, has undergone phase I, II and III clinical trials as a vascular disrupting agent in the treatment of non- small cell, anaplastic thyroid and ovarian cancers .It failed however as a single agent. Its lack of conformational stability and brief half-life were also issues. It is currently undergoing trials in combination with existing anti-cancer drugs. It was granted orphan drug status by the European medicines agency in 2013 for treating ovarian cancer when it was found that fosbretabulin tromethamine, when combined with paclitaxel or carboplatin, caused an improvement in patient responses. In 2016 fosbretabulin was awarded orphan drug status for treating gastro- entero- pancreatic neuroendocrine tumours when the effect of fosbretabulin tromethamine on these tumours was discovered (McLoughlin & O'Boyle, 2020).

1.13.2 Ombrabulin

Ombrabulin, structure shown in figure 55, has been entered into phase II clinical trials for treating ovarian cancer. It was developed by Sanofi Aventis and granted orphan drug status in 2011 for treating soft tissue sarcoma. This orphan drug status was later withdrawn however due to poor patient responses in phase III clinical trials and Sanofi Aventis discontinued clinical investigation into its use (McLoughlin & O'Boyle, 2020).

1.13.3 Oxi4503

Oxi4503, structure shown in figure 19, is a diphosphorylated CA- 1 analogue. In 2017 it was awarded orphan drug status by the FDA and is being developed by Mateon therapeutics for treating acute myeloid leukaemia. Clinical trials were started in 2015 investigating the use of Oxi4503 and cytarabine together, for treating acute myeloid leukaemia and myelodysplastic syndrome (McLoughlin & O'Boyle, 2020).

1.14 Combination therapies

CA- 4 as a vascular disrupting agent exerts its effect mostly on the inner core of the tumour. Existing drug treatments and radiation therapy act mainly on the outer, peripheral region of the tumour, therefore combining CA- 4 administration with radiation therapy or the existing treatments means that the entirety of the tumour is targeted (McKeage, 2011).

1.14.1 CA- 4 and radiotherapy

The effectiveness of radiotherapy on treating tumour cells depends on the amount of oxygen in the tumour environment. Radiation therapy is not efficient at eliminating tumour cells in the central region of the tumour, where there is a lack of oxygen. Due to their complementary regions of tumour targeting, the combination of CA- 4 and radiotherapy as a treatment makes sense. Tests have shown that this combination, utilizing radiotherapy on specific regions, results in an increase in death of tumour cells compared to with just the action of radiation therapy alone (Siemann, 2011) . When using this combination however, to achieve the maximum effect, the scheduling of the different treatments is vitally important. The action of CA- 4, causing shutdown of tumour vasculature, resulting in oxygen depletion results in diminished effectiveness of subsequent radiotherapy, therefore VDA administration should follow radiotherapy (Pérez-Pérez et al., 2016).

1.14.2 CA- 4 and chemotherapeutic agents combination

The combination of CA- 4 with current chemotherapeutic agents was shown in studies to be more effective than either one alone. The combination of VDAs with paclitaxel, in treating xenografts of non- small cell lung cancer proved to be more effective than either agent alone. A similar situation was observed when treating xenografts of anaplastic thyroid cancer with the combination of CA- 4P with carboplatin or combining CA- 4P with paclitaxel and manumycin A (Siemann, 2011). The combination of CA- 4P with 5- fluorouracil was very successful in treating tumours in mouse models (Kretzschmann & Fürst, 2013). Combining docetaxel with AVE8062 was shown to improve survival in Hey- A8 cancer cell line mouse models (Siemann, 2011). It was shown in studies that when AVE8062 was combined with doxorubicin, cisplatin, oxaliplatin or carboplatin in treating tumours in mice models, the antitumor activity was greater than that of either agent alone. The most successful combinations

were those of AVE8062 with either oxaliplatin or doxorubicin, which produced their synergistic effect at very low, well tolerated dosages (Kretzschmann & Fürst, 2013).

The reason for the success of these combinations is that the VDAs affect tumour regions which have poor perfusion and are not accessible to chemotherapeutic agents for this reason. The loss of blood flow around the tumour as a result of VDA action also leads to drugs being entrapped in the tumour vicinity, causing improved effectiveness of the treatment due to extended exposure of the tumour to the drugs.

As is the case with radiation therapy, the scheduling of the different types of treatment is crucial, as first administering the VDA results in tumour vasculature shutdown, denying access to the tumour for subsequent administration of chemotherapeutic agents, therefore VDA administration should follow administration of chemotherapy (Siemann, 2011).

Combining VDAs and Chemotherapeutic agents does not however always give positive results. Combining CA-4P with paclitaxel and carboplatin for treating anaplastic thyroid cancer did not result in improvement in survival rates, the same can be said for the combination of Ombrabulin with taxane for the treatment of metastatic NSCLC (Pérez-Pérez et al., 2016).

1.14.3 Combination therapies and tumour environment

The administration of a VDA such as CA- 4 to a tumour is thought to alter the environment of a tumour and therefore possibly make the tumour more susceptible to the effect of a second agent. As an example, administering Ombrabulin to tumour cells results in an increase in the expression of the protein p32 on tumour cell surface. This means that subsequent administration of a second agent; able to target p32 could be highly successful (Pérez-Pérez et al., 2016).

1.14.4 Combination therapy with nitric oxide inhibitors

Neutrophils are white blood cells with anti- tumour activity (Oberg, Wesch, Kalyan & Kabelitz, 2019). Tumours generate nitric oxide, which has activity against neutrophils (Siemann, 2011). Investigations have therefore been carried out (Siemann, 2011) to see the effect of combining VDA, such as CA- 4P, administration with inhibition of the enzymes that catalyze nitric oxide

generation in tumour cells, nitric oxide synthases (Fu, 2014). N- nitro- L- arginine is a nitric oxide synthase inhibitor ("No-Nitro- L -arginine = 98 TLC 2149-70-4", 2022). The CA- 4P/ N- nitro- L- arginine combination showed increased anti- tumour activity in mouse tumour models (Siemann, 2011). Further investigation needs to be carried out.

1.15 Combretastatin hybrid molecules

Hybrid molecules are a new development. They involve the incorporation of two drugs into a single molecule. This results in the drug molecule having multiple targets and also reduces the drug toxicity to normal cells. An example is illustrated in figure 57.

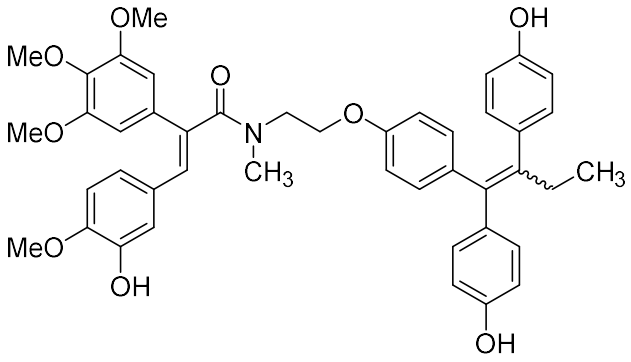

Figure 57. CA- 4 / Tamoxifen hybrid molecule (Piekuś-Słomka, Mikstacka, Ronowicz & Sobiak, 2019).

The hybrid shown in figure 57 incorporates CA- 4 and the drug tamoxifen, which is an estrogen receptor modulator used in treating breast cancer. When tested against the MCF- 7 breast cancer cell line, this compound showed an IC_{50} of 5nM, compared to CA-4's value of 8nM. The compound was tested against a wide range of other cancer cell lines and displayed potent anti- cancer activity in many of them (Piekuś-Słomka, Mikstacka, Ronowicz & Sobiak, 2019).

A group of hybrid molecules was synthesized by Vilanova et al., (2014), structure of the most potent shown in figure 58, incorporating the structures of CA- 4 and Pironetin, which is a natural product, also possessing anticancer activity (Dias, de Oliveira & de Sousa, 2003). Analogues were made with various lengths of linkers joining the two drug molecules. The most potent derivative was that with a length of carbon units in linker of 15. This derivative was

found to have anticancer activity comparable to CA- 4, with less toxicity against healthy cells (Tangutur, Kumar, Krishna & Kantevari, 2017).

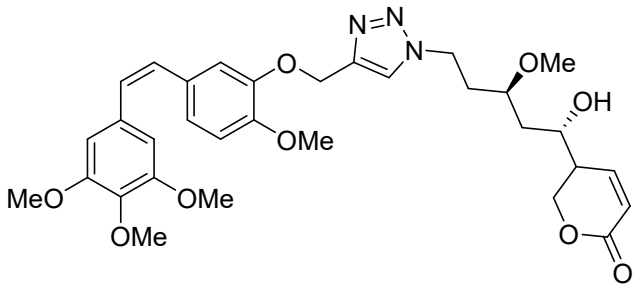

Figure 58. CA- 4 / Pironetin hybrid molecule (Tangutur, Kumar, Krishna & Kantevari, 2017).

1.16 CA- 4 derivatives and molecular modelling

The crystal structure of the protein tubulin has now been obtained. This structure is being developed with ever increasing resolution (Pérez-Pérez et al., 2016). It is now therefore possible to investigate the interactions between various chemical compounds and tubulin using computer software. Now having access to a tubulin crystal structure, it was necessary to construct a pharmacophore model for interaction of drugs with tubulin. This model was a collaborative effort between several research groups, and it has continually been refined. The model can then be utilized in virtual screening of chemical databases to find compounds that will bind to tubulin and the strength of those interactions. Molecular modelling provides a value for the IC_{50} of compounds, and there is "very good correlation between the calculated and observed IC_{50}s for the cytotoxic effect of synthesized compounds" (Mikstacka, Stefański & Różański, 2013, p.386). Compounds found to have favourable interactions with tubulin in silico can then be selected for synthesis in the lab, followed by testing them for activity. The molecular modelling process results in a huge reduction of costs incurred in the lab (Mikstacka, Stefański & Różański, 2013).

An issue with molecular modelling is the occurrence of different tubulin isoforms, tubulin exhibits polymorphism (Mikstacka, Stefański & Różański, 2013). The different isoforms of tubulin in cancer cells can all interact differently to a drug. A future development would therefore be to tailor molecular modelling to a particular tubulin isoform (Li et al., 2018).

The more that is known regarding the structure of tubulin and in particular the colchicine binding site and its interaction with various chemical compounds the better for the development of novel vascular disrupting agents (Pérez-Pérez et al., 2016).

1.17 Fluorine and drug development

Fluorine has a major role in the process of development of drugs, this includes for CA-4 derivatives. This is due to fluorine's distinctive properties. It is now common practice to introduce fluorine atom or atoms into the structure of compounds being investigated for particular biological activity. Fluorine has a profound effect on the activity of a compound, without drastically changing the compound's size. The fluorine atom's small size allows for the compound it has been included in to still interact effectively with its biological receptor. The fluorine atom is highly electronegative, resulting in a highly polarized carbon- fluorine bond which has a major effect on the interactions between the drug and its target (Zong, Shea, Maffucci & Ojima, 2017). . This highly polar C-F bond in compounds containing fluorine exhibits polar hydrophobicity, which describes when a compound is highly hydrophobic in spite of its polar bonds (Accioni, García-Gómez & Rubio, 2021). The insertion of fluorine in a structure increases the lipophilicity of a compound, which increases the absorption of the compound into biological membranes. The importance of fluorine in drug development is shown by the fact that more than one in five of all drugs currently on the market have at the very least one fluorine atom in their structure (Zong, Shea, Maffucci & Ojima, 2017).

1.18 Wittig reaction and alternative methods for combretastatin synthesis

1.18.1 Wittig reaction

Figure 59 shows the overall chemical equation for the formation of a combretastatin, via a Wittig reaction between a substituted benzaldehyde and a phosphonium salt (McNulty & McLeod, 2013).

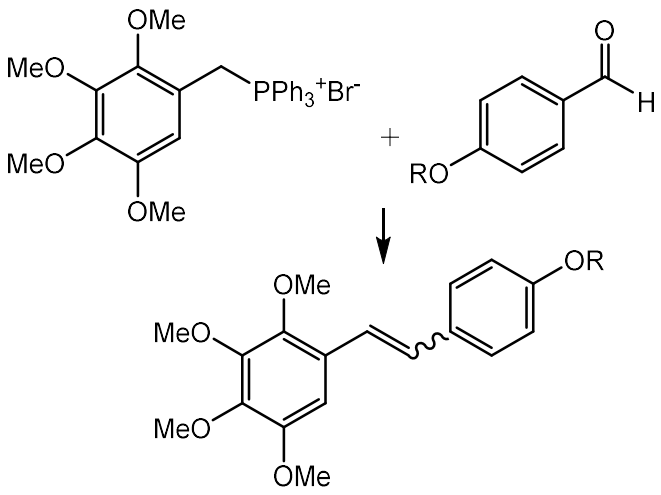

Figure 59. Chemical equation for Wittig reaction

There are many different synthetic routes for synthesis of combretastatin derivatives. Synthesizing the same derivative, but with a different method results in different *E*: *Z* stereoselectivity of the compound as well as differences in yield (Roman et al., 2013). The Wittig reaction was one of the first methods used for synthesizing combretastatins, and it is very frequently used (McNulty & McLeod, 2011). The Wittig reaction does however have advantages and disadvantages. Advantages include that the reaction can be carried out using water as the solvent, which as well as being environmentally friendly, also solves the issue of how to deal with the phosphine oxide which is produced as a by-product of the Wittig reaction, the oxide is removed during the separation techniques employed in the synthesis (McNulty & Das, 2009). The bases used alongside using water as a solvent, which is either lithium hydroxide or potassium carbonate , are also more environmentally friendly(McNulty & McLeod, 2013). Also, the Wittig reaction is very tolerant of the functional groups not involved in the reaction, with the exception being the hydroxyl group, which must be protected when present (McNulty, McLeod, Das & Zepeda-Velázquez, 2015), which is because a phenolic hydroxyl group will have a lower pKa than water and would therefore most likely be fully deprotonated under the basic conditions of the reaction.

1.18.2 Alternative routes for combretastatin synthesis

1.18.2.1 Aldol condensation

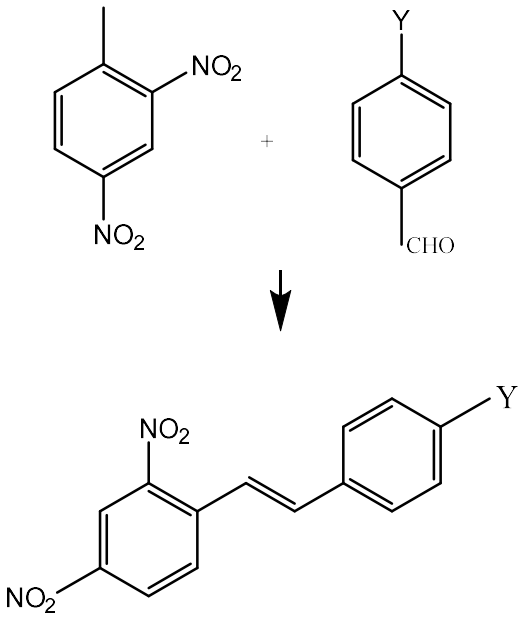

Figure 60. Equation for aldol condensation stilbene synthesis (Likhtenshtein, 2010).

For the reaction shown in figure 60, first a carbanion is formed by the reaction of the toluene with a base, the carbanion then adds to the aldehyde's carbonyl group.

1.18.2.2 Coupling reactions

The equation in figure 61 is for stilbene formation in the reaction between a haloarene and a substituted cinnamic acid, with a Pd catalyst and a base present (Rameau, Russo, Mangematin, Pinel & Djakovitch, 2018).

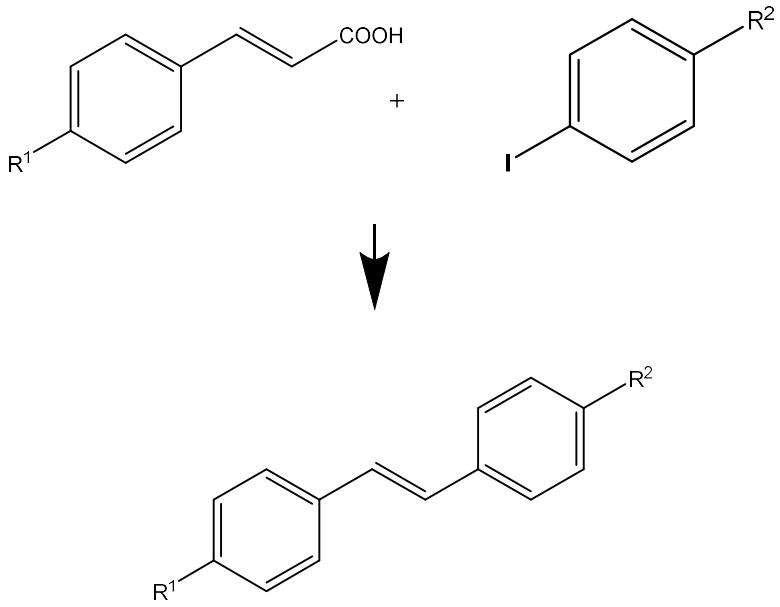

Figure 61. Coupling reaction to produce stilbenes (Rameau, Russo, Mangematin, Pinel & Djakovitch, 2018).

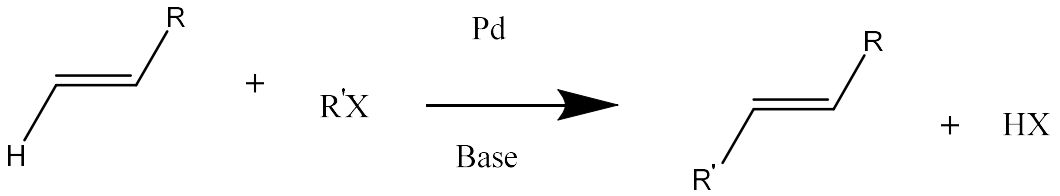

Figure 62. Equation for Heck coupling ("Heck Reaction", 2017).

The equation in figure 62 is that for the coupling reaction known as Heck coupling, which is the reaction between a halocarbon compound and a suitably substituted alkene. It happens in the presence of a Pd catalyst and a base ("Heck Reaction", 2017).

1.19 Drug delivery systems

There are various methods available for dealing with the poor solubility in water and the issues with metabolism within the body of the compound CA- 4. These include the use of nanotechnology such as nanoparticles, nanocells, nanocomplexes and nanoliposomes, and polymeric micelles and dendrimers (Pérez-Pérez et al., 2016), which are both nanoscale, as well as carbon nanotubes (Cho, Wang, Nie, Chen & Shin, 2008), all of which are used to carry and deliver drugs to tumour sites. The various systems are illustrated in figure 63.

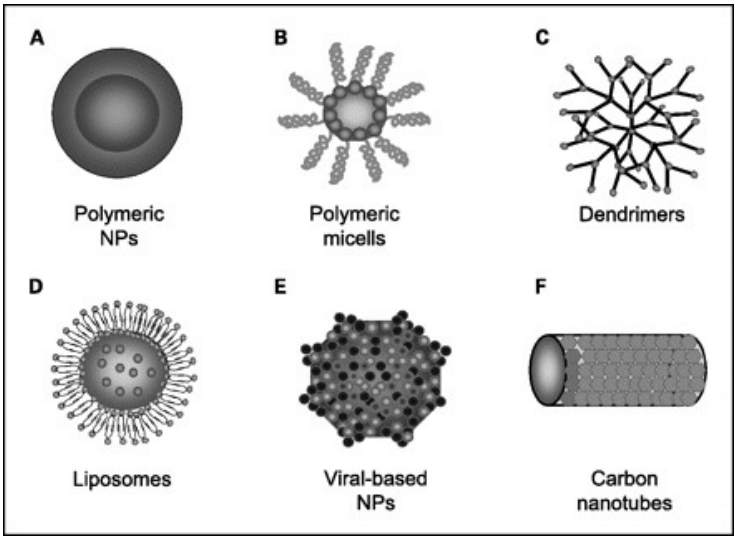

Figure 63. Diagram illustrating various drug delivery systems (Cho, Wang, Nie, Chen & Shin, 2008).

These methods can also bring about site specific delivery of the drug, which means there is a reduction in the toxic effect of the drug to non- cancer cells in other parts of the body (Anderson & Sydor, 2016).

1.19.1 Nanoparticles

The fact that nanoparticles are so small means they have high permeability into tumour cells. The surface area of nanoparticles is also very large, meaning that a large amount of drugs can be carried by them. They are very stable, which means that the drug reaches the target without getting degraded along the way (Anderson & Sydor, 2016). Both hydrophobic and hydrophilic drug compounds can be carried by them (Gelperina, Kisich, Iseman & Heifets, 2005).

An example of the use of nanoparticles in drug delivery is the method used by Song et al., (2015) in which the administration of CA- 4P was coupled with administration of *cis*-diaminedichloroplatinum (CDDP) loaded nanoparticles to mouse models carrying MDA-MB-435 and C26 cancer cell lines. The drug loaded nanoparticles took advantage of what is known as the enhanced permeability and retention (EPR) effect (Pérez-Pérez et al., 2016), which means that nanoparticles, due to their small size, tend to accumulate more in tumour tissue than in normal tissue (Alasvand et al., 2017). The CA- 4P acted on the tumour core while the CDDP acted on the tumour edges. The combination of the two treatments produced better results than either treatment alone (Pérez-Pérez et al., 2016).

1.19.2 Nanocells

Sengupta et al., (2005) developed a structure known as a nanocell (Pérez-Pérez et al., 2016). A nanocell allows for the consecutive delivery of first one drug and then another, over a period of time. The nanocell has two regions, an inner core, made up of one drug, encased within a vesicle made up of the second drug ("Nanocell drug delivery system - Patent CA-2558263-A1 - PubChem", 2005). A pair of drugs that can be administered in this way is CA- 4 and doxorubicin (Pérez-Pérez et al., 2016).

1.19.3 Nanocomplexes

Another delivery system that utilises nanotechnology is the use of nanocomplexes. In an example, poly (D, L- co-glycolic acid)-b- poly (ethylene glycol) was used to encase CA- 4. The surface of the complex was also coated with cetuximab, an antibody targeting the epidermal growth factor receptor, which is over expressed in human liver cancer. This is an example of targeted drug delivery (Pérez-Pérez et al., 2016).

1.19.4 Nanoliposomes

Also used for drug delivery are nanoliposomes, structure shown in figure 64. One of the advantages of using these for drug delivery is that their structures can be easily manipulated, changing properties such as size and surface charge. Nanoliposomes are chemically stable,

have increased bioavailability, increased ability to target tumours and demonstrated reduced toxicity, which is due to a decreased amount of CA- 4 in the general bloodstream and the already mentioned EPR effect. Drugs to be delivered to tumours can be incorporated into the liposomal core or the bilayer, depending on if they are hydrophobic or hydrophilic. CA-4 is therefore inserted into the liposome's lipid bilayer. The surfaces of nanoliposomes can have incorporated into them molecules which facilitate specific targeting of tumour tissues, such as antibodies. The release rate of drugs carried by the nanoliposomes can be influenced by among other things, the composition of the bilayer.

A drawback to the use of nanoliposome drug carriers is the fact that they are removed from the bloodstream by the reticuloendothelial system, decreasing the amount of the drug that reaches the tumour tissue. This problem is solved by making modifications to the liposomal surface to counteract this process, such as incorporation of polyethylene glycols (PEGs) (Nik et al., 2019).

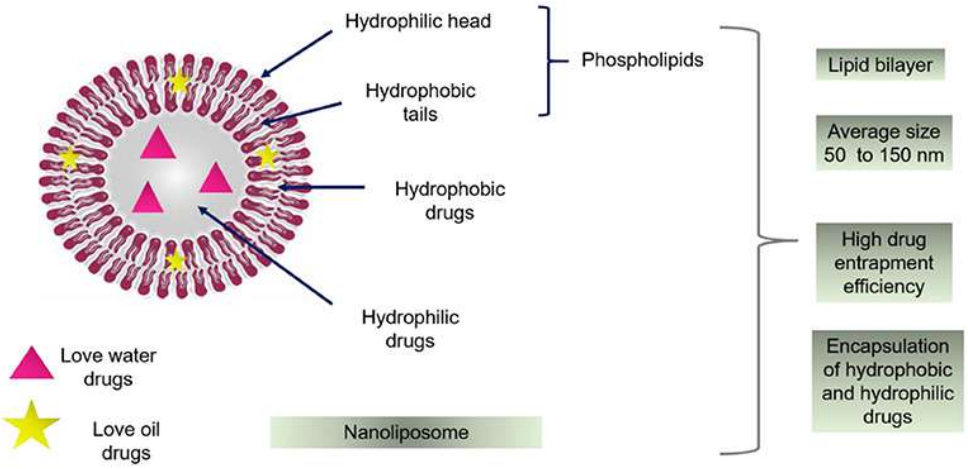

Figure 64. Structure of nanoliposome (Aguilar-Pérez, Avilés-Castrillo, Medina, Parra-Saldivar & Iqbal, 2020).

1.19.5 Polymeric micelles

Polymeric micelles are nanomeric scale materials used to transport drugs. They are formed when hydrophilic and hydrophobic polymers, linked together to form an amphiphilic structure, automatically arrange themselves in aqueous solution, forming a micelle, as shown in figure 65. The interior of the micelle is thus hydrophobic and used to transport hydrophobic drugs such a CA- 4 (Amin, Butt, Amjad & Kesharwani, 2017).

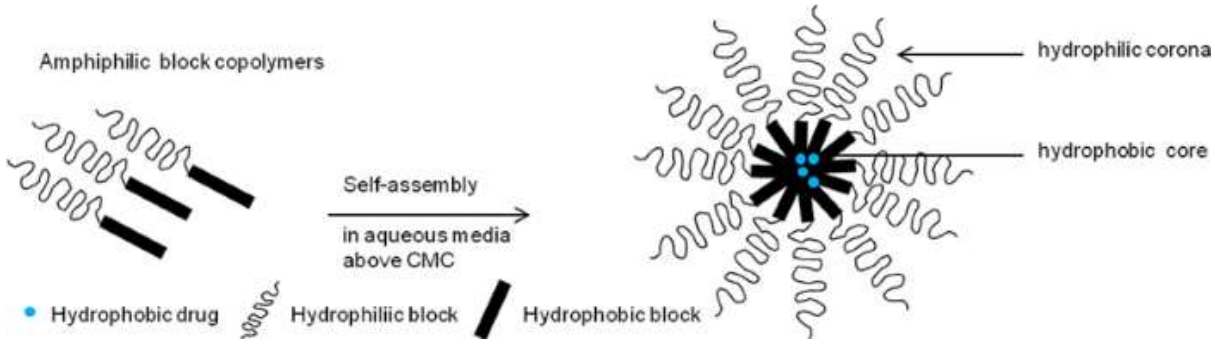

Figure 65. Diagram showing micelle structure (Jhaveri & Torchilin, 2014).

In a study by Yang et al (2012), the two polymers used to form the amphiphilic structure were the polymers polyethylene glycol- b- poly lactic acid (PEG-b-PLA) and cyclic arginine-glycine- aspartic acid- tyrosine- lysine (CRGDyK). The two polymers and the drugs CA- 4 and doxorubicin were mixed together via the process of solution casting. The end result was a dual drug polymeric micelle. The amino acids of the CRGDyK and the nanomeric size of the micelle both resulted in targeted delivery of the drugs to tumour tissue (Yang et al., 2012).

1.19.6 Nanoemulsions

Nanoemulsions are another delivery system; they are made by combining water, an oil insoluble in water and a surfactant with a drug such as CA- 4, using processes of homogenisation and ultrasonication. Nanodroplets of oil are formed, suspended in the water; the presence of the surfactant brings this about and also prevents the nanodroplets from coalescing. Nanodroplets smaller than 300 nm in diameter can be produced. The size of the nanodroplets produced changes depending on the pressure used in the homogenisation process, the surfactant used, and the viscosity of the oil used. In this delivery system, the hydrophobic drug CA- 4 is contained in the oil, within the droplet (Mico et al., 2017).

1.20 Combretastatin analogues of last few years

ABI- 231 was a CA- 4 analogue developed by Chen et al., (2011, 2012); its structure is shown as compound 1 in figure 66. It consists of a carbonyl group and imidazole linking the rings and a bicyclic structure replacing the B ring. It is a colchicine binding site inhibitor with high potency. ABI- 231 displayed an IC_{50} of 5.2 nM on average, against a wide range of cancer cell lines. Recently they synthesized two ABI- 231 analogues with high activity, shown as structures two and three in figure 66. Both compounds were highly potent, bind to the colchicine binding site, inhibit tubulin polymerization and also inhibit metastasis. Compound two, the ABI- 231 analogue, with a methyl group substituent on the bicyclic structure, structure shown in figure 66, was more potent than ABI- 231, with an IC_{50} of between 1.7 and 3.2 nM against WM164, A375 and MI4 cancer cell lines. Compound three, structure shown in figure 66, was also more potent than its parent compound ABI- 231, with IC_{50} values of between 1.6 and 3.7 nM against the WM164, A375 and MI4 cancer cell lines. ABI- 231 displayed IC_{50} values of between 5.6 and 8.1 nM against the same cell lines. All three compounds showed activity against multi- drug resistant cancer cell lines, showing promise for future development.

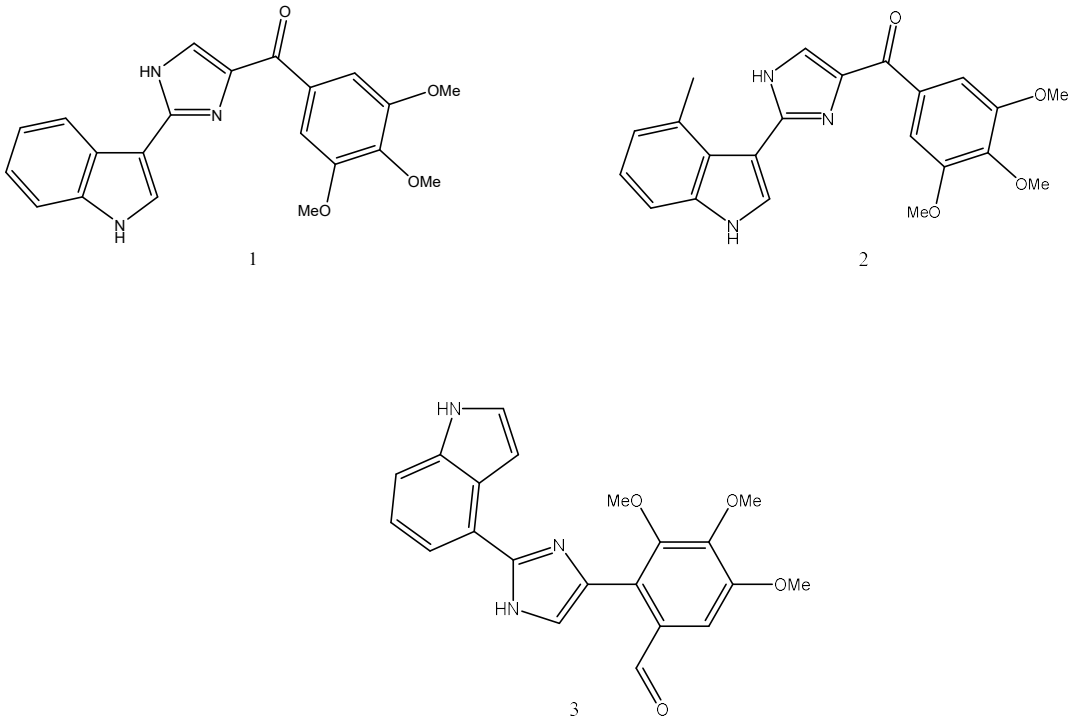

Figure 66. Structures of ABI- 231 analogues (McLoughlin & O'Boyle, 2020).

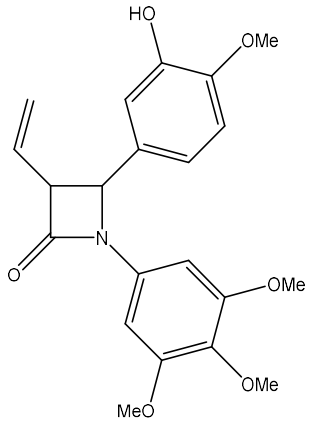

Figure 67. Structure of CA- 4 analogue with vinyl- substituted β- lactam ring as linker (McLoughlin & O'Boyle, 2020).

McLoughlin & O'Boyle (2020) synthesized CA- 4 analogues with vinyl substituted β- lactam rings as the linker. The compound shown in figure 67 demonstrated the highest potency, with an average GI_{50} value of 23 nM when tested against a wide range of NCI cancer cell lines. This compound was exceptionally active against the MCF- 7 breast cancer cell line, against which it had an IC_{50} value of 8 nM. The results obtained show promise for developing these compounds as analogues, more stable than CA-4 with regard to unwanted *cis- trans* isomerism, since they lack the isomerizable olefinic bond.

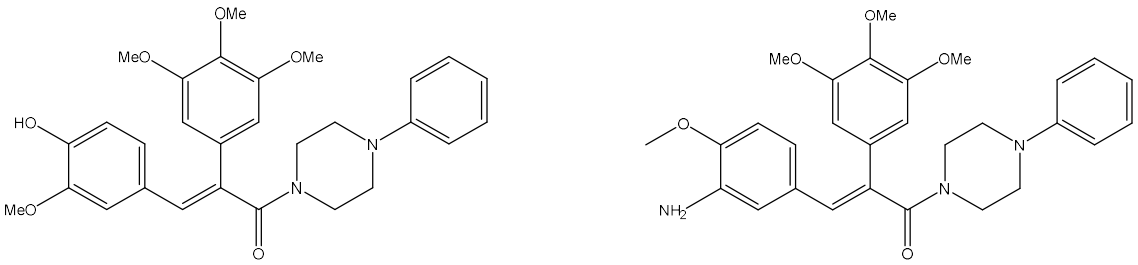

Figure 68. Structures of piperazine CA- 4 analogues (McLoughlin & O'Boyle, 2020).

McLoughlin & O'Boyle (2020) also recently synthesized a series of CA- 4 analogues with a piperazine moiety joined to the linking double bond, structures of some of them shown in figure 68. The piperazine group both prevented isomerisation and improved aqueous solubility. The two compounds shown in figure 68 demonstrated good activities against the MCF-7 breast

cancer cell line in *in vitro* testing, showing promise for their development as a treatment for this type of cancer (McLoughlin & O'Boyle, 2020).

IsoCA- 4 analogues were synthesized by Naret et al (2019), in which both the A and B rings were replaced by other ring systems, the A ring by a quinazolinyl, pyrimidine- dionyl or quinolynl and the B ring by an indolyl or carbazolyl. The compound shown in figure 69 displayed the highest potency

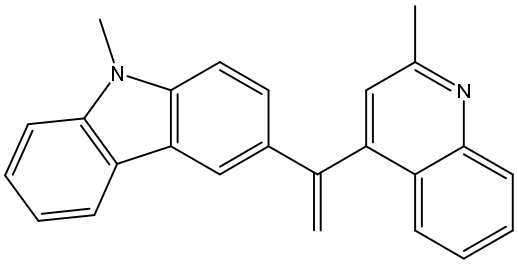

Figure 69. Structure of IsoCA- 4 analogue (McLoughlin & O'Boyle, 2020).

In this compound, the A- ring was replaced with a 2- methylquinoline and the B- ring with a 9- methylcarbazole. This compound showed higher activity than isoCA- 4 against U87- MG and A549 cancer cell lines and it was many times more potent than CA- 4 against the A549 lung cancer cell line. It was also more active than CA- 4 against the MDR HT- 29 cancer cell line.

The fact that it possesses a high partition coefficient, which allows it to cross the blood- brain barrier, coupled with the fact that it shows activity against glioblastoma cancer cells means that this compound shows promise for treating this particular form of cancer (McLoughlin & O'Boyle, 2020).

2 Results and discussion

2.1 Preparation of compounds (phosphonium salt)

The first step in this project was the synthesis of a tetramethoxy phosphonium salt, a novel compound. This was achieved in six synthetic steps, starting from and using readily available materials throughout. The reaction scheme is outlined in figure 70.

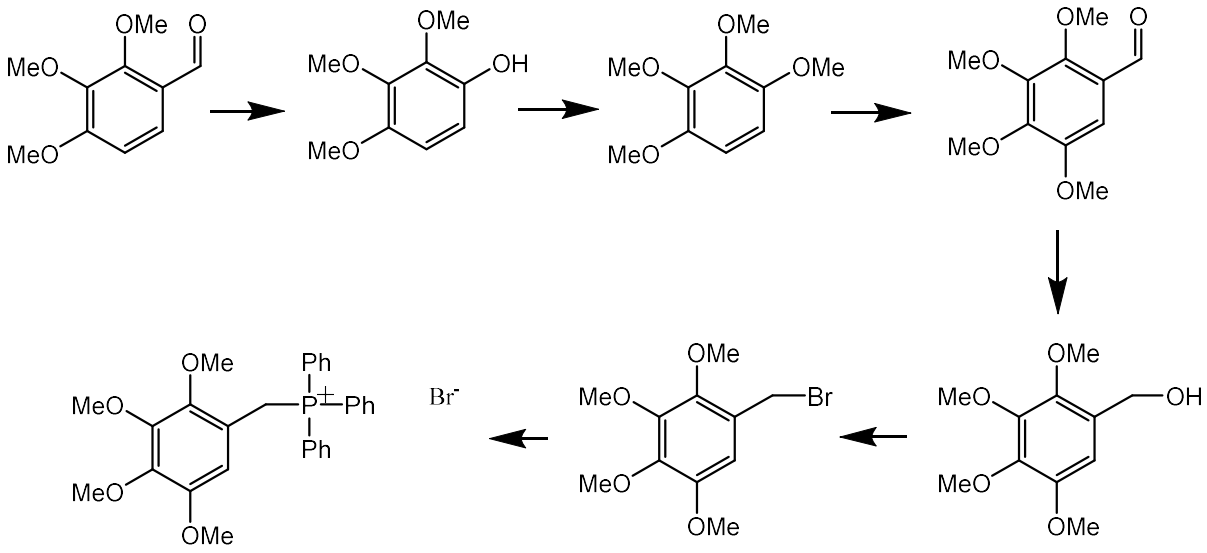

Figure 70. Diagram showing reaction scheme for tetramethoxy phosphonium salt synthesis.

The very first starting material was 2, 3, 4 – trimethoxybenzaldehyde, which was reacted with a H_2SO_4 / MeOH mixture and hydrogen peroxide in an acid – catalysed Dakin oxidation, producing 2, 3, 4- trimethoxyphenol (Tremblay & Sames, 2005) . The reaction mechanism is shown in figure 71. The original procedure used was by Tremblay & Sames, 2005; however various changes were carried out when using it in our synthesis, to optimize the reaction.

To start with, it was not required to carry the reaction out under an atmosphere of argon. It was also found that the addition of three aliquots of hydrogen peroxide, at intervals, instead of just one and then leaving the reaction mixture to stand overnight after the reaction was completed and before the workup, resulted in obtaining the phenol in high purity, without the need of flash chromatography as outlined in the original procedure. Without these amendments to the original procedure, the phenol was only obtained in a maximum purity of around 80 %, before columning. The reaction yield was 53 %.

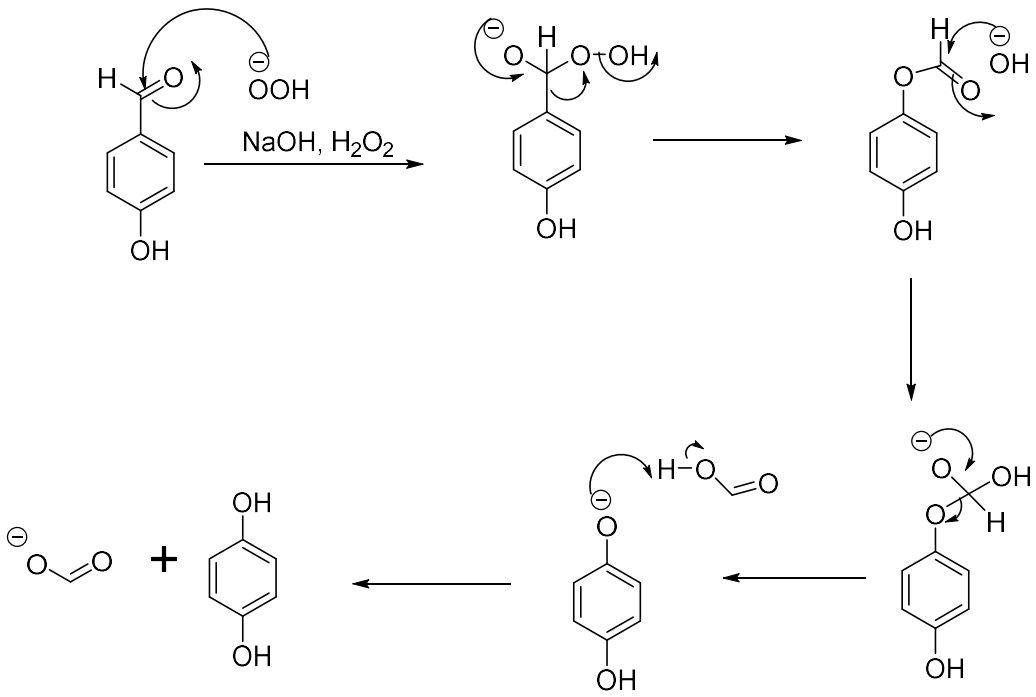

Figure 71. Diagram showing reaction mechanism for acid- catalysed Dakin oxidation

The next synthetic step was the synthesis of 1, 2, 3, 4 – tetramethoxybenzene from the trimethoxy phenol. This involved reaction with potassium carbonate and methyl iodide (Tremblay & Sames, 2005), in a nucleophilic substitution of the halide with the alkoxide produced in the reaction between the phenol and the potassium carbonate. The reaction mechanism is shown in figure 72.

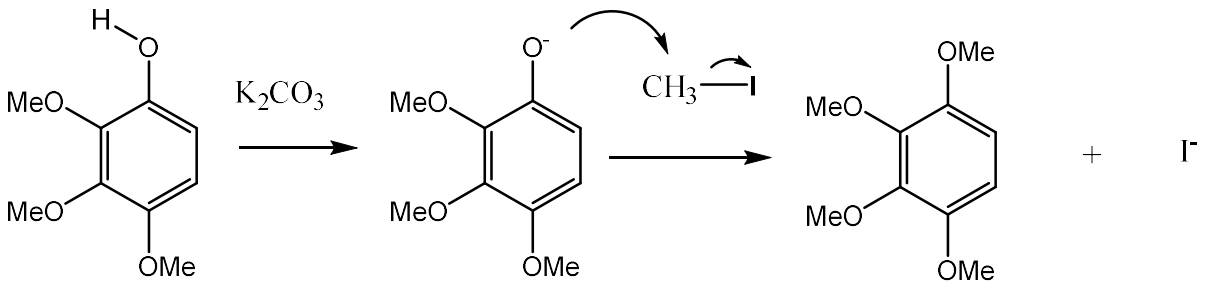

Figure 72. Reaction mechanism for 1, 2, 3, 4- tetramethoxybenzene synthesis.

In a change to the original procedure by Tremblay & Sames, 2005, the reaction was refluxed for eight hours instead of six. Also, after this, the work up resulted in crystals of the product, with high purity, without the need for recrystallization as was outlined in the original procedure. The reaction yield was 73.5 %.

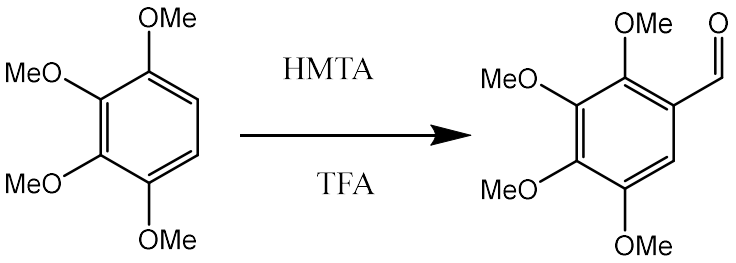

Figure 73. Reaction for synthesis of tetramethoxybenzaldehyde from tetramethoxybenzene

The next synthetic step on the pathway to the tetramethoxy phosphonium salt was the synthesis of the 2, 3, 4, 5- tetramethoxybenzaldehyde from the tetramethoxybenzene. This was achieved by reacting the tetramethoxybenzene with hexamethylenetetramine and trifluoroacetic acid (Bai et al., 2019) in a Duff reaction. This is outlined in figure 73. Various changes were made to the original procedure. Reaction time was eight and a half hours instead of eight. Heating of the reaction mixture was carried out at 72° C instead of 70°C. During the work- up, extraction using dichloromethane was carried out five times instead of two. The eluent used in purification of the product via flash column chromatography was hexane / ethyl acetate (7: 3) instead of the originally outlined petroleum ether/ dichloromethane/ ethyl acetate (9:1:1). During the column chromatography, TLC analysis of fractions coming off the column showed significant amounts of another compound coming off the column at the same time as the desired product; however, the presence of this second compound did not have any impact on the success of the next synthetic step, production of the tetramethoxy benzyl alcohol. The synthesis of the 2, 3, 4, 5-tetramethoxybenzaldehyde was very low yielding, at 17.2 %, which was the lowest of the six synthetic steps and so the synthesis of this compound proved to be the bottleneck for the overall phosphonium salt synthesis.

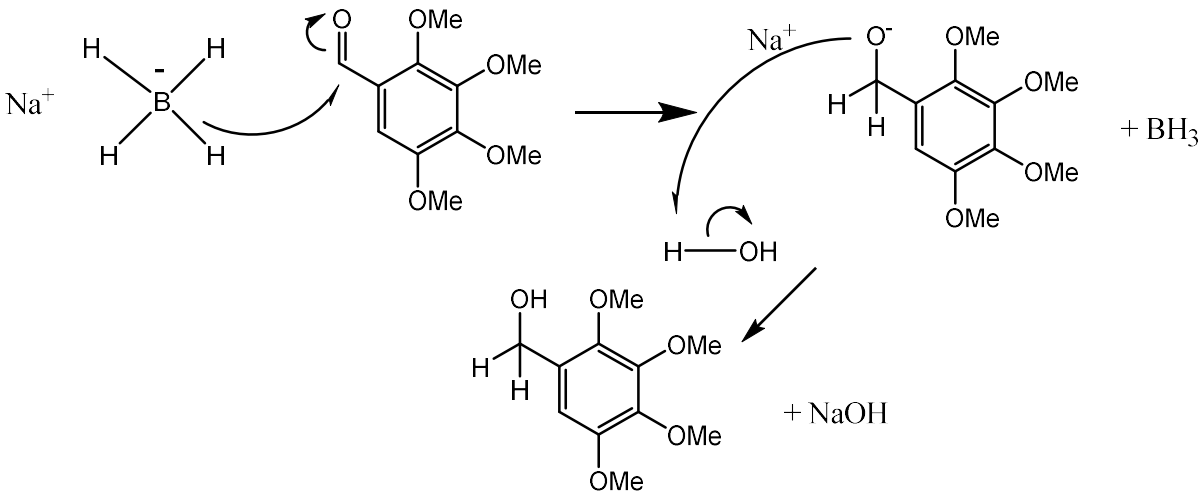

Figure 74. Reaction mechanism for tetramethoxybenzyl alcohol synthesis.

The next synthetic step was formation of the 2, 3, 4, 5- tetramethoxybenzyl alcohol, from reaction of the tetramethoxybenzaldehyde with sodium borohydride (Macé et al., 2015) in a straightforward reduction reaction. The reaction mechanism is shown in figure 74. The procedure used differed from the original in that the reaction at 0°C was stirred for one and a half hours instead of the outlined just one. The reaction yield was 55.6%.

The next synthetic step was synthesis of 2, 3, 4, 5- tetramethoxybenzyl bromide, from the tetramethoxybenzyl alcohol which underwent an S_N2 reaction with potassium tribromide (ElSohly, Ma, Turner & ElSohly, 1984). The reaction mechanism is outlined in figure 75. The difference between the method used and the original method was that the amount of reaction time after adding the second PBr_3 portion was one hour instead of half an hour. The reaction yield was 96.8 %.

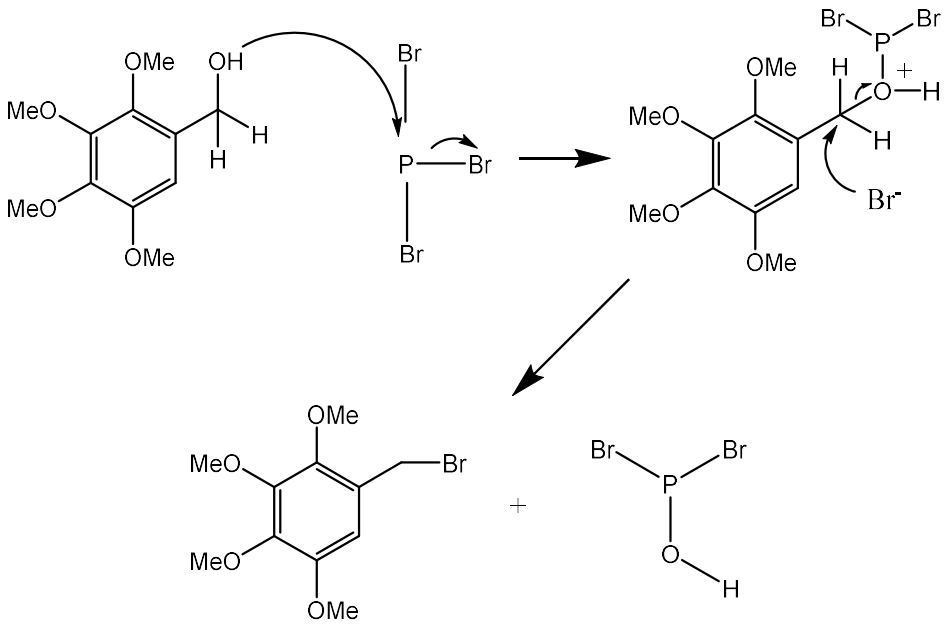

Figure 75. Reaction mechanism for tetramethoxybenzyl bromide synthesis

The final step for synthesis of the tetramethoxybenzyltriphenyl phosphonium salt was the S_N2 reaction between the tetramethoxybenzyl bromide and triphenylphosphine (Pettit, Singh, Niven, Hamel & Schmidt, 1987), resulting in the formation of an ylide. This synthetic step was carried out immediately following the bromide synthesis, due to the fact that the bromide readily hydrolyses with moisture in the air to form a benzyl alcohol. The reaction mechanism is outlined in figure 76. The reaction yield was 66 %.

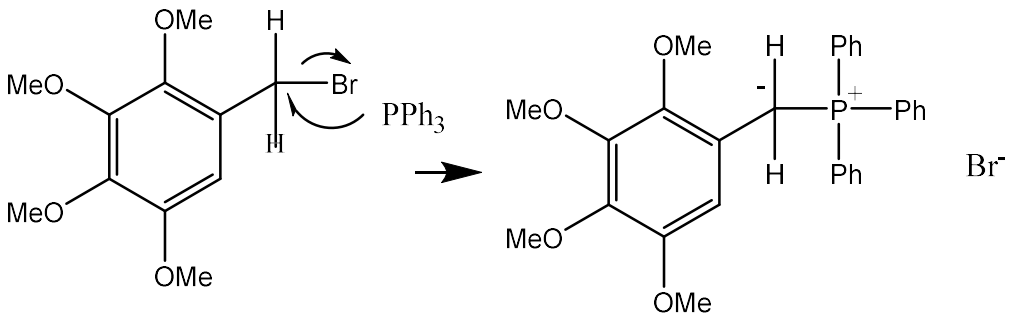

Figure 76. Mechanism for synthesis of phosphonium salt from bromide

For each of the outlined synthetic steps, the compounds were produced in small batches which were then collected together for the next step, with reaction conditions such as the amount of reagents which were known to be successful. Each step resulted in products together with small amounts of impurities, but the final product, the phosphonium salt was obtained in very high purity.

2.2 Synthesis of CA -4 analogues

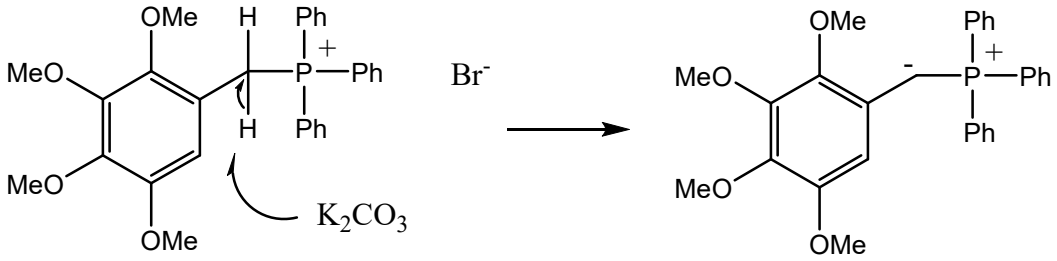

Figure 77. Mechanism of first part of Wittig reaction.

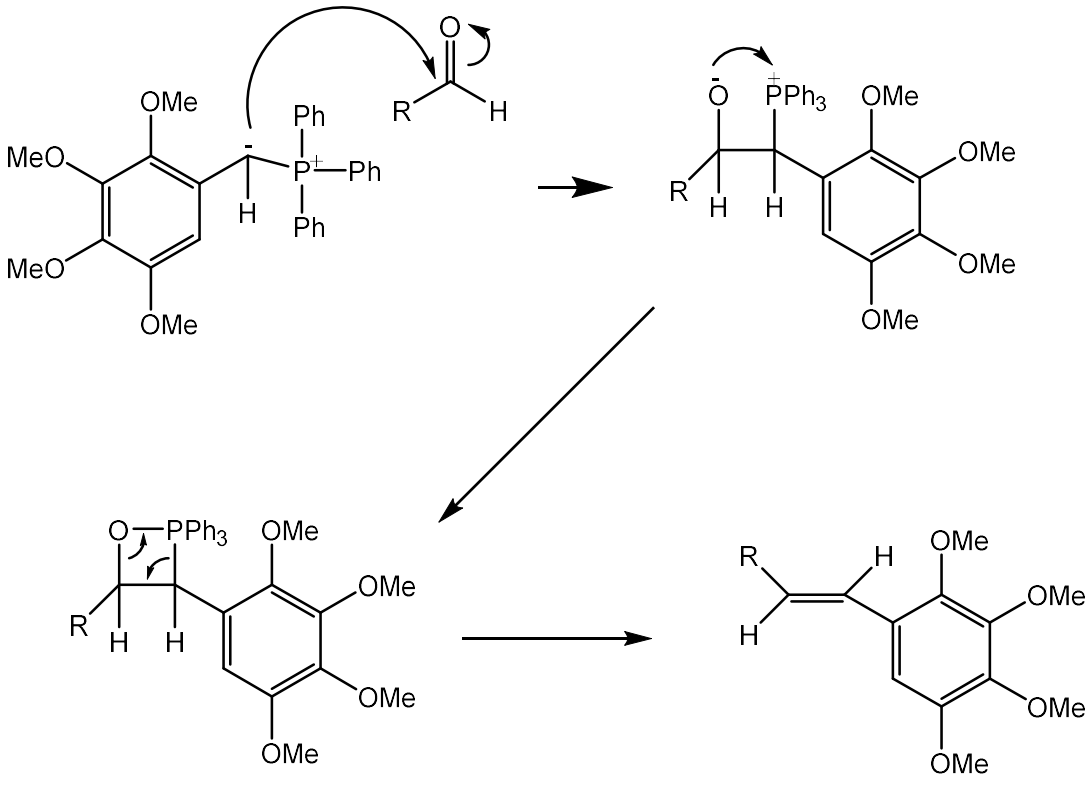

Figure 78. Mechanism of following steps of Wittig reaction.

After successfully synthesizing a large amount of the tetramethoxy phosphonium salt (about 8g), the next step was the reaction between phosphonium salt and various substituted benzaldehydes to produce stilbenes, in a Wittig reaction, using potassium carbonate as a base (Rambaud, Vecchio & Villieras, 1984). In the first part of the Wittig reaction, the K_2CO_3 removes an acidic proton from the phosphonium salt, forming a carbanion. The mechanism of this reaction step is outlined in figure 77.

The reaction mechanism for the steps that follow in the Wittig reaction are outlined in figure 78.

As a point of interest, the Wittig reaction was carried out using water as the solvent, which had the advantages that the reaction was more environmentally friendly and the work- up was easier compared to using organic solvents.

The method used for the Wittig reaction was based on a study by Rambaud et al, 1984. The original procedure suggested a reaction time for the Wittig reaction of 1.25 hours but during this project reaction time used was between four and seven hours, in an attempt to make the reaction proceed to completion as much as possible. Even after seven hours refluxing, some benzaldehyde still remained for many of the reactions, as evidenced by a clearly identifiable carbonyl peak in the proton NMR spectrum of the product. The structures of the ten CA- 4 analogues that were synthesized in this project are shown in figure 79.

The experimental conditions, such as the presence of salts and the solvent used for the reaction have a hand in determining the Wittig reaction selectivity (Robiette, Richardson, Aggarwal & Harvey, 2006) .

When the Wittig reaction is carried out using semi-stabilized triphenyl phosphonium ylides, as in this project, it is normal to obtain mixtures of *Z* and *E* isomers (Robiette, Richardson, Aggarwal & Harvey, 2006)

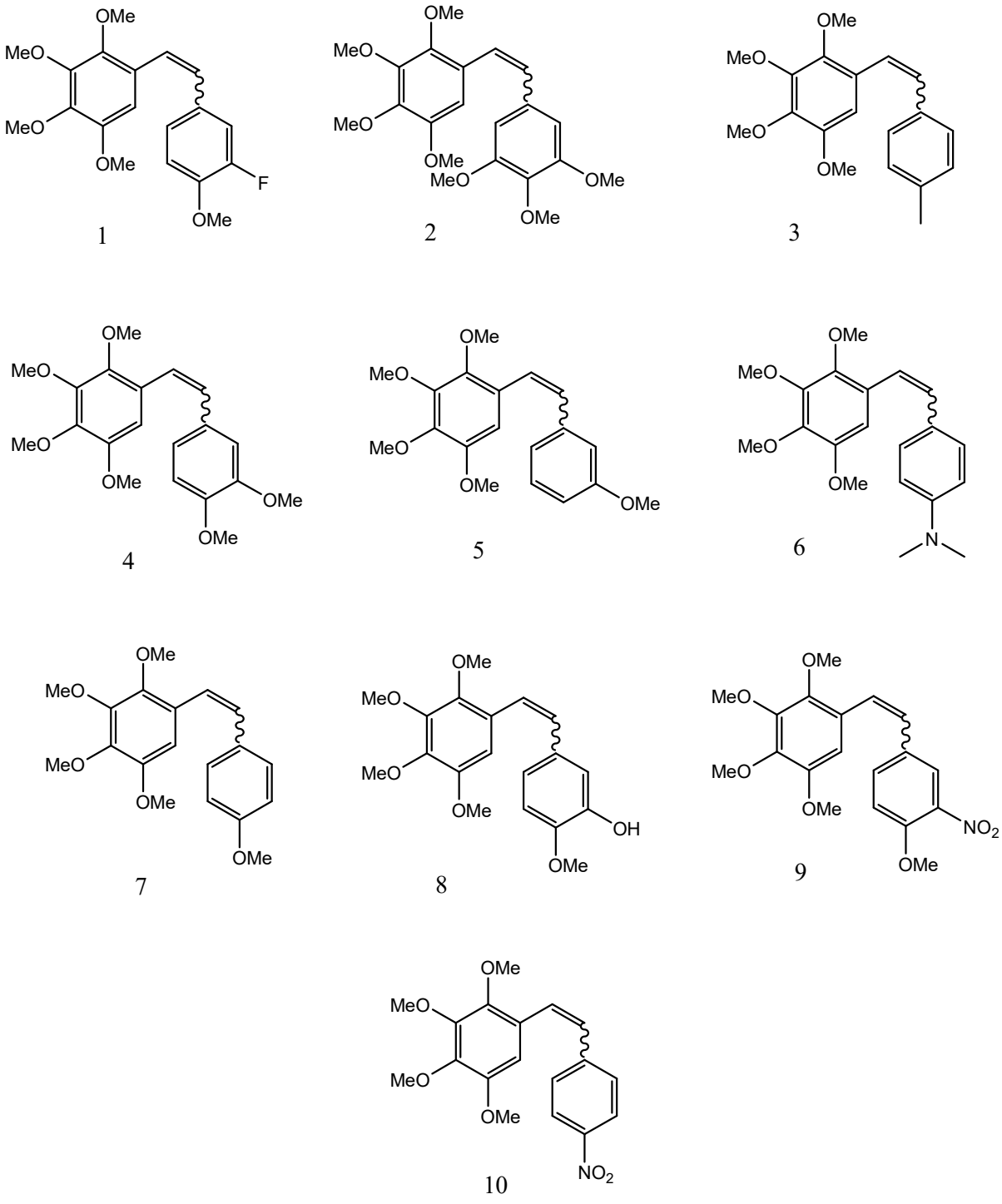

Figure 79. Diagram showing structures of CA- 4 analogues synthesized in this project.

Figure 80 is a table listing the various aldehydes which were utilised for synthesizing each of the compounds.

Compound	Aldehyde
1	3- fluoro- 4- methoxybenzaldehyde
2	3,4,5 - trimethoxybenzaldehyde
3	p - tolualdehyde
4	veratraldehyde
5	m - anisaldehyde
6	4 - dimethylaminobenzaldehyde
7	4 - methoxybenzaldehyde
8	3 - hydroxy -4 - methoxybenzaldehyde
9	4 - methoxy -3 - nitrobenzaldehyde
10	4 - nitrobenzaldehyde

Figure 80. Table showing substituted benzaldehydes used for CA -4 analogue syntheses in this project.

The Wittig reaction used resulted in both *cis* and *trans* isomers being obtained as the products for each separate reaction. The isomers were obtained with very poor stereoselectivity, with some product *cis* to *trans* ratios being close to 50: 50. Flash column chromatography was used both in an attempt to separate *cis* and *trans* isomers of synthesized stilbenes and also to separate stilbene products from leftover starting materials, with varying degrees of success. Each synthesized stilbene was put through a column, with a different hexane/ ethyl acetate eluent composition determined by TLC analysis of the stilbene product. In the cases of three of the stilbenes, after TLC analysis of fractions coming off the column, it was attempted to separate the *cis* and *trans* isomers in appreciable amounts. Subsequent NMR analysis however showed that separation was not complete, contrary to TLC evidence. With compounds 1 and 7 it was attempted to isolate both the *cis* isomer and the *trans* isomer. With compound 1 it was possible to isolate the *cis* isomer but on attempting to isolate the *trans* isomer the best that could be achieved was a *cis*: *trans*, 23:77 mixture. Likewise, in the case of compound 7, on attempting to isolate the *cis* isomer, the best that could be achieved was a *cis*: *trans*, 87: 13 mixture and on attempting to isolate the *trans* isomer the best that could be achieved was a *cis*: *trans*, 18: 82 mixture. On attempting to isolate the *cis* isomer of compound 9, the best that could be achieved was a *cis: trans* , 85: 15 mixture. It was found during this project that TLC techniques cannot be relied upon for separation of isomers, as even when a TLC plate appears to indicate the presence in a fraction off the column of just one isomer, small amounts of the other isomer are still present. With seven of the synthesized stilbenes, on putting them through a column, the

retention factors of the isomers coming off the column were so similar that separation of the isomers in appreciable amounts was observed to be impossible and it was therefore not attempted. In almost all cases therefore, the final product obtained for each stilbene synthesis was a mixture of *cis* and *trans* isomers. There was however one exception, it was possible to successfully isolate the *cis* isomer of the stilbene product formed in the Wittig reaction involving the 3- fluoro- 4- methoxybenzaldehyde in a measurable amount. The ratio of *cis* to *trans* isomers for each synthesized stilbene that separation was not possible for was obtained by mathematical manipulation of relevant integrated peaks in their proton NMR. The *E*/ *Z* ratios are the mathematical ratios of *cis* to *trans* isomers obtained for each synthesized CA-4 derivative. The *E*/*Z* ratios were obtained using the ^{1}H spectra of the mixture of isomers obtained for each synthesized compound. The first step was identification of all the relevant peaks. The next step was their integration. The peaks corresponding to the protons in the *cis* and *trans* double bonds were easily identifiable as quartets with coupling constant of approx. 12 Hz for the *cis* isomer and approx. 16 Hz for the *trans* isomer. The ratio of the integration of the peak of the *cis* olefinic bond to the integration of the peak of the *trans* olefinic bond was used to determine the *E*/ *Z* ratios for each compound.

The ratio of *cis* to *trans* isomers for each of the synthesized CA- 4 analogues is shown in figure 81.

Compound	Cis : trans ratio
1	100 : 0
2	30 : 70
3	47 : 53
4	49 : 51
5	43 : 57
6	43 : 57
7	87 : 13
8	52 : 48
9	85 : 15
10	n.d.

Figure 81. Table showing *cis*: *trans* ratio of synthesized CA- 4 analogues.

The yields obtained for the synthesized CA-4 derivatives were for compounds 2, 3, 4, 5, 6, and 8, for a mixture of the *cis* and *trans* isomers, due to the fact that the isomers could not be significantly separated. In the case of compounds 7 and 9, it was not possible to obtain a yield of isomers coming off the column due to the fact that unsuccessful separation of isomers was attempted and therefore not all fractions coming off the column were weighed.

One of the synthesized CA- 4 analogues, compound 8, was synthesized by the reaction between the phosphonium salt and protected 3- hydroxy- 4- methoxybenzaldehyde. Formation of the desired product requires that the hydroxyl group is protected during the Wittig reaction. This was initially attempted using a silyl protecting group. The silyl protected aldehyde (11) was successfully synthesized, however, on reacting it with the phosphonium salt; the yield of the stilbene product was exceptionally poor and therefore this reaction route was abandoned. It was then attempted to use a pyran protecting group on the 3-hydroxyl-4-methoxybenzaldehyde. The pyran protected aldehyde (12) was successfully synthesized and also successfully underwent the Wittig reaction with appreciable yields. The product of the Wittig reaction was then deprotected using acid, producing the desired compound.

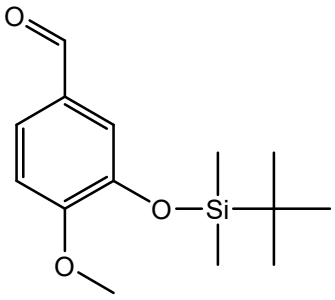

11

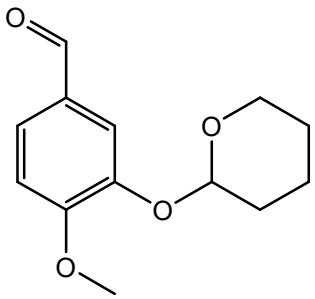

12

Figure 82. Diagram showing structures of protected 3-hydroxy-4-methoxybenzaldehyde

In the case of trimethoxy compound 2, following the Wittig reaction, TLC analysis of the crude product showed that the leftover aldehyde starting material and the *cis* and *trans* product isomers were co running i.e., had the same R_f value, making their separation impossible. This problem was solved by reacting the mixture with sodium borohydride. The sodium borohydride reacted with only the aldehyde, reducing it to an alcohol, with a different R_f value and allowing separation of product from starting material.

Compound 10 was synthesized but NMR analysis showed it was so impure after coming off the column that it was decided not to carry on with testing its biological activity.

2.3 Biological testing

The cytotoxic activities of the synthesized CA- 4 analogues against two cell lines, human liver cancer (HepG2) and human lung cancer (A549) were obtained using a MTT assay. The testing was performed by Dr Muna Abubaker, at the University of Salford.

2.3.1 MTT assay

The cytotoxic activities of synthesized CA- 4 analogues were obtained by determining cell viability in an MTT assay. For this, the Mosmann protocol, with certain changes was used. Each cell line underwent culturing within a sterilized flask (75 cm^3), containing RPMI- 1640 media, L – glutamine, 10 % calf serum and 1 % penicillin / streptomycin in a 37° C, 5 % CO_2 environment. Once the cultured cells had become confluent, the media was taken out, followed by washing of the flask three times with phosphate buffer saline. Trypsin – EDTA (2 ml) was then added to the flask followed by incubation for two minutes in a 5 % CO_2 , 100 % humidity, and 37° C atmosphere. After this, cells were dislodged from the flask surface by with gentle tapping. This was followed by adding 5 ml of media to the flask and then transferring the resulting suspension to a falcon tube. The suspension in the falcon tube underwent centrifugation for five minutes at 1500 rpm. The supernatant portion was then removed, and the solid portion was suspended again in three ml of media. 10 µL of the suspension was transferred to an Eppendorf tube and mixed with 10 µL of tryptan blue and mixed. A haemocytometer was then used to perform a cell count. Based on this cell count, appropriate dilution of cell suspensions was then carried out, followed by transferral to a 96 well plate at 5 × 10^3 cells /100µL / well. Incubation of the plates was then carried out for 24 hours in an atmosphere of 5 % CO_2, 37°C and 100 % humidity, to make sure cells adhered to the plates. With the test compounds, different concentrations of test solutions to be used were made up from a stock solution. 100 µL of test compound solution was added to each well, this was done for each of the different concentrations of test compound solution. Addition of each compound concentration to a well was carried out in triplicate. Some of the wells were left untreated to act as positive controls. As well as the sample compounds, the cells were also treated with cisplatin (Sigma- Aldrich) and CA- 4 (Sigma- Aldrich), to serve as controls. Following incubation for five days, MTT solution (50 µL) was added to each well, followed by another

three hours of incubation. Removal of the liquid left behind in the well a purple crystal, which was then dissolved in DMSO (200 µL). The plate was then placed on a plate reader to measure absorption values, which are directly linked to the number of viable cells left in each well after treatment. From the absorption values IC_{50} values were then calculated (Mosmann, 1983).

An assay was not run in this project for tubulin polymerization

2.3.2 IC_{50} values

The IC_{50} values for synthesized CA – 4 analogues against A549 and HepG2 cell line are shown in figure 83.

A549 cell line

Compound	IC 50
1	698.6 nM
2	9.7 µM
3	15.0 µM
4	16.0 µM
5	14.2 µM
6	1.6 µM
7	1.9 µM
8	1.2 µM
9	3.5 µM
10	n.d
CA- 4	516.9 nM
Cisplatin	4.6 µM

HepG2 cell line

Compound	IC 50
1	112.0 nM
2	9.9 µM
3	15.5 µM
4	13.1 µM
5	12.3 µM
6	553.5 nM
7	711.0 nM
8	297.8 nM
9	1.1 µM
10	n.d
CA - 4	20.7 nM
Cisplatin	2.4 µM

Figure 83. Tables showing IC_{50} values of synthesized CA- 4 analogues against A549 and HepG2 cancer cell lines.

The IC_{50} values shown in the tables represent activities of the *cis* isomer for each compound. The testing for most compounds was carried out on *cis*/ *trans* isomer mixtures. Assuming, as has been generally acknowledged that the *trans* isomer is close to inactive (McLoughlin & O'Boyle, 2020), IC_{50} values for each compound were calculated using the *cis*: *trans* ratios for each compound, obtained from the proton spectra. For instance, for compound 2,against the

A549 cell line, the IC_{50} of the *cis*: *trans* mixture was 32.3 µM and the *cis*: *trans* ratio was 30:70, therefore the activity of the *cis* isomer is 30 % of 32.3 µM which is 9.7 µM.

In this cytotoxicity assay, the two controls used were CA- 4 and cisplatin. Nine synthesized CA- 4 analogues were tested against human lung cancer (A549) and human liver cancer (HepG2) cell lines. All nine compounds showed good to excellent activity. Seven of the nine compounds tested, as well as the controls showed greater activity against the HepG2 cell line compared to the A549 cell line, in certain cases as much as six times more.

Compounds seven and eight, structures shown in figure 84, showed the same pattern that was observed in their corresponding trimethoxy analogues, as was mentioned earlier in this thesis under the heading 'modifications to the B ring', section 1.11.2, where the loss of the OH group on ring B of CA- 4 resulted in a compound that still displayed high cytotoxicity, even better than CA- 4 against some cell lines. In this case, compound eight, containing the OH group had an IC_{50} of 298 nM against the HepG2 cell line, while compound seven, the same compound minus the OH group was still highly active, but less so, displaying an IC_{50} of 711 nM.

7 8

Figure 84. Diagram showing structures of compounds seven and eight.

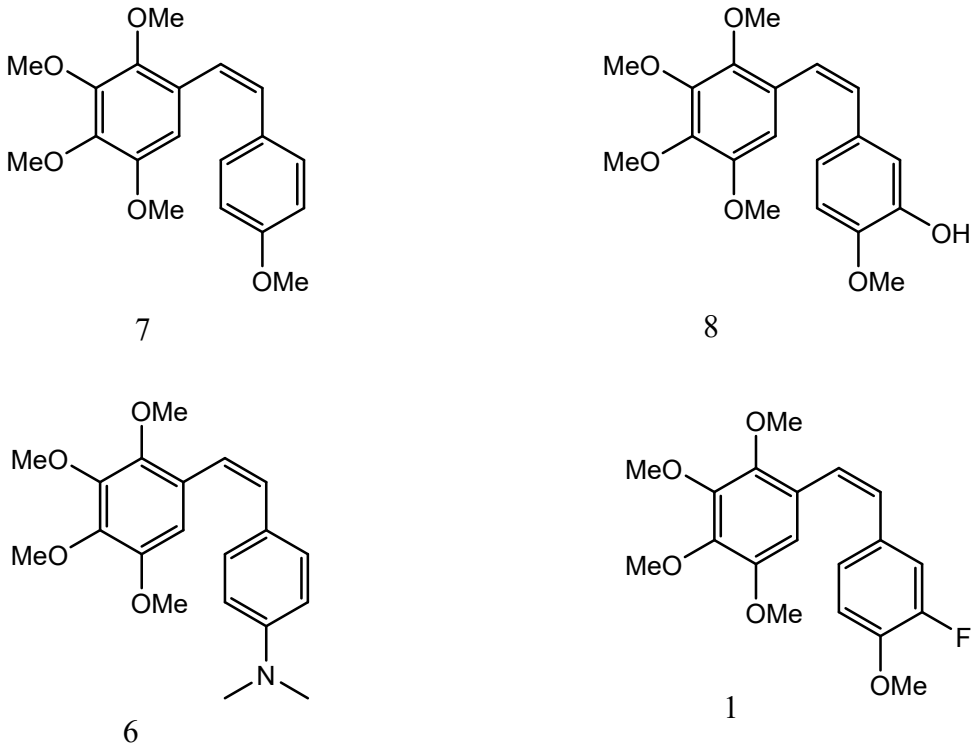

Figure 85. Diagram showing structures of synthesized compounds with highest activity

Of the four compounds displaying nanomolar activity against at least one cell line, structures shown in figure 85, three of them do not have an OH group at the 3' position on ring B.

Comparing compounds 1, 6 and 7 to compound eight, regarding activity against the HepG2 cell line, whilst compounds 6 and 7 which are still highly active but which don't have an OH group are less active than compound 8, with IC_{50} values of 554 and 711 nM respectively, compared to compound 8's IC_{50} of 298 nM, compound 1, the most active compound of all those synthesized, has a fluorine atom replacing the OH group and it is almost three times more active than compound 8, with an IC_{50} of 112 nM. A similar pattern was found for these compounds and the A549 cell line

These results support what is already established regarding the SAR of CA- 4 and its derivatives, which is that the OH group on ring B is not essential for activity.

Of the four compounds with nanomolar activity, three of them, compounds 6, 7and 8 displayed it against only the HepG2 cell line, while one of them, compound 1 displayed nanomolar activity against both cell lines. Compound 1 was however six times more potent against the HepG2 cell line, with an IC_{50} of 112 nM, compared to its activity against the A549 cell line of 699 nM.

Comparing the activity of the most potent synthesized compound, compound 1, to that of CA-4; while CA- 4 was five times more active than compound 1 against the HepG2 cell line, it was only 1.4 times more active than compound 1 against the A549 cell line.

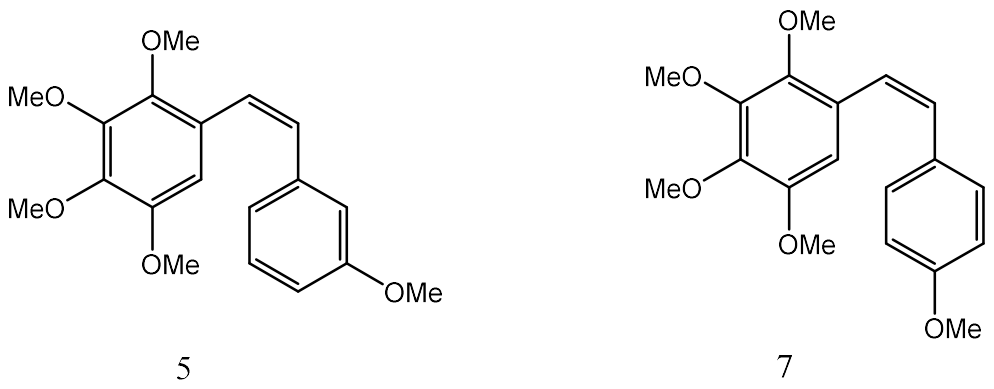

Figure 86. Diagram comparing structures of compounds 5 and 7.

As was found in the literature regarding trimethoxy CA- 4 analogues, where a shift in the position of the methoxy group on ring B from the four to the three-position resulted in a huge loss of activity, a similar effect was displayed with these analogues. With this project this was a comparison of compounds 5 and 7, structures shown in figure 86. Compound 7 has the methoxy group in the four position and displayed an IC_{50} of 711 nM against the HepG2 cell line, while compound 5 with the methoxy group in the three position displayed an IC_{50} of 12.3 µM against the same cell line. A similar pattern was observed for these compounds and the A549 cell line.

With CA- 4 derivatives, removal or substitution of the methoxy group on the B ring usually results in a huge loss of activity, however with trimethoxy CA- 4 analogues where a dimethylamino group replaced the methoxy group the compound was still highly active. It was a similar case with compound 6 in this project, a tetramethoxy dimethylamino derivative which displayed an IC_{50} value of 554 nM against the HepG2 cell line and 1.6 µM against the A549 cell line.

A search was carried out in literature in an attempt to obtain the activities of the trimethoxy analogues of all compounds synthesized in this project against both cell lines, for direct comparison of the activities of trimethoxy and tetramethoxy CA- 4 derivatives. Five were

discovered, the trimethoxy analogues of compounds 2, 3, 5, 6 and 7. Also, one of the synthesized compounds was the tetramethoxy analogue of CA- 4, which also allowed for direct comparison of trimethoxy and tetramethoxy analogues of CA- 4 derivatives.

Compound 2 displayed an IC_{50} of 9.7 μM against the A549 cell line, compared to its trimethoxy analogue which had a literature value of 5.6 μM against the same cell line (Blasco et al., 2018), an almost two-fold difference in activity.

Compound 7 displayed an IC_{50} of 1.9 μM against the A549 cell line, compared to its trimethoxy analogue which had a literature value of 2.2×10^{-5} μM against the same cell line. There is a drastic change in activity comparing compound seven and its trimethoxy analogue.

Compound 6 displayed an IC_{50} of 1.6 μM against the A549 cell line, compared to its trimethoxy analogue which had a literature value of 4.1 nM against the same cell line, an almost four hundred times difference in activity.

Compound 5 displayed an IC_{50} of 14.2 μM against the A549 cell line, compared to its trimethoxy analogue which had a literature value of 1.3×10^{-1} μM against the same cell line, an over hundredfold difference in activity (Cushman et al., 1991).

Compound 3 displayed an IC_{50} of 15 μM against the A549 cell line, compared to its trimethoxy analogue which had an average literature value of 6.9 nM against A549, MCF7, HT29, SKMEL5 and MLM cell lines (Nam, 2003). Also, a huge change in activity, over two thousand-fold.

Compound 8 displayed an IC_{50} value of 1.2 μM against the A549 cell line, compared to its trimethoxy analogue (CA- 4), which displayed an IC_{50} of 517 nM against the same cell line, over twice the activity. Against the HepG2 cell line, compound eight displayed an IC_{50} of 298 nM, compared to CA- 4 which displayed an IC_{50} of 21 nM against the same cell line, over 14 times more active.

In all 6 cases where tetramethoxy and trimethoxy analogues were directly compared, it was found that the trimethoxy analogues displayed higher cytotoxicity towards the A549 cell line. The same pattern was shown in the case of the HepG2 cell line and CA- 4 and its tetramethoxy analogue.

Five of the nine synthesized compounds were more active than the clinically used drug Cisplatin against both cell lines. In the case of the A549 cell line, compounds one, six, seven,

eight and nine displayed IC_{50} values of 698.6 nM, 1.6 μM, 1.9 μM, 1.2 μM and 3.5 μM respectively compared to Cisplatin's value of 4.6 μM against the same cell line. In the case of the HepG2 cell line, compounds one, six, seven, eight and nine displayed IC_{50} values of 112 nM, 553.5 nM, 711 nM, 297.8 nM and 1.1 μM respectively compared to Cisplatin's value against the same cell line of 2.4 μM.

All of the nine tested compounds were less active than CA- 4 against both cell lines.

From these results it is thought that the extra methoxy group on the A ring of the compounds influences the interaction of the compound with the Colchicine binding site (CBS) on tubulin. Tetramethoxy compounds are less active due to decreased strength of binding to the CBS.

3 Experimental

3.1 General experimental

TLC analysis was carried out using TLC silica gel 60 F_{254}, aluminium sheets. A 254 nm UV lamp was used for viewing plates.

Compound purification was achieved using flash column chromatography, with silica gel.

NMR analysis was carried out at the University of Salford on a Bruker Avance III 400/ 600 MHz spectrometer with the Topspin 4.1.0 software package used for analysing data.

The biological testing of synthesized compounds was carried out by Dr Muna Abubaker at the University of Salford.

High resolution mass spectrometry was carried out at the University of Cambridge. Liquid chromatography- mass spectrometry was carried out by Lee Harman at University of Salford.

IR spectra were obtained at University of Salford, using a Varian FTIR spectrometer and an OMNIC software package. Frequencies are shown as reciprocal cms.

3.2 Synthesized compounds

3.2.1 2, 3, 4- Trimethoxyphenol

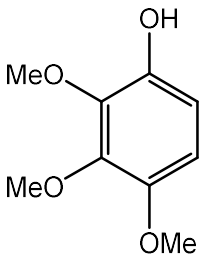

To a stirred solution of 2, 3, 4- trimethoxybenzaldehyde (11.76 g, 60 mmol) in H_2SO_4 / MeOH (1.2 : 120 v/v, 120 ml) at 0°C was added 27 % aqueous H_2O_2 (9.6 ml, 76.8 mmol). After 2 hours vigorous stirring at 0°C, a further aliquot of H_2O_2 (2.6 ml) was added and stirring was continued for a further hour. Another aliquot of aq. H_2O_2 (4.8 ml) was added and stirred for an hour, followed by another portion of aq. H_2O_2 (2.0 ml) another hour later. The reaction mixture was allowed to stir, under the same conditions for a further hour. The reaction mixture was allowed to stand overnight, at room temperature. Diethyl ether (300 ml) was then used to dilute the reaction mixture. The ethereal mixture was washed with H_2O (150 ml) followed by saturated aqueous brine (150 ml). The extract was dried with $MgSO_4$ and filtered. The diethyl ether was then removed using a rotary evaporator, leaving the title compound as a reddish-brown liquid (5.25 g, 53 %) (Tremblay & Sames, 2005).

^{1}H NMR ($CDCl_3$, 400 MHz): δ 3.82 (3H, s, CH_3O), 3.90 (3H, s, CH_3O), 3.96 (3H, s, CH_3O), 5.58 (1H, s, OH), 6.57 (1H, d, J = 8.92, H5), 6.64 (1H, d, J = 8.92, H6).

^{13}C NMR ($CDCl_3$, 100 MHz): δ 56.57 (CH_3O), 60.91 (CH_3O), 61.24 (CH_3O), 107.67 (C5), 108.65 (C6), 140.53 (C2), 142.3 (C3), 143.37 (C1), 146.94 (C4).

Liquid chromatography- mass spectrometry (negative electrospray ionization): $[M-H]^-$: calculated for $C_9H_{12}O_4$, 183; found 183.

IR: 3413 (OH str), 2996 (Ar CH str), 2940 (Al CH str), 1478 (CH bend).

3.2.2 1, 2, 3, 4-Tetramethoxybenzene

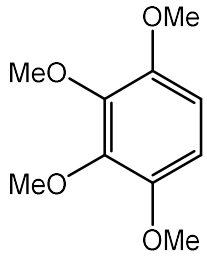

To a stirred solution of 2, 3, 4-trimethoxyphenol (5.25g, 28.6 mmol, 1.0 eq) and K_2CO_3 (11.78 g, 85.7 mmol, 3.0 eq) in acetone (64 ml) was added CH_3I (10.62 ml, 171.5 mmol, 6.0 eq). The reaction mixture was refluxed with stirring for 8 hours after which it was left to cool and stand overnight. The acetone was removed using a rotary evaporator. The solid product remaining was dissolved in CH_2Cl_2 and then filtered. The filtrate was dried with $MgSO_4$ and filtered again. The CH_2Cl_2 was then removed using a rotary evaporator, leaving the title compound as yellow-orange crystals, m.pt 87° C (4.15 g, 73.5 %) (Tremblay & Sames, 2005).

^{1}H NMR ($CDCl_3$, 400 MHz): δ 3.84 (6H, s, 2 × CH_3O), 3.92 (6H, s, 2 × CH_3O), 6.60 (2H, s, H5 & H6).

^{13}C NMR ($CDCl_3$, 100 MHz): δ 56.38 (2 × CH_3O), 61.2 (2 × CH_3O), 106.4 (C5 & C6), 143.35 (C2 & C3), 147.78 (C1 & C4).

Liquid chromatography – mass spectrometry (ESI^+): $[M-H]^+$: calculated for $C_{10}H_{14}O_4$, 199; found 199.

IR: 2941, 2861, 2835 (Al CH Str), 1493, 1479, 1461, 1445, 1425 (CH bend).

3.2.3 2, 3, 4, 5- Tetramethoxybenzaldehyde

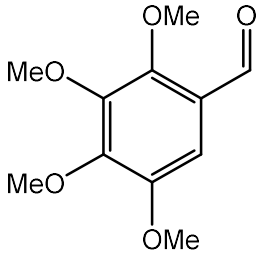

A solution of 1, 2, 3, 4- tetramethoxybenzene (6.25 g, 31.6 mmol) and hexamethylenetetramine (5.34 g, 27 mmol) in trifluoroacetic acid (85 ml) was stirred at 72°C for eight and a half hours then left to cool and stand at room temperature overnight. The trifluoroacetic acid was then removed using a rotary evaporator. The reaction mixture was then neutralized to a pH of approx. 7 using cold saturated aqueous $NaHCO_3$. The product was extracted using DCM (5 × 115 ml) followed by washing with brine (2 × 115 ml). The extract was dried with $MgSO_4$ and filtered. The DCM was then removed using a rotary evaporator. The product was purified using silica gel column chromatography (hexane / ethyl acetate, 7: 3) resulting in the title compound as a yellow-orange liquid (1.24 g, 17.2 %) (Bai et al., 2019).

^{1} H NMR ($CDCl_3$, 400 MHz): δ 3.88 (3H, s, CH_3O), 3.94 (3H, s, CH_3O), 3.98 (3H, s, CH_3O), 4.00 (3H, s, CH_3O), 7.11 (1H, s, H6), 10.30 (1H, s, CHO).

^{13} C NMR ($CDCl_3$, 100 MHz): δ 56.12 (CH_3O), 61.27 (CH_3O), 61.28 (CH_3O), 62.86 (CH_3O), 103.7 (C6), 124.0 (C1), 146.61 (C3), 149.32 (C4), 149.81 (C5), 152.32 (C2), 188.8 (CHO).

Liquid chromatography- mass spectrometry (ESI+): $[M-H]^+$: calculated for $C_{11}H_{14}O_5$, 227 ; found 227.

IR: 2940, 2843 (CHO Str), 1680 (C=O Str).

3.2.4 2, 3, 4, 5- Tetramethoxybenzyl alcohol

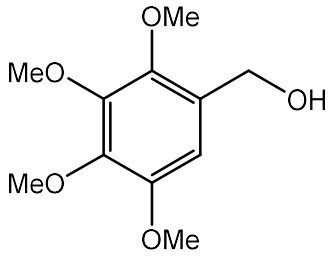

To a stirred solution of 2, 3, 4, 5- tetramethoxybenzaldehyde (2.55 g, 11.3 mmol) in methanol (25 ml) at 0°C was added $NaBH_4$ (0.725 g, 19 mmol) in small portions. After 15 mins stirring at 0°C, stirring was continued at room temp. for 1.5 hrs. The methanol was then removed using a rotary evaporator. Water (20 ml) was added, and the product was extracted using ethyl acetate (3 × 20 ml). The combined organic phases were dried with $MgSO_4$ and filtered. The ethyl acetate was removed using a rotary evaporator leaving the title compound as a dark, green liquid (1.43 g, 55.6 %) (Macé et al., 2015).

^{1} H NMR ($CDCl_3$, 400 MHz): δ 3.24 (1H, s, OH), 3.81 (3H, s, CH_3O), 3.82 (3H, s, CH_3O), 3.86 (3H, s, CH_3O), 3.91 (3H, s, CH_3O), 4.63 (2H, s, CH_2), 6.69 (1H, s, H6).

^{13} C NMR ($CDCl_3$, 100 MHz): δ 56.02 (CH_3O), 60.34 (CH_2OH), 60.96 (CH_3O), 61.03 (CH_3O), 61.22 (CH_3O), 106.29 (C6), 128.9 (C1), 142.18 (C4), 144.74 (C3), 146.69 (C2), 149.41 (C5).

High resolution mass spectrometry (ESI+): $[M-H]^+$: calculated for $C_{11}H_{16}O_5$, 228.0998; found 228.0995.

IR : 3432 (OH Str), 2938, 2875 (Al CH Str), 1490, 1464 (CH Bend).

3.2.5 2, 3, 4, 5- Tetramethoxybenzyl bromide

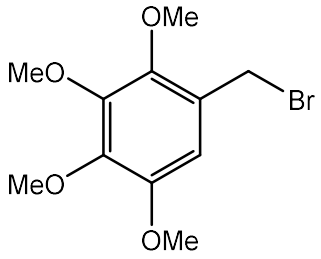

To a stirred solution of 2, 3, 4, 5- tetramethoxybenzyl alcohol (3.22 g, 14.1 mmol) in DCM (20 ml) at 0°C was added PBr_3 (0.46 ml, 4.9 mmol). After 1 hour stirring at 0°C a further aliquot of PBr_3 (0.46 ml, 4.9 mmol) was added. The reaction mixture was then allowed to stir for a further hour. The mixture was then washed with saturated aqueous $NaHCO_3$ (30 ml) followed by H_2O (30 ml) and brine (30 ml).The mixture was dried with $MgSO_4$ and filtered. The solvent was then removed using a rotary evaporator leaving the title compound as a light brown liquid (2.71 g, 96.8 %) (ElSohly, Ma, Turner & ElSohly, 1984).

^{1} H NMR ($CDCl_3$, 400 MHz): δ 3.83 (3H, s, CH_3O), 3.89 (3H, s, CH_3O), 3.91 (3H, s, CH_3O), 3.93 (3H, s, CH_3O), 4.53 (2H, s, CH_2), 6.63 (1H, s, H6).

^{13} C NMR ($CDCl_3$, 100 MHz): δ 28.76 (CH_2Br), 56.19 (CH_3O), 61.04 (CH_3O), 61.16 (CH_3O), 61.26 (CH_3O), 107.99 (C6), 125.64 (C1), 143.72 (C4), 145.92 (C3), 147.13 (C2), 149.50 (C5).

3.2.6 2, 3, 4, 5-Tetramethoxybenzyltriphenyl bromide

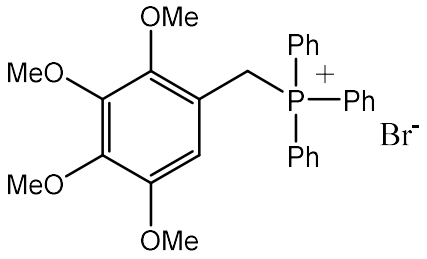

To a stirred solution of 2, 3, 4, 5- tetramethoxybenzyl bromide (3.15 g, 12.1 mmol) in toluene (20 ml) was added dropwise a solution of triphenylphosphine (2.32 g, 11.1 mmol) in toluene (20 ml). The reaction mixture was then vigorously stirred for 24 hour after which the title compound was filtered off as a white solid. M.pt 164 – 168 °C. Novel compound. (3.98 g, 66 %) (Pettit, Singh, Niven, Hamel & Schmidt, 1987).

^{1} H NMR ($CDCl_3$, 400 MHz): δ 3.55 (3H, s, CH_3O), 3.56 (3H, s, CH_3O), 3.69 (3H, s, CH_3O), 3.84 (3H, s, CH_3O), 5.34 (2H, d, CH_2, J = 14.05), 6.75 (1H, d, J= 2.17 Hz, CH).

^{13} C NMR ($CDCl_3$, 100 MHz): δ 25.44 (C7, CH_2), 109.82 (C6, CH), 118.1 (C8), 130.06 (C9), 134.32 (C10), 134.92 (C11), 114.42, 143.37, 146.0, 146.68 & 149.31 (C1→ C5).

High resolution mass spectrometry (ESI+): $[M-H]^+$: calculated for $C_{29}H_{30}O_4P$, 473.1882; found 473.1890.

3.2.7 Protocol A

A stirred mixture of 2, 3, 4, 5- tetramethoxybenzyltriphenylphosphonium bromide (1.0 eq), potassium carbonate (2.0 eq) and a benzaldehyde (1.0 eq) in water (30 ml) was heated under reflux for several hours. The reaction mixture was left to stand at room temperature overnight and extracted with DCM (50 ml × 3). The combined extracts were washed with saturated brine solution (50 ml × 2) followed by drying with magnesium sulphate. After vacuum filtration, the solvent was removed using a rotary evaporator to give the crude stilbene as a mixture of *E*- and *Z*- isomers (Rambaud, Vecchio & Villieras, 1984). Separation and purification of the isomers was attempted by chromatography, using hexane/ ethyl acetate as eluent. The diagram shown in figure 87 shows how protons and carbon atoms were assigned for NMR analysis.

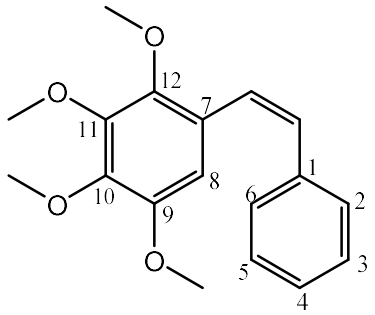

Figure 87. Diagram showing proton and carbon assignments

3.2.8 (*Z*)-1-(3-Fluoro-4-methoxyphenyl)-2-(2, 3, 4, 5-tetramethoxyphenyl)-ethene (1)

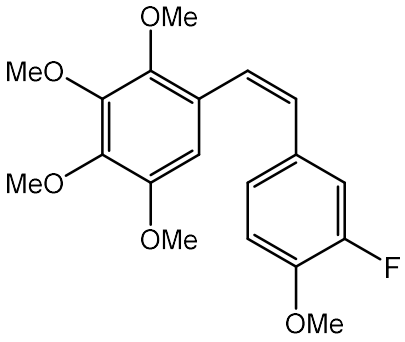

Protocol A was carried out using phosphonium salt (0.5 g, 0.9 mmol), potassium carbonate (0.25 g, 1.8 mmol) and 3- fluoro- 4- methoxy benzaldehyde (0.14 g, 0.9 mmol). The reaction was heated in water (30 ml) under reflux for seven hours. The crude stilbene (0.46 g, 146 %) was purified on silica (hexane/ ethyl acetate, 30: 1). The *Z*- isomer came off the column as a light-yellow liquid (0.044 g, 13.97 %).

^{1} H NMR ($CDCl_3$, 400 MHz): δ 3.56 (3H, s, CH_3O), 3.83 (3H, s, CH_3O), 3.88 (3H, s, CH_3O), 3.92 (3H, s, CH_3O), 3.96 (3H, s, CH_3O), 6.51 (1H, s, H8), 6.52 (1H, d, *J*= 12.3, C=CH), 6.62 (1H, d, *J*= 12.3, C=CH), 6.84 (1H, t, *J*= 8.61, H5), 7.01 (1H, dd, *J*= 8.54, H6), 7.05 (1H, dd, *J*= 1.69, *J*= 12.56, H2).

^{13} C NMR ($CDCl_3$, 100 MHz): δ 55.95 (CH_3O), 56.2 (CH_3O), 56.38 (CH_3O), 61.27 (CH_3O), 61.38 (CH_3O), 107.2 (CH, C8), 112.9 (C=C), 116.3 (CH, C2), 124.8 (C=C), 125.2 (CH, C5), 128.8 (CH, C6), 130.3 (C, C1), 146.7 (C, C4), 151.9 (C, C3), 142.6, 145.81, 147.12 & 149.01 (C9, C10, C11 & C12), 125.81/ 127.87 (C7).

High resolution mass spectrometry (ESI+): $[M-H]^+$: calculated for $C_{19}H_{21}FO_5$, 349.1451; found 349.1451.

IR: 2935 (Ar CH Str), 2838 (Al CH Str), 1616 (C=C).

3.2.9 (*Z*)-1-(3, 4, 5-Trimethoxyphenyl)-2-(2, 3, 4, 5-tetramethoxyphenyl)-ethene (2)

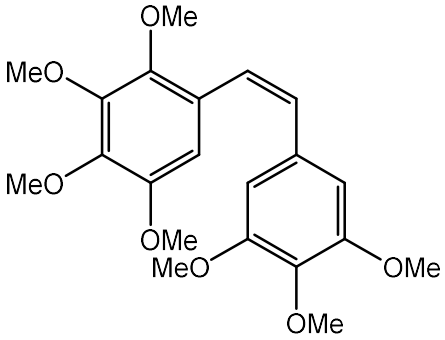

Protocol A was carried out using phosphonium salt (0.75 g, 1.4 mmol), potassium carbonate (0.375 g, 2.7 mmol) and 3, 4, 5- trimethoxybenzaldehyde (0.27 g, 1.4 mmol). The reaction was heated in water (30 ml) under reflux for seven hours. The crude stilbene (0.78 g, 147 %) was purified on silica (hexane/ ethyl acetate, 8: 2). A mixture of *E*- and *Z*- isomers came together off the column as a white solid (0.19 g, 35 %, *cis* : *trans*, 30 : 70).

^{1} H NMR ($CDCl_3$, 400 MHz): δ 3.57, 3.71, 3.83, 3.85, 3.87, 3.89, 3.90, 3.93, 2 × 3.95, 3.96, 3.98 (7 × CH_3O, *cis* and *trans* methoxy groups indistinguishable), 6.51 (2H, s, H2 & H6), 6.53 (1H, s, H8), 6.58 (1H, d, *J*= 12.14, C=CH), 6.67 (1H, d, *J*= 12.14, C=CH).

^{13} C NMR ($CDCl_3$, 100 MHz): δ 55.87, 55.96, 2 × 56.17, 56.24, 60.87, 60.97, 61.2, 61.23,2 × 61.29, 61.68 (7 × CH_3O, *cis* and *trans* methoxy groups indistinguishable), 106.14 (2 × CH, C2 & C6), 107.51 (CH, C8), 124.99 (C=C), 125.68 (C, C7), 130.35 (C=C), 132.58 (C, C1), 137.24 (C, C4), 142.45 (C, C10), 145.66 (C, C11), 147.11 (C, C9), 149.01 (C, C12), 152.87 (C, C3 & C5).

High resolution mass spectrometry (ESI+): $[M-H]^+$: calculated for $C_{21}H_{26}O_7$, 391.1757; found 391.1753.

IR: 2937 (Ar CH Str), 2837 (Al CH Str), 1580 (C=C).

3.2.10 (*E*)-1-(3, 4, 5-Trimethoxyphenyl)-2-(2, 3, 4, 5-tetramethoxyphenyl)-ethene (2)

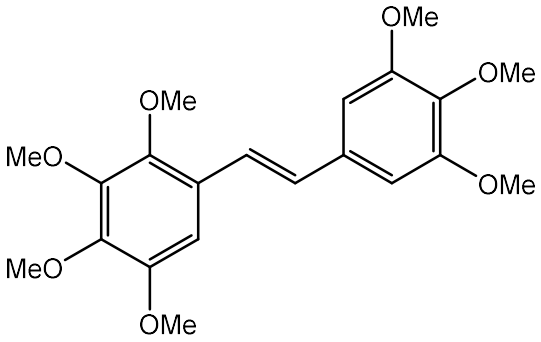

This compound was produced together with its isomer (*Z*)-1-(3, 4, 5-Trimethoxyphenyl)-2-(2, 3, 4, 5-tetramethoxyphenyl)-ethene and therefore involves the same method of preparation.

^{1} H NMR ($CDCl_3$, 400 MHz): δ 3.57, 3.71, 3.83, 3.85, 3.87, 3.89, 3.90, 3.93, 2 × 3.95, 3.96, 3.98 (7 × CH_3O, *cis* and *trans* methoxy groups indistinguishable), 6.78 (2H, s, H2 & H6), 6.88 (1H, s, H8), 6.99 (1H, d, *J*= 16.33, C=CH), 7.29 (1H, d, *J* = 16.33, C=CH).

^{13} C NMR ($CDCl_3$, 100 MHz): δ 55.87, 55.96, 2 × 56.17, 56.24, 60.87, 60.97, 61.2, 61.23,2 × 61.29, 61.68 (7 × CH_3O, *cis* and *trans* methoxy groups indistinguishable), 103.26 (CH, C8), 103.66 (2 × CH, C2 & C6), 122.35 (C=C), 125.68 (C, C7), 128.86 (C=C), 133.41 (C, C1), 137.99 (C, C4), 142.91 (C, C10), 145.67 (C, C11), 147.26 (C, C9), 149.79 (C, C12), 153.43 (2 × C, C3 & C5).

High resolution mass spectrometry (ESI+): $[M-H]^+$: calculated for $C_{21}H_{26}O_7$, 391.1757; found 391.1753.

IR: 2937 (Ar CH Str), 2837 (Al CH Str), 1580 (C=C).

3.2.11 (*Z*)-1-(4-Methylphenyl)-2-(2, 3, 4, 5-tetramethoxyphenyl)-ethene (3)

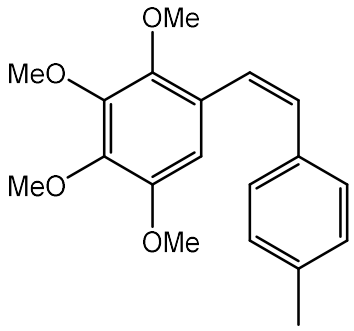

Protocol A was carried out using phosphonium salt (0.5 g, 0.9 mmol), potassium carbonate (0.25 g, 1.8 mmol) and 4- tolualdehyde (0.11 g, 0.9 mmol). The reaction was heated under reflux for seven hours. The crude stilbene (0.33 g, 114 %) was purified on silica (hexane/ ethyl acetate, 15: 1). A mixture of *E*- and *Z*- isomers came together off the column as a thick yellow oil (0.13 g, 47 %, *cis*: *trans*, 47:53).

^{1} H NMR ($CDCl_3$, 400 MHz): δ 2.29 (3H, s, CH_3), 3.46, 3.82, 3.83, 3.89, 3.90, 3.91,3.94, 3.95 (4 × CH_3O, *cis* and *trans* indistinguishable), 6.48 (1H, s, H8),6.59 (1H, d, *J*= 12.17, C= CH), 6.63 (1H, d, *J*= 12.17, C= CH),7.04 (2H, d, *J*= 8.39, H2 & H6), 7.17 (2H, d, *J*= 8.39, H3 & H5).

^{13} C NMR ($CDCl_3$, 100 MHz): δ 21.22 & 21.27 (CH_3, *cis* and *trans* indistinguishable), 55.76, 56.23, 2 × 61.25, 61.27, 61.3, 61.4, 61.6 (4 × CH_3O, *cis* and *trans* indistinguishable), 107.43 (CH, C8),124.34 (C= C), 125.69 (C, C7), 128.75 (CH, C3 & C5), 128.85 (CH, C2 & C6), 130.3 (C=C), 134.29 (C, C1), 136.88 (C, C10), 142.32 (C, C11), 145.77 (C, C4), 146.99 (C, C9), 148.81 (C, C12).

High resolution mass spectrometry: $[M + H]^+$: Calculated for $C_{19}H_{22}O_4$, 315.1596; found 315.1595.

IR: 2934 (Ar CH Str), 2865, 2834 (Al CH Str), 1574 (C=C).

3.2.12 (*E*)-1-(4-Methylphenyl)-2-(2, 3, 4, 5-tetramethoxyphenyl)-ethene (3)

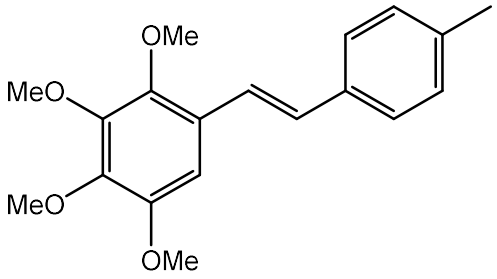

This compound was produced together with its isomer (*Z*)-1-(4-Methylphenyl)-2-(2, 3, 4, 5-tetramethoxyphenyl)-ethene and therefore involves the same method of preparation.

^{1} H NMR ($CDCl_3$, 400 MHz): δ 2.36 (3H, s, CH_3), 3.46, 3.82, 3.83, 3.89, 3.90, 3.91, 3.94, 3.95 (4 × CH_3O, *cis* and *trans* indistinguishable), 6.87 (1H, s, H8), 7.01 (1H, d, *J*= 16.42, C=CH), 7.17 (2H, d, *J*= 7.98, H2 & H6), 7.33 (1H, d, *J*= 16.42, C=CH), 7.43 (2H, d, *J*= 7.98, H3 & H5).

^{13} C NMR ($CDCl_3$, 100 MHz): δ 21.22 & 21.27 (CH_3, *cis* and *trans* indistinguishable), 55.76, 56.23, 2 × 61.25, 61.27, 61.3, 61.4, 61.6 (4 × CH_3O, *cis* and *trans* indistinguishable), 103.09 (C8, CH), 121.81 (C=C), 126.03 (C7, C), 126.45 (C3 & C5, CH), 128.8 (C=C), 128.88 (C2 & C6, CH), 134.88 (C1, C), 137.47 (C10, C), 142.73 (C11, C), 145.61 (C4, C), 147.26 (C9, C), 149.77 (C12, C).

High resolution mass spectrometry: $[M + H]^+$: calculated for $C_{19}H_{22}O_4$, 315.1596; found 315.1595

IR: 2934 (Ar CH Str), 2865, 2834 (Al CH Str), 1574 (C=C).

3.2.13 *(Z)*-1-(3, 4-Dimethoxyphenyl)-2-(2, 3, 4, 5-tetramethoxyphenyl)-ethene (4)

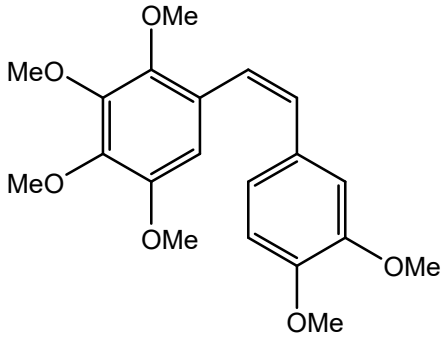

Protocol A was carried out using phosphonium salt (0.75 g, 1.4 mmol), potassium carbonate (0.37 g, 2.8 mmol) and veratraldehyde (0.23 g, 1.4 mmol). The reaction was heated in water (30 ml) under reflux for seven hours. The crude stilbene (0.84 g, 171 %) was purified on silica (hexane, ethyl acetate, 8: 2). A mixture of *E*- and *Z*- isomers came together off the column as a thick, yellow oil (0.34 g, 70 %, *cis*: *trans*, 49: 51).

^{1} H NMR ($CDCl_3$, 400 MHz): δ 3.54, 3.65, 3.82, 3.84, 3.85, 3.88, 3.896, 3.90, 3.92, 2 × 3.94, 3.96 (6 × CH_3O*, cis* and *trans* methoxy groups indistinguishable), 6.53 (1H, s, H8), 6.55 (1H, d, *J*= 12.11, C=CH), 6.59 (1H, d, *J*= 12.11, C=CH), 6.75 (1H, d, *J*= 8.29, H5), 6.79 (1H, d, *J*=1.91, H2). The H6 proton, with 2/ 8 Hz coupling was not visible on the spectrum due to too many overlapping signals.

^{13} C NMR ($CDCl_3$, 100 MHz): δ 55.46, 55.8, 55.9, 2 × 55.92, 56.2, 61.19, 61.2, 3 × 61.3, 61.6 (6 × CH_3O, *cis* and *trans* methoxys indistinguishable), 107.44 (CH, C8), 110.76 (CH, C5), 111.74 (CH, C2), 123.83 (C=C), 125.96 (C, C7), 129.81 (C, C1), 130.15 (C=C), 142.28 (C, C10), 145.63 (C, C11), 147.1 (C, C9)148.19 (C, C12), 148.9 (C, C3), 148.98 (C, C4). Not being able to identify the H6 proton in turn means that the C6 carbon cannot be identified on the HMQC.

High resolution mass spectrometry (ESI+): $[M\text{-}H]^+$: calculated for $C_{20}H_{24}O_6$, 361.1651; found 361.1646.

IR: 2995 (Ar CH Str), 2934, 2834 (Al CH Str), 1683 (C=C).

3.2.14 (*E*)-1-(3, 4-Dimethoxyphenyl)-2-(2, 3, 4, 5-tetramethoxyphenyl)-ethene (4)

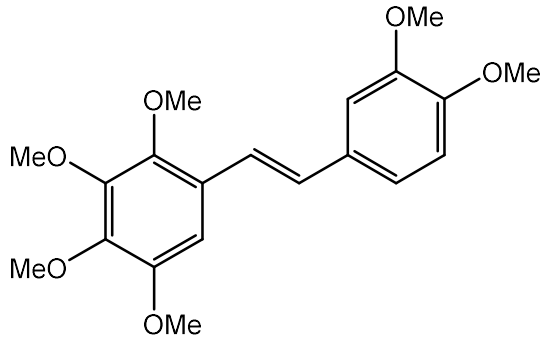

This compound was produced together with its isomer (*Z*)-1-(3, 4-Dimethoxyphenyl)-2-(2, 3, 4, 5-tetramethoxyphenyl)-ethene and therefore involves the same method of preparation

^{1} H NMR ($CDCl_3$, 400 MHz): δ 3.54, 3.65, 3.82, 3.84, 3.85, 3.88, 3.896, 3.90, 3.92, 2 × 3.94, 3.96 (6 × CH_3O, *cis* and *trans* methoxy groups indistinguishable), 6.84 (1H, d, *J*= 1.94, H2), 6.87 (1H, s, H8), 6.99 (1H, d, *J*= 16.49,C=CH), 7.08 (1H, d, *J*= 8.73, H5), 7.24 (1H, d, *J*= 16.49, C=CH). The H6 proton, with 2/ 8 Hz coupling is not visible on the spectrum due to too many overlapping signals.

^{13} C NMR ($CDCl_3$, 100 MHz): δ 55.46, 55.8, 55.9, 2 × 55.92, 56.2, 61.19, 61.2, 3 × 61.3, 61.6 (6 × CH_3O, *cis* and *trans* methoxys indistinguishable), 120.9 (C=C), 126.01 (C7, C), 128.65 (C=C), 130.78 (C1, C), 142.61 (C10, C), 145.46 (C11, C), 147.23 (C9, C), 148.3 (C12, C), 149.12 (C4, C), 149.75 (C3, C). C2, C5, C6 and C8 signals could not be identified on the HMQC.

High resolution mass spectrometry (ESI+): $[M-H]^+$: calculated for $C_{20}H_{24}O_6$, 361.1651; found 361.1646.

IR: 2995 (Ar CH Str), 2934, 2834 (Al CH Str), 1683 (C=C).

3.2.15 *(Z)*-1-(3-Methoxyphenyl)-2-(2, 3, 4, 5-tetramethoxyphenyl)-ethene (5)

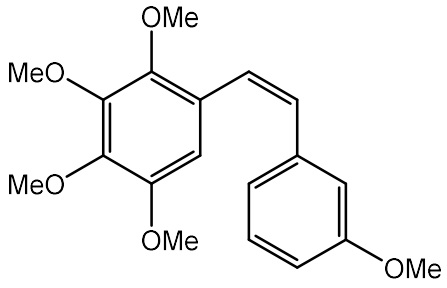

Protocol A was carried out using phosphonium salt (0.75 g, 1.4 mmol), potassium carbonate (0.38 g, 2.8 mmol) and 3- anisaldehyde (0.19 g, 1.4 mmol). The reaction was heated in water (30 ml) under reflux for seven hours. The crude stilbene (0.79 g, 176 %) was purified on silica (hexane/ ethyl acetate, 12: 1). A mixture of *E*- and *Z*- isomers came together off the column as a clear liquid (0.26 g, 57 %, *cis* : *trans*, 43:57).

^{1} H NMR ($CDCl_3$, 400 MHz): δ 3.50 (CH_3O), 3.82 (CH_3O), 3.83 (CH_3O), 3.84 (CH_3O), 3.9 (CH_3O), 6.47 (1H, s, H8), 6.60 (1H, d, *J*= 12.21, C=CH), 6.68 (1H, d, *J*= 12.21, C=CH), 6.73 (1H, multiplet, *J*= 2.64, *J*= 8.28, H4), 6.81 (1H, dd, H2), 6.87 (1H, multiplet,H6), 7.15 (1H, dd, *J*= 7.9 Hz, H5).

^{13} C NMR ($CDCl_3$, 100 MHz): δ 55.2 (CH_3O), 56.2 (CH_3O), 61.2 (CH_3O), 61.3 (CH_3O), 61.6 (CH_3O), 107.5 (CH, C8), 113.0 (CH, C4), 114.0 (CH, C2), 121.5 (CH, C6), 125.3 (C=C), 125.4 (C, C7), 129.6 (CH, C5), 130.2 (C=C), 138.6 (C, C1), 139.1 (C, C12), 142.4 (C, C11), 147.0 (C, C10), 148.8 (C, C9), 159.4 (C, C3).

High resolution mass spectrometry (ESI+): $[M-H]^+$: calculated for $C_{19}H_{22}O_5$, 331.1545; found 331.1537.

IR: 2995 (Ar CH Str), 2935, 2873 (Al CH Str), 1596 (C=C).

3.2.16 (*E*)-1-(3-Methoxyphenyl)-2-(2, 3, 4, 5-tetramethoxyphenyl)-ethene (5)

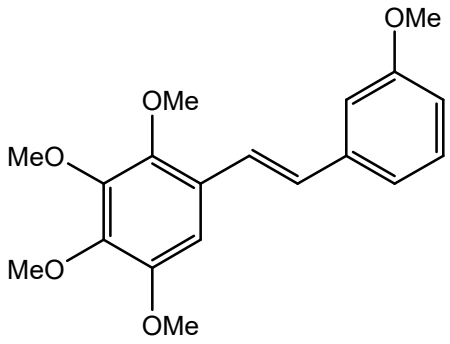

This compound was produced together with its isomer (*Z*)-1-(3-Methoxyphenyl)-2-(2, 3, 4, 5-tetramethoxyphenyl)-ethene and therefore involves the same method of preparation.

^{1} H NMR ($CDCl_3$, 400 MHz): δ 3.67 (CH_3O), 3.88 (CH_3O), 3.91 (CH_3O), 3.93 (CH_3O), 3.95 (CH_3O), 6.87 (1H, multiplet, H4), 6.88 (1H, s, H8), 7.07 (1H, dd, *J*= 1.9, H2), 7.13 (1H, multiplet, H6), 7.27 (1H, dd, *J*= 7.8, H5).

^{13} C NMR ($CDCl_3$, 100 MHz): δ 55.0 (CH_3O), 55.7 (CH_3O), 61.2 (CH_3O), 61.3 (CH_3O), 61.4 (CH_3O), 103.2 (CH, C8), 111.8 (CH, C2), 113.1 (CH, C4), 123.1 (C=C), 125.7 (C, C7), 128.7 (C=C), 128.7 (CH, C6), 129.2 (CH, C5), 138.6 (C, C12), 139.1 (C, C1), 143.0 (C, C10), 147.2 (C, C11), 149.8(C, C9), 159.9 (C, C3).

High resolution mass spectrometry (ESI+): $[M-H]^+$: calculated for $C_{19}H_{22}O_5$, 331.1545; found 331.1537.

IR: 2995 (Ar CH Str), 2935, 2873 (Al CH Str), 1596 (C=C).

3.2.17 (*Z*)-1-(4-Dimethylaminophenyl)-2-(2, 3, 4, 5-tetramethoxyphenyl)-ethene (6)

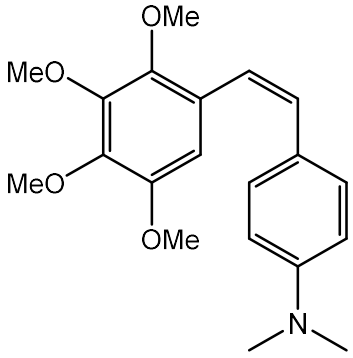

Protocol A was carried out using phosphonium salt (0.75 g, 1.4 mmol), potassium carbonate (0.375 g, 2.8 mmol) and 4- dimethylaminobenzaldehyde (0.2 g, 1.4 mmol). The reaction was heated in water (30 ml) under reflux for 7.5 hours. The crude stilbene (0.73 g, 156 %) was purified on silica (hexane/ ethyl acetate, 9: 1). A mixture of *E*- and *Z*- isomers came together off the column as a dark yellow liquid (0.302 g, 64.24 %, *cis* : *trans,* 43 : 57)

^{1} H NMR ($CDCl_3$, 400 MHz): δ 2.91 (6H, s, 2 × NCH_3), 3.06, 3.54, 3.81, 3.83, 3.89, 3.90, 3.901, 3.95 (4 × CH_3O, *cis* and *trans* indistinguishable), 6.44 (1H, d, *J*= 12.25, C=CH), 6.51 (1H, d, *J*= 12.25, C=CH), 6.58 (2H, d, *J*= 8.57, H3 & H5), 6.63 (1H, s, H8), 6.72 (2H, d, *J*= 8.57, H2 & H6).

^{13} C NMR ($CDCl_3$, 100 MHz): δ 40.46 (2 × NCH_3), 55.95, 56.22, 61.24, 61.26, 2 × 61.3, 61.33, 61.56 (4 × CH_3O, *cis* and *trans* methoxy groups indistinguishable), 107.44 (CH, C8), 111.54 (2 × CH, C3 & C5), 112.51 (2 × CH, C2 & C6), 121.59 (C=C), 125.2 (C, C7), 126.55 (C, C1), 130.46 (C=C), 142.0 (C, C10), 145.64 (C, C11), 147.02 (C, C9), 148.9 (C, C12), 149.62 (C, C4).

High resolution mass spectrometry (ESI+): $[M-H]^+$: calculated for $C_{20}H_{25}NO_4$, 344.1862; found 344.1862.

IR: 2933 (Ar CH Str), 2823 (AL CH Str), 1679 (C=C).

3.2.18 (*E*)-1-(4-Dimethylaminophenyl)-2-(2, 3, 4, 5-tetramethoxyphenyl)-ethene (6)

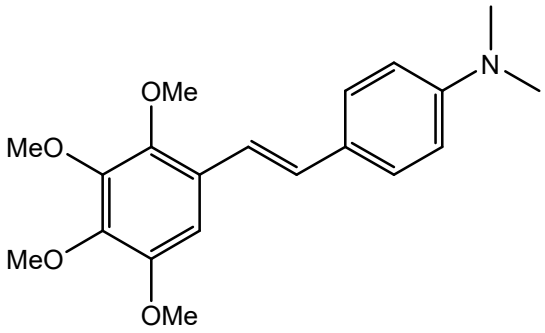

This compound was produced together with its isomer (*Z)*-1-(4-Dimethylaminophenyl)-2-(2, 3, 4, 5-tetramethoxyphenyl)-ethene and therefore involves the same method of preparation

^{1} H NMR ($CDCl_3$, 400 MHz): δ 2.97 (6H, s, 2 × NCH_3), 3.06, 3.54, 3.81, 3.83, 3.89, 3.90, 3.901, 3.95 (4 × CH_3O, *cis* and *trans* indistinguishable), 6.87 (1H, s, H8), 6.97 (1H, d, *J*= 16.42, C=CH), 7.24 (1H, d, *J*= 16.42, C=CH), 7.44 (2H, d, *J*= 8.79, H3 & H5), 7.73 (2H, d, *J*= 8.79, H2 & H6).

^{13} C NMR ($CDCl_3$, 100 MHz): δ 40.51 (2 × NCH_3), 55.95, 56.22, 61.24, 61.26, 2 × 61.3, 61.33, 61.56 (4 × CH_3O, *cis* and *trans* methoxy groups indistinguishable), 102.83 (CH, C8), 126.14 (C, C7), 126.74 (C, C1), 127.61 (2 × CH, C3 & C5), 128.98 (C=C), 131.99 (2 × CH, C2 & C6), 142.11 (C, C10), 145.19 (C, C11), 147.25 (C, C9), 149.75 (C, C12), 150.1 (C, C4). One of the trans olefinic carbon signals was not visible on the spectrum.

High resolution mass spectrometry (ESI+): $[M-H]^+$: calculated for $C_{20}H_{25}NO_4$, 344.1862; found 344.1862.

IR: 2933 (Ar CH Str), 2823 (AL CH Str), 1679 (C=C).

3.2.19 (*Z*)-1-(4-Methoxyphenyl)-2-(2, 3, 4, 5- tetramethoxyphenyl) – ethene (7)

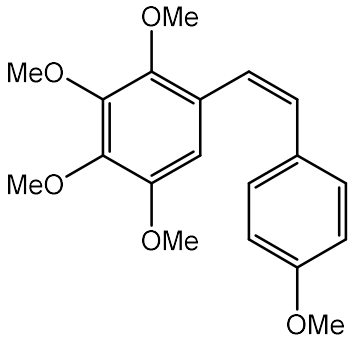

Protocol A was carried out using phosphonium salt (2.46 g, 4.5 mmol), potassium carbonate (1.26 g, 9mmol) and 4- methoxybenzaldehyde (0.62 g, 4.5 mmol). The reaction was heated in water (25 ml) under reflux for four hours. The crude stilbene (2.17 g, 145.6 %) was purified on silica (hexane/ ethyl acetate, 40:1). A mixture of *E*- and *Z*- isomers came together off the column as a dark, yellow liquid. Yield not available as unsuccessful isomer separation was attempted and not all fractions coming off the column were weighed.

^{1} H NMR ($CDCl_3$, 400 MHz): δ 3.49 (3H, s, CH_3O), 3.77 (6H, s, 2 × CH_3O), 3.82 (3H, s, CH_3O), 3.90 (3H, s, CH_3O), 6.53 (1H, s, H8), 6.56 (1H, d, *J*= 12.28, C=CH), 6.61 (1H, d, *J*= 12.28, C=CH), 6.82 (2H, d, *J*= 8.83, H3 &H5), 7.22 (2H, d, *J*= 8.83, H2 & H6).

^{13} C NMR ($CDCl_3$, 100 MHz): δ 55.23 (CH_3O), 55.86 (CH_3O), 61.27 (CH_3O), 61.3 (CH_3O), 61.39 (CH_3O), 107.4 (CH, C8), 113.59 (2 × CH, C3 & C5), 123.58 (C=C), 126.23 (C, C7), 129.71 (C, C1), 129.9 (C=C), 130.31 (2 × CH, C2 & C6), 142.62 (C, C10), 145.82 (C, C11), 147.1 (C, C9), 148.94 (C, C12), 159.35 (C, C4).

High resolution mass spectrometry (ESI+): $[M-H]^+$: calculated for $C_{19}H_{22}O_5$, 331.1545; found 331.1543.

IR: 2957 (Ar CH Str), 2931, 2836 (Al CH Str), 1607 (C=C).

3.2.20 (*E*)-1-(4-Methoxyphenyl)-2-(2, 3, 4, 5- tetramethoxyphenyl) – ethene (7)

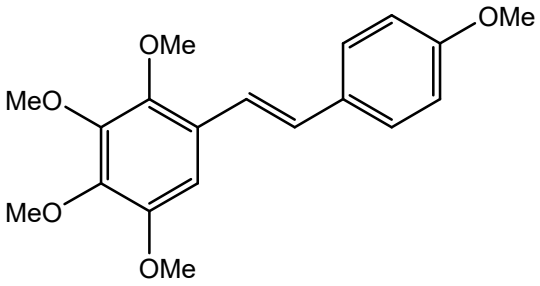

This compound was produced together with its isomer (*Z*)-1-(4-Methoxyphenyl)-2-(2, 3, 4, 5-tetramethoxyphenyl) - ethene and therefore involves the same method of preparation.

^{1} H NMR ($CDCl_3$, 400 MHz): δ 3.81 (3H, s, CH_3O), 3.83 (3H, s, CH_3O), 3.85 (3H, s, CH_3O), 3.88 (3H, s, CH_3O), 3.91 (3H, s, CH_3O), 7.27 (1H, d, *J*= 16.6, C=CH). These were the only trans signals identifiable, due to small amount of isomer present being obscured by impurities

^{13} C NMR ($CDCl_3$, 100 MHz): δ 55.33 (CH_3O), 56.25 (CH_3O), 61.32 (CH_3O), 61.62 (CH_3O), 125.86 (C, C7), 130.53 (C, C1), 142.32 (C, C10), 145.53 (C, C11), 147.32 (C, C9), 149.81 (C, C12), 158.76 (C, C4). Not identifying proton signals meant that in turn HMQC could not be used to identify certain carbon signals.

High resolution mass spectrometry (ESI+): $[M-H]^+$: calculated for $C_{19}H_{22}O_5$, 331.1545; found 331.1543.

IR : 2957 (Ar CH Str), 2931, 2836 (Al CH Str), 1607 (C=C).

3.2.21 (*Z*)-1-(3-Hydroxy-4-methoxyphenyl)-2-(2, 3, 4, 5-tetramethoxyphenyl)-ethene (8)

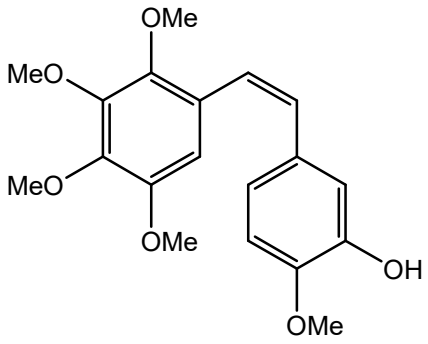

A stirred mixture of 2, 3, 4, 5- tetramethoxybenzyltriphenylphosphonium bromide (0.83 g, 1.5 mmol), potassium carbonate (0.42 g, 3.0 mmol) and 4-methoxy-3-(tetrahydro-2H-pyran-2-yloxy) benzaldehyde (0.55g, 2.3 mmol) in water (30 ml) was heated under reflux for 7.5 hours. The reaction mixture was left to stand at room temperature overnight. To deprotect the crude stilbene (1.05 g, 162%), 10 % HCl (5ml) was added to the stilbene in ethanol (10 ml), and the reaction mixture was stirred at room temperature for an hour. Extraction with ethyl acetate was unsuccessfully attempted and so the deprotected crude stilbene (0.96 g, 148 %) was obtained by evaporating all solvents from the reaction mixture using a rotary evaporator. The crude stilbene was purified on silica (hexane/ ethyl acetate, 8: 2). A mixture of *E*- and *Z*- isomers came together off the column as thick viscous, orange oil (0.25 g, 47 %, *cis*: *trans*, 52: 48).

^{1} H NMR ($CDCl_3$, 400 MHz): δ 3.53, 3.81, 3.83, 3.86, 3.896, 3.90, 3.91, 3.92, 3.94, 3.95 (5 × CH_3O, *cis* and *trans* methoxys indistinguishable),6.51 (1H, d, *J*= 12.34, C=CH), 6.55 (1H, s, H8), 6.56 (1H, d, *J*= 12.34, C=CH), 6.72 (1H, d, *J*= 8.41, H5), 6.78 (1H, dd, *J*= 2.07, *J*= 8.38, H6), 6.90 (1H, d, *J*= 2.17, H2).

^{13} C NMR ($CDCl_3$, 100 MHz): δ 55.95, 56.04, 56.2, 56.26, 61.22, 61.25, 61.27, 61.28, 61.4, 61.6 (5 × CH_3O, *cis* and *trans* methoxy groups indistinguishable), 107.6 (C8, CH), 110.3 (C5, CH), 115.0 (C2, CH), 121.2 (C6, CH), 123.8 (C=C), 125.6 (C7, C), 129.9 (C=C), 131.4 (C1, C), 142.6 (C10, C), 145.2 (C11, C), 145.8 (C9, C), 145.8 (C3, C), 147.0 (C12, C), 148.9 (C4, C).

High resolution mass spectrometry (ESI+): $[M-H]^+$: calculated for $C_{19}H_{22}O_6$, 347.1494; found 347.1483.

IR: 3410 (OH Str), 2936, 2837 (Al CH Str), 1688 (C=C).

3.2.22 (*E*)-1-(3-Hydroxy-4-methoxyphenyl)-2-(2, 3, 4, 5-tetramethoxyphenyl)-ethene (8)

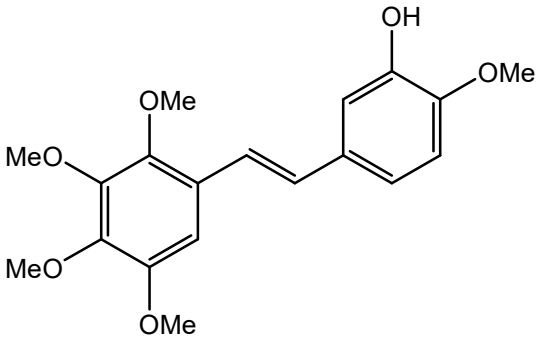

This compound was produced together with its isomer (*Z*)-1-(3-Hydroxy-4-methoxyphenyl)-2-(2, 3, 4, 5-tetramethoxyphenyl)-ethene and therefore involves the same method of preparation

^{1} H NMR ($CDCl_3$, 400 MHz): δ 3.53, 3.81, 3.83, 3.86, 3.896, 3.90, 3.91, 3.92, 3.94, 3.95 (5 × CH_3O, *cis* and *trans* methoxys indistinguishable), 6.84 (1H, d, *J*= 8.34, H5), 6.85 (1H, s, H8), 6.93 (1H, d, *J*= 16.55, C=CH), 6.99 (1H, dd, *J*= 2.15, *J*= 8.16, H6), 7.18 (1H, d, *J*= 2.13, H2), 7.23 (1H, d, *J*= 16.55, C=CH).

^{13} C NMR ($CDCl_3$, 100 MHz): δ 55.95, 56.04, 56.2, 56.26, 61.22, 61.25, 61.27, 61.28, 61.4, 61.6 (5 × CH_3O, *cis* and *trans* methoxy groups indistinguishable), 103.1 (C8, CH), 110.7 (C5, CH), 111.9 (C2, CH), 119.3 (C6, CH), 121.2 (C=C), 126.1 (C7, C), 128.4 (C=C), 130.6 (C1, C), 142.4 (C10, C), 145.5 (C9, C), 145.8 (C11, C), 146.5 (C3, C), 147.2 (C12, C), 149.7 (C4, C).

High resolution mass spectrometry (ESI+): $[M-H]^+$: calculated for $C_{19}H_{22}O_6$, 347.1496; found 347.1483.

IR: 3410 (OH Str), 2936, 2837 (Al CH Str), 1688 (C=C).

3.2.23 (*Z*)-1-(4-Methoxy-3-nitrophenyl)-2-(2, 3, 4, 5-tetramethoxyphenyl)-ethene (9)

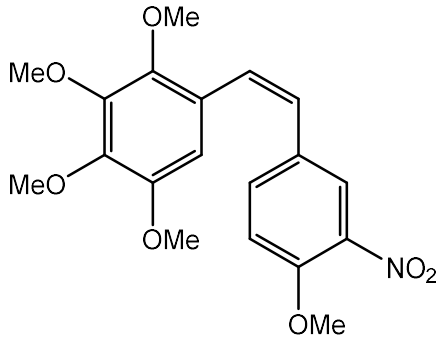

Protocol A was carried out using phosphonium salt (0.5 g, 0.9 mmol), potassium carbonate (0.25 g, 1.8 mmol) and 4- methoxy-3- nitrobenzaldehyde (0.16 g, 0.9 mmol). The reaction was heated in water (25 ml) under reflux for 4.5 hours. The crude stilbene (0.36 g, 106 %) was purified on silica (hexane/ ethyl acetate, 9: 1). A mixture of *E*- and *Z*- isomers came together off the column as a yellow/ green liquid. Yield not available as unsuccessful isomer separation was attempted and not all fractions coming off the column were weighed.

^{1} H NMR ($CDCl_3$, 400 MHz): 3.50 (3H, s, CH_3O), 3.73 (3H, s, CH_3O), 3.84 (3H, s, CH_3O), 3.86 (3H, s, CH_3O), 3.87 (3H, s, CH_3O), 6.36 (1H, s, H8), 6.43 (1H, d, *J*= 12.25, C=CH), 6.63 (1H, d, *J*= 12.25, C=CH), 6.86 (1H, d, *J*= 8.66, H5), 7.35 (1H, dd, *J*= 2.27, *J*= 8.76, H6), 7.70 (1H, d, *J*= 2.21, H2).

^{13} C NMR ($CDCl_3$, 100 MHz): δ 55.03 (CH_3O), 55.52 (CH_3O), 60.27 (CH_3O), 60.28 (CH_3O), 60.34 (CH_3O), 105.88 (CH, C8), 112.0 (CH, C5), 123.6 (C, C7), 124.8 (CH, C2), 125.39 (C=C), 126.33 (C=C), 128.74 (C, C1), 133.51 (CH, C6), 138.32 (C, C10), 141.95 (C, C11), 144.78 (C, C3), 146.3 (C, C9), 148.22 (C, C12), 150.65 (C, C4).

High resolution mass spectrometry (ESI+): $[M-H]^+$: calculated for $C_{19}H_{21}NO_7$, 376.1396; found 376.1394.

IR: 2937, 2867, 2838 (Al CH Str), 1617 (C=C), 1528, 1339 (NO_2).

3.2.24 (*E*)-1-(4-Methoxy-3-nitrophenyl)-2-(2, 3, 4, 5-tetramethoxyphenyl)-ethene (9)

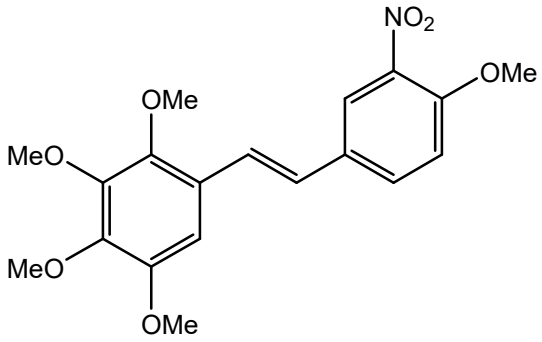

This compound was produced together with its isomer (*Z*)-1-(4-Methoxy-3-nitrophenyl)-2-(2, 3, 4, 5-tetramethoxyphenyl)-ethene and therefore involves the same method of preparation.

^{1} H NMR ($CDCl_3$, 400 MHz): δ 3.79 (3H, s, CH_3O), 3.85 (3H, s, CH_3O), 3.88 (3H, s, CH_3O), 3.92 (3H, s, CH_3O), 6.76 (1H, s, H8), 7.02 (1H, d, *J*= 8.74, H5), 7.23 (1H, d, *J*= 16.52, C=CH), 7.63 (1H, dd, *J*= 2.25, J= 8.73, H6), 7.93 (1H, d, *J*= 2.36, H2). The fifth methoxy group and one of the olefinic protons were not visible on the spectra.

^{13} C NMR ($CDCl_3$, 100 MHz): δ 55.2 (CH_3O), 55.65 (CH_3O), 60.19 (CH_3O), 60.65 (CH_3O), 102.08 (CH, C8), 112.74 (CH, C5), 122.3 (CH, C2), 122.68 (C=C), 123.99 (C, C7), 129.67 (C, C1), 130.72 (CH, C6), 138.77 (C, C10), 142.22 (C, C11), 144.82 (C, C3), 146.24 (C, C9), 148.76 (C, C12), 151.05 (C, C4). One of the methoxy carbons and an olefinic bond carbon atom were not visible in the spectrum.

High resolution mass spectrometry (ESI+): $[M-H]^+$: calculated for $C_{19}H_{21}NO_7$, 376.1396; found 376.1394.

IR: 2937, 2867, 2838 (Al CH Str), 1617 (C=C), 1528, 1339 (NO_2).

3.2.25 *(Z)*-1-(4- nitrophenyl)-2-(2, 3, 4, 5- tetramethoxyphenyl) - ethene (10)

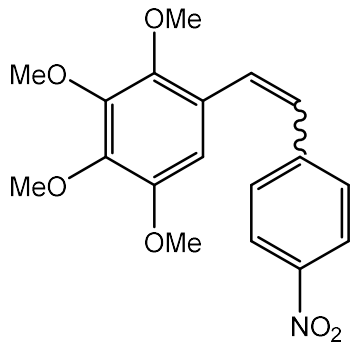

Protocol A was carried out using phosphonium salt (1.0 g, 1.8 mmol), potassium carbonate (0.5 g, 3.6 mmol) and 4- nitrobenzaldehyde (0.27 g, 1.8 mmol). The reaction was heated in water (30 ml) under reflux for 5 hours. It was attempted unsuccessfully to purify the crude stilbene (0.82 g, 132 %) on silica (hexane/ ethyl acetate, 50:1). The compound coming off the column was so impure; it was decided not to continue with processing this compound.

High resolution mass spectrometry (ESI+): $[M-H]^+$: calculated for $C_{18}H_{19}NO_6$, 346.1291; found 346.1291.

3.2.26 3-[*tert*-Butyldimethylsilyl) oxy]-4-methoxybenzaldehyde (11)

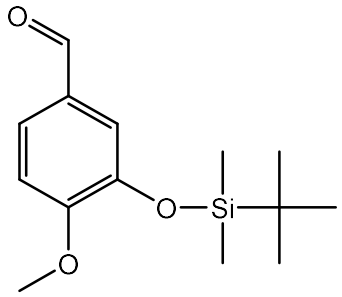

To a stirred solution of 3- hydroxyl-4-methoxybenzaldehyde (2.0 g, 13.0 mmol) in dimethylformamide (20 ml), under an argon atmosphere was added diisopropylethylamine (3.4 ml, 19.5 mmol). This was followed by the addition of *tert*- butyldimethylsilyl chloride (2.34 g, 15.6 mmol). After 1.5 hours of stirring at room temperature, H_2O (4 ml) was added, and the mixture stirred for a further 30 minutes. Diethyl ether (60 ml) and saturated $NaHCO_3$ solution were the added and the mixture stirred for a further 30 minutes. The organic phase was then separated, followed by extraction of the aqueous phase with diethyl ether (40 ml). The combined organic phase was washed with saturated brine solution (40 ml) followed by washing with H_2O (40 ml). The solvent was then removed using a rotary evaporator, leaving the title compound as a yellow liquid (2.35 g, 68 %) (Pettit, Singh & Cragg, 1985).

^{1} H NMR ($CDCl_3$, 400 MHz): δ 0.0003 (6H, s, 2 × $SiCH_3$), 0.83 (9H, s, 3 × CH_3), 3.71 (3H, s, CH_3O), 6.78 (1H, d, *J*= 8.28), 7.2 (1H, d, *J*= 2.05), 7.3 (1H, dd, *J*= 2.06, *J*= 8.31), 9.64 (1H, s, CHO).

^{13} C NMR ($CDCl_3$, 100 MHz): δ – 4.67 (2 × $SiCH_3$), 18.39 (quaternary carbon), 25.62 (3 × CH_3), 55.52 (CH_3O), 111.16 (C5), 119.94 (C2), 126.34 (C6), 130.18 (C1), 145.54 (C3), 156.58 (C4). 190.84 (CHO).

3.2.27 4-Methoxy-3-(tetrahydro-2*H*-pyran-2-yloxy) benzaldehyde (12)

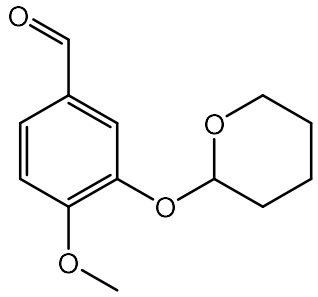

To a stirred solution of 3- hydroxyl-4- methoxybenzaldehyde (1.52 g, 10 mmol)in dry DCM (40ml) was added pyridinium- *p*- toluenesulfonate (0.11 g, 0.44 mmol) and 3,4- dihydro- 2H-pyran (6.5 g, 77.3 mmol). After 24 hours stirring at room temperature under an argon atmosphere, saturated $NaHCO_3$ (50 ml) was added, and the reaction mixture was extracted with DCM (3 × 100 ml).The combined extracts were dried by magnesium sulphate followed by vacuum filtration. The solvent was removed using a rotary evaporator to give the title compound as a thick yellow liquid (1.4 g, 77%) (Dakdouki, Villemin & Bar, 2010).

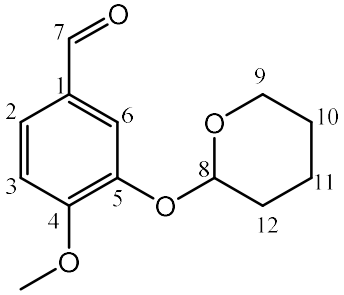

The diagram above shows how protons and carbon atoms were assigned for NMR analysis.

^{1} H NMR ($CDCl_3$, 400 MHz): δ 1.4 – 2.0 (6 × H, m, 2 × H10, 2 × H11, 2 × H12), 3.30 (1H, m, CH-O, H9), 3.80 (1H, m, CH-O, H9), 3.81 (3H, s, CH_3O), 5.3 (1H, t, H8), 6.89 (1H, d, *J*= 8.5, H3), 7.40 (1H, dd, *J*= 1.73, *J*= 8.42, H2), 7.53 (1H, d, *J*= 1.73, H6), 9.72 (1H, s, CHO).

^{13} C NMR ($CDCl_3$, 100 MHz): δ 18.7 (CH, C11), 25.0 (CH, C10), 30.1 (CH, C12), 56.6 (CH_3O), 62.5 (CH, C9), 97.2 (CH, C8), 111.3 (CH, C3), 116.4 (CH, C6), 126.6 (CH, C2), 129.9 (C, C1), 146.5 (C, C4), 155.5 (C, C5), 190.7 (CHO).

4 Conclusion

In the steps leading up to the formation of the tetramethoxy phosphonium salt, the intermediates were all obtained in high purity and the impurities which were present in each of the steps did not matter as overall, the final step on the pathway to the phosphonium salt, the salt itself was obtained with excellent purity, virtually no impurities in the samples at all, as verified by NMR analysis.

The Wittig reactions to produce the desired CA- 4 derivatives were all easily carried out and successful, as verified by NMR analysis and mass spectrometry. There was however an issue in many instances where there was difficulty in getting rid of traces of the aldehyde starting material from the *cis*/ *trans* mixture of isomers coming off the column, as frequently the R_f of the aldehyde was similar to that of the product isomers. Only a couple of the Wittig reactions went to completion as far as the aldehyde was concerned i.e., resulted in no trace of the aldehyde starting material in product mixture. The R_f value of the other starting material, the phosphonium salt was very much significantly different from that of the product isomers and so its separation on the column from the product isomers was not an issue. The leftover aldehyde starting material in the product mixture was there in spite of the fact that recommended reaction times for the Wittig reaction, given in the text of the method used were increased from 2.5 hours to up to seven hours in some instances. It might be worthwhile trying the use of catalysts or microwave conditions for such reactions. In the case of compound 2 the aldehyde starting material was all removed by its reduction with sodium borohydride forming a benzyl alcohol and its subsequent separation on the column.

For the compounds synthesized, it was virtually impossible to separate the product isomers from each other in appreciable amounts, with the isolation of the *cis* isomer only successful in one instance. This is due to the very similar R_f values that both the *cis* and *trans* isomers of these compounds have. TLC cannot be relied on for the separation process, as its results can be contradicted by NMR analysis i.e., TLC will indicate no traces of the *trans* isomer present in a collection of fractions coming off the column, however NMR analysis, which is very accurate will show there is still the presence of the *trans* isomer. For these reasons, the majority of the CA- 4 derivatives which were synthesized were tested for biological activity as mixtures, samples containing both *cis* and *trans* isomers. This was not an issue as it is known that the *trans* isomers of CA- 4 derivatives display little or no cytotoxic activity (McLoughlin & O'Boyle, 2020) and therefore activity of the samples tested was from the *cis* isomer.

Five of the nine compounds tested displayed very good to excellent activity against both cell lines tested against, HepG2 and A549. These five compounds were all less active than CA- 4 but more active than cisplatin.

It was observed from the overall experimental results that the introduction of an extra methoxy group at the 2 position of a trimethoxy CA- 4 analogue does not improve cytotoxic activity against cancer cells, but in fact has the opposite effect.

In future projects it is worth considering the synthesis and testing of tetramethoxy A- ring CA- 4 derivatives with methoxy groups in the 2, 3, 5, 6 positions instead of 2, 3, 4, and 5 as with this project. CA- 4 derivatives with pentamethoxy A- ring structure are also worth investigating.

5.0 References

Accioni, F., García-Gómez, D., & Rubio, S. (2021). Exploring polar hydrophobicity in organized media for extracting oligopeptides: application to the extraction of opiorphin in human saliva. *Journal Of Chromatography A*, *1635*, Article number 461777. doi: 10.1016/j.chroma.2020.461777

Aguilar-Pérez, K., Avilés-Castrillo, J., Medina, D., Parra-Saldivar, R., & Iqbal, H. (2020). Insight into nanoliposomes as smart nanocarriers for greening the twenty-first century biomedical settings. *Frontiers In Bioengineering And Biotechnology*, *8,* Article number 579536. doi: 10.3389/fbioe.2020.579536.

Akselsen, Ø., Odlo, K., Cheng, J., Maccari, G., Botta, M., & Hansen, T. (2012). Synthesis, biological evaluation and molecular modeling of 1, 2, 3-triazole analogs of combretastatin A-1. *Bioorganic & Medicinal Chemistry*, *20*(1), 234-242. doi: 10.1016/j.bmc.2011.11.010.

Alasvand, N., Urbanska, A., Rahmati, M., Saeidifar, M., Gungor-ozkerim, P., & Sefat, F. et al. (2017). *Multifunctional Systems for Combined Delivery, Biosensing And Diagnostics* (pp. 245-259). Elsevier.

Alberts, J., Johnson, A., Lewis, J., Raff, M., Roberts, K., & Walter, P. (2002). An overview of the cell cycle. *Molecular biology of the cell* (4th ed.). New York: Garland Science.

Ali, R., Mirza, Z., Ashraf, G., Kamal, M., Ansari, S., & damanhouri, G. et al. (2012). New anticancer agents: recent developments in tumour therapy. *Anticancer Research*, *32*(7), 2999-3005.

Amin, M., Butt, A., Amjad, M., & Kesharwani, P. (2017). Chapter 5 - polymeric micelles for drug targeting and delivery. *Nanotechnology - Based Approaches For Targeting And Delivery Of Drugs And Genes*, 167 - 202.

Amos, L. (2011). What tubulin drugs tell us about microtubule structure and dynamics. *Seminars In Cell & Developmental Biology*, *22*(9), 916-926. doi: 10.1016/j.semcdb.2011.09.014.

Anderson, D., & Sydor, M. (2016). Nanotechnology: The risks and benefits for medical diagnosis and treatment. *Journal Of Nanomedicine & Nanotechnology*, *7*(4), Article number 1000e143. doi: 10.4172/2157-7439.1000e143.

Bai, Y., He, X., Bai, Y., Sun, Y., Zhao, Z., & Chen, X. et al. (2019). Polygala tenuifolia-Acori tatarinowii herbal pair as an inspiration for substituted cinnamic α-asaronol esters: Design, synthesis, anticonvulsant activity, and inhibition of lactate dehydrogenase study. *European Journal Of Medicinal Chemistry*, *183*, Article number 111650. doi: 10.1016/j.ejmech.2019.111650.

Blasco, V., Murga, J., Falomir, E., Carda, M., Royo, S., & Cuñat, A. et al. (2018). Synthesis and biological evaluation of cyclic derivatives of combretastatin A-4 containing group 14 elements. *Organic & Biomolecular Chemistry*, *16*(32), 5859-5870. doi: 10.1039/c8ob01148f.

Bolomsky, A., Vogler, M., Köse, M., Heckman, C., Ehx, G., Ludwig, H., & Caers, J. (2020). MCL-1 inhibitors, fast-lane development of a new class of anti-cancer agents. *Journal Of Hematology & Oncology*, *13*(1), Article number 173. doi: 10.1186/s13045-020-01007-9.

Bowne-Anderson, H., Zanic, M., Kauer, M., & Howard, J. (2013). Microtubule dynamic instability: A new model with coupled GTP hydrolysis and multistep catastrophe. *Bioessays*, *35*(5), 452-461. doi : 10.1002/bies.201200131.

Brouhard, G., & Rice, L. (2014). The contribution of αβ-tubulin curvature to microtubule dynamics. *Journal Of Cell Biology*, *207*(3), 323-334. doi: 10.1083/jcb.201407095

Bukhari, S., Kumar, G., Revankar, H., & Qin, H. (2017). Development of combretastatins as potent tubulin polymerization inhibitors. *Bioorganic Chemistry*, *72*, 130-147. doi: 10.1016/j.bioorg.2017.04.007.

Cancer. (2022). Retrieved 30 January 2022, from https://www.who.int/news-room/fact-sheets/detail/cancer.

Cancer and carcinogens - Cell division - Edexcel - GCSE Combined Science Revision - Edexcel - BBC Bitesize. (2022). Retrieved 1 February 2022, from https://www.bbc.co.uk/bitesize/guides/zpkx8mn/revision/4

Cancer cells. (2020). Retrieved 1 February 2022, from https://www.cancerresearchuk.org/about-cancer/what-is-cancer/how-cancer-starts/cancer-cells

Caul, S. (2021). Are there more people diagnosed with cancer? | National Statistical. Retrieved 22 July 2021, from https://blog.ons.gov.uk/2019/04/26/are-there-more-people-diagnosed-with-cancer/.

Cheynier, V., Schneider, R., Salmon, J., & Fulcrand, H. (2010). *Comprehensive natural products II* (1st ed., pp. 1119-1172). Elsevier.

Cho, K., Wang, X., Nie, S., Chen, Z., & Shin, D. (2008). Therapeutic nanoparticles for drug delivery in cancer. *Clinical Cancer Research*, *14*(5), 1310 - 1316.

Cooper, G. (2000). *The cell: a molecular approach* (2nd ed.). Sunderland (MA): Sinauer associates.

Cragg, G., Kingston, D., & Newman, D. (2011). *Anticancer agents from natural products* (2nd ed., p. 28). CRC press.

Cushman, M., Nagarathnam, D., Gopal, D., Chakraborti, A., Lin, C., & Hamel, E. (1991). Synthesis and evaluation of stilbene and dihydrostilbene derivatives as potential anticancer agents that inhibit tubulin polymerization. *Journal Of Medicinal Chemistry*, *34*(8), 2579-2588. doi: 10.1021/jm00112a036.

Dakdouki, S., Villemin, D., & Bar, N. (2010). Solid-phase reactive chromatography (SPRC): A new methodology for Wittig and Horner-Emmons reactions on a column under microwave Irradiation. *European Journal Of Organic Chemistry*, 2010(2), 333-337. doi: 10.1002/ejoc.200901032.

Devi, S., & Mehendale, H. (2014). *Encyclopedia of toxicology* (3rd ed., pp. 26-28). Amsterdam: Elsevier.

Dias, L., de Oliveira, L., & de Sousa, M. (2003). Total synthesis of (−)-Pironetin†. *Organic Letters*, *5*(3), 265-268. doi: 10.1021/ol027211o.

Dick, A., & Cocklin, S. (2020). Bioisosteric Replacement as a Tool in Anti-HIV Drug Design. *Pharmaceuticals*, *13*(3), 36. doi: 10.3390/ph13030036

Downing, K., & Nogales, E. (1998). Tubulin and microtubule structure. *Current Opinion In Cell Biology*, *10*(1), 16-22. doi: 10.1016/s0955-0674(98)80082-3.

Downing, K., & Nogales, E. (1998). Tubulin structure: Insights into microtubule properties and functions. *Current Opinion In Structural Biology*, *8*(6), 785-791. doi: 10.1016/s0959-440x(98)80099-7.

Duan, Y., Man, R., Tang, D., Yao, Y., Tao, X., & Yu, C. et al. (2016). Design, synthesis and antitumor activity of novel link-bridge and B-ring modified combretastatin A-4 (CA-4) analogues as potent antitubulin agents. *Scientific Reports*, *6*(1), 1-13. doi: 10.1038/srep25387.

ElSohly, H., Ma, G., Turner, C., & ElSohly, M. (1984). Constituents of Cannabis sativa, XXV. Isolation of two new dihydrostilbenes from a Panamanian variant. *Journal Of Natural Products*, *47*(3), 445-452. doi: 10.1021/np50033a008.

Faustino, C., Francisco, A., Isca, V., & Duarte, N. (2019). Cytotoxic stilbenes and derivatives as promising antimitotic leads for cancer therapy. *Current Pharmaceutical Design*, *24*(36), 4270-4311. doi: 10.2174/1381612825666190111123959.

Forster, J., Harriss-Phillips, W., Douglass, M., & Bezak, E. (2017). A review of the development of tumour vasculature and its effects on the tumour microenvironment. *Hypoxia*, *Volume 5*, 21-32. doi: 10.2147/hp.s133231.

Fu, Y. (2014). *Progress in molecular biology and translational science* (vol. 121, pp. 293-319). Amsterdam: Elsevier.

Garbicz, D., Mielecki, D., Wrzesinski, M., Pilzys, T., Marcinkowski, M., & Piwowarski, J. et al. (2018). Evaluation of anti-cancer activity of stilbene and methoxydibenzo [b, f] oxepin derivatives. *Current Cancer Drug Targets*, *18*(7), 706-717. doi: 10.2174/1568009617666170623120742.

Gaspari, R., Prota, A., Bargsten, K., Cavalli, A., & Steinmetz, M. (2017). Structural basis of cis - and trans -combretastatin binding to tubulin. *Chem*, *2*(1), 102-113. doi: 10.1016/j.chempr.2016.12.005.

Gaukroger, K., Hadfield, J., Hepworth, L., Lawrence, N., & McGown, A. (2001). Novel syntheses of cis and trans isomers of combretastatin A-4. *The Journal Of Organic Chemistry*, *66*(24), 8135-8138. doi: 10.1021/jo015959z.

Gaukroger, K., Hadfield, J., Lawrence, N., Nolan, S., & McGown, A. (2003). Structural requirements for the interaction of combretastatins with tubulin: How important is the trimethoxy unit? *Org. Biomol. Chem.*, *1*(17), 3033-3037. doi: 10.1039/b306878a.

Gelperina, S., Kisich, K., Iseman, M., & Heifets, L. (2005). The potential advantages of nanoparticle drug delivery systems in chemotherapy of tuberculosis. *American Journal Of*

Respiratory And Critical Care Medicine, *172*(12), 1487-1490. doi: 10.1164/rccm.200504-613pp.

Greene, L., Meegan, M., & Zisterer, D. (2015). Combretastatins: More than just vascular targeting agents?. *Journal Of Pharmacology And Experimental Therapeutics*, *355*(2), 212-227. doi: 10.1124/jpet.115.226225.

Griggs, J., Metcalfe, J., & Hesketh, R. (2001). Targeting tumour vasculature: The development of combretastatin A4. *The Lancet Oncology*, *2*(2), 82-87. doi: 10.1016/s1470-2045(00)00224-2.

Grisham, R., Ky, B., Tewari, K., Chaplin, D., & Walker, J. (2018). Clinical trial experience with CA4P anticancer therapy: Focus on efficacy, cardiovascular adverse events, and hypertension management. *Gynecologic Oncology Research And Practice*, *5*(1), Article number 1. doi: 10.1186/s40661-017-0058-5.

Haupt, A., & Minc, N. (2018). How cells sense their own shape – mechanisms to probe cell geometry and their implications in cellular organization and function. *Journal Of Cell Science*, *131*(6), Article number jcs214015. doi: 10.1242/jcs.214015.

Hori, K. (2011). Starvation tactics for solid tumours: Tumour blood flow interruption via a combretastatin derivative (Cderiv), and its microcirculation mechanism. *Cancer And Metastasis Reviews*, *31*(1-2), 109-122. doi: 10.1007/s10555-011-9333-9.

How can cancer kill you? | Dying with cancer | Cancer Research UK. (2021). Retrieved 22 July 2021, from https://www.cancerresearchuk.org/about-cancer/coping/dying-with-cancer/how-can-cancer-kill-you.

Ibrahim, M., Do, D., Sepah, Y., Shah, S., Van Anden, E., & Hafiz, G. et al. (2013). Vascular disrupting agent for neovascular age related macular degeneration: A pilot study of the safety and efficacy of intravenous combretastatin a-4 phosphate. *BMC Pharmacology And Toxicology*, *14*(1), Article number 7. doi: 10.1186/2050-6511-14-7.

Jackman, M. (2011). *Encyclopedia of cancer* (p. 126). Berlin: Springer.

Jhaveri, A., & Torchilin, V. (2014). Multifunctional polymeric micelles for delivery of drugs and siRNA. *Frontiers In Pharmacology*, *5*, Article number 77. doi: 10.3389/fphar.2014.00077.

Jiang, J., Shen, N., Song, W., Yu, H., Sakurai, K., Tang, Z., & Li, G. (2019). Combretastatin A4 nanodrug combined plerixafor for inhibiting tumour growth and metastasis simultaneously. *Biomaterials Science*, *7*(12), 5283-5291. doi: 10.1039/c9bm01418g.

Jung, J., Lim, E., Lee, Y., Kang, J., Kim, H., & Jang, S. et al. (2009). Synthesis of novel trans-stilbene derivatives and evaluation of their potent antioxidant and neuroprotective effects. *European Journal Of Medicinal Chemistry*, *44*(8), 3166-3174. doi: 10.1016/j.ejmech.2009.03.011.

Karatoprak, G., Küpeli Akkol, E., Genç, Y., Bardakcı, H., Yücel, Ç., & Sobarzo-Sánchez, E. (2020). Combretastatins: An overview of structure, probable mechanisms of action and potential applications. *Molecules*, *25*(11), Article number 2560. doi: 10.3390/molecules25112560.

Kaur, R., Kaur, G., Gill, R., Soni, R., & Bariwal, J. (2014). Recent developments in tubulin polymerization inhibitors: An overview. *European Journal Of Medicinal Chemistry*, *87*, 89-124. doi: 10.1016/j.ejmech.2014.09.051.

Khan, K., Yap, T., Yan, L., & Cunningham, D. (2013). Targeting the PI3K-AKT-mTOR signaling network in cancer. *Chinese Journal Of Cancer*, *32*(5), 253-265. doi: 10.5732/cjc.013.10057

Khan, Z., Iqbal, A., & Shahzad, S. (2017). Synthetic approaches toward stilbenes and their related structures. *Molecular Diversity*, *21*(2), 483-509. doi: 10.1007/s11030-017-9736-9.

Kinghorn, A., Chin, Y., & Swanson, S. (2009). Discovery of natural product anticancer agents from biodiverse organisms. *Current Opinions In Drug Discovery And Development*, *12*(2), 189-196.

Kingston, D. (2009). Tubulin-interactive natural products as anticancer agents. *Journal Of Natural Products*, *72*(3), 507-515. doi: 10.1021/np800568j.

Kounakis, K., & Tavernarakis, N. (2019). The cytoskeleton as a modulator of aging and neurodegeneration. *Advances in experimental medicine and biology* (Vol. 1178, pp. 227-245). Cham: Springer.

Kretzschmann, V., & Fürst, R. (2013). Plant-derived vascular disrupting agents: Compounds, actions, and clinical trials. *Phytochemistry Reviews*, *13*(1), 191-206. doi: 10.1007/s11101-013-9304-6.

Kumar, B., Sharma, P., Gupta, V., Khullar, M., Singh, S., Dogra, N., & Kumar, V. (2018). Synthesis and biological evaluation of pyrimidine bridged combretastatin derivatives as potential anticancer agents and mechanistic studies. *Bioorganic Chemistry*, *78*, 130-140. doi: 10.1016/j.bioorg.2018.02.027.

Kumbhar, B., Bhandare, V., Panda, D., & Kunwar, A. (2019). Delineating the interaction of combretastatin A-4 with αβ tubulin isotypes present in drug resistant human lung carcinoma using a molecular modelling approach. *Journal Of Biomolecular Structure And Dynamics*, *38*(2), 426-438. doi: 10.1080/07391102.2019.1577174.

Kwak, Y., Joo, S., Gansukh, E., Mistry, B., & Keum, Y. (2019). Synthesis and anticancer activities of polymethylenedioxy analogues of combretastatin A-2. *Applied Biological Chemistry*, *62*(1), Article number 25. doi: 10.1186/s13765-019-0434-4

Li, L., Jiang, S., Li, X., Liu, Y., Su, J., & Chen, J. (2018). Recent advances in trimethoxyphenyl (TMP) based tubulin inhibitors targeting the colchicine binding site. *European Journal Of Medicinal Chemistry*, *151*, 482-494. doi: 10.1016/j.ejmech.2018.04.011.

Li, Y., Lei, Y., Yao, N., Wang, C., Hu, N., & Ye, W. et al. (2017). Autophagy and multidrug resistance in cancer. *Chinese Journal Of Cancer*, *36*(1), Article number 25 . doi: 10.1186/s40880-017-0219-2

Li, Y., Luo, P., Wang, J., Dai, J., Yang, X., & Wu, H. et al. (2014). Autophagy blockade sensitizes the anticancer activity of CA-4 via JNK-Bcl-2 pathway. *Toxicology And Applied Pharmacology*, *274*(2), 319-327. doi: 10.1016/j.taap.2013.11.018.

Liekens, S., Schols, D., & Hatse, S. (2010). CXCL12-CXCR4 Axis in Angiogenesis, Metastasis and Stem Cell Mobilization. *Current Pharmaceutical Design*, *16*(35), 3903-3920. doi: 10.2174/138161210794455003

Lin, Y., Xu, J., & Lan, H. (2019). Tumour-associated macrophages in tumour metastasis: Biological roles and clinical therapeutic applications. *Journal Of Hematology & Oncology*, *12*(1), Article number 76. doi: 10.1186/s13045-019-0760-3.

Liang, W., Lai, Y., Zhu, M., Huang, S., Feng, W., & Gu, X. (2016). Combretastatin A4 regulates proliferation, migration, invasion, and apoptosis of thyroid cancer cells via

PI3K/Akt signalling pathway. *Medical Science Monitor*, *22*, 4911-4917. doi: 10.12659/msm.898545.

Likhtenshtein, G. (2010). *Stilbenes. Applications in chemistry, life sciences and materials science* (pp. 2-3). Weinheim: Wiley-VCH Verlag GmbH & Co. KGaA.

Lippert, J. (2007). Vascular disrupting agents. *Bioorganic & Medicinal Chemistry*, *15*(2), 605-615. doi: 10.1016/j.bmc.2006.10.020

Mabeta, P., & McGaw, L. (2018). *Studies in natural products chemistry* (pp. 53 -67). Elsevier science.

Macé, Y., Bony, E., Delvaux, D., Pinto, A., Mathieu, V., & Kiss, R. et al. (2015). Cytotoxic activities and metabolic studies of new combretastatin analogues. *Medicinal Chemistry Research*, *24*(8), 3143-3156. doi: 10.1007/s00044-015-1363-3.

Madu, C., Wang, S., Madu, C., & Lu, Y. (2020). Angiogenesis in breast cancer progression, diagnosis, and treatment. *Journal Of Cancer*, *11*(15), 4474-4494. doi: 10.7150/jca.44313.

Mao, J., Wang, D., Wang, Z., Tian, W., Li, X., & Duan, J. et al. (2016). Combretastatin A-1 phosphate, a microtubule inhibitor, acts on both hepatocellular carcinoma cells and tumour-associated macrophages by inhibiting the Wet/β-catenin pathway. *Cancer Letters*, *380*(1), 134-143. doi: 10.1016/j.canlet.2016.06.020.

Matis, M. (2020). The mechanical role of microtubules in tissue remodelling. *Bioessays*, *42*(5), Article number 1900244. doi: 10.1002/bies.201900244.

McKeage, M. (2011). Clinical trials of vascular disrupting agents in advanced non–small-cell lung cancer. *Clinical Lung Cancer*, *12*(3), 143-147. doi: 10.1016/j.cllc.2011.03.010.

McLoughlin, E., & O'Boyle, N. (2020). Colchicine-binding site inhibitors from chemistry to clinic: A review. *Pharmaceuticals*, *13*(1), Article number 8. doi: 10.3390/ph13010008.

McNulty, J., & Das, P. (2009). Aqueous Wittig reactions of semi-stabilized ylides. A straightforward synthesis of 1, 3-dienes and 1, 3, 5-trienes. *Tetrahedron Letters*, *50*(41), 5737-5740. doi: 10.1016/j.tetlet.2009.07.133.

McNulty, J., & McLeod, D. (2011). Amine- and sulfonamide-promoted Wittig olefination reactions in water. *Chemistry - A European Journal*, *17*(32), 8794-8798. doi: 10.1002/chem.201101153.

McNulty, J., & McLeod, D. (2011). An iterative approach toward the synthesis of discrete oligomeric p-phenylene vinylene organic dyes employing aqueous Wittig chemistry. *Tetrahedron Letters*, *52*(42), 5467-5470. doi: 10.1016/j.tetlet.2011.08.040.

McNulty, J., & McLeod, D. (2013). A scalable process for the synthesis of (E)-pterostilbene involving aqueous Wittig olefination chemistry. *Tetrahedron Letters*, *54*(47), 6303-6306. doi: 10.1016/j.tetlet.2013.09.019.

McNulty, J., McLeod, D., Das, P., & Zepeda-Velázquez, C. (2015). Wittig Reactions of Trialkylphosphine-derived Ylides: New Directions and Applications in Organic Synthesis. *Phosphorus, Sulfur, And Silicon And The Related Elements*, *190*(5-6), 619-632. doi: 10.1080/10426507.2014.980907

Mico, V., Charalambous, A., Peyman, S., Abou-Saleh, R., Markham, A., Coletta, P., & Evans, S. (2017). Evaluation of lipid-stabilised tripropionin nanodroplets as a delivery route for combretastatin A4. *International Journal Of Pharmaceutics*, *526*(1-2), 547-555. doi: 10.1016/j.ijpharm.2017.05.009.

Mikstacka, R., Stefański, T., & Różański, J. (2013). Tubulin-interactive stilbene derivatives as anticancer agents. *Cellular And Molecular Biology Letters*, *18*(3), 368-397. doi: 10.2478/s11658-013-0094-z.

Mosmann, T. (1983). Rapid colorimetric assay for cellular growth and survival: Application to proliferation and cytotoxicity assays. *Journal Of Immunological Methods*, *65*(1-2), 55-63. doi: 10.1016/0022-1759(83)90303-4.

Mühlethaler, T., Gioia, D., Prota, A., Sharpe, M., Cavalli, A., & Steinmetz, M. (2021). Comprehensive analysis of binding sites in tubulin. *Angewandte Chemie*, *133*(24), 13443-13454. doi: 10.1002/ange.202100273.

Nakamura, M., Kajita, D., Matsumoto, Y., & Hashimoto, Y. (2013). Design and synthesis of silicon-containing tubulin polymerization inhibitors: Replacement of the ethylene moiety of combretastatin A-4 with a silicon linker. *Bioorganic & Medicinal Chemistry*, *21*(23), 7381-7391. doi: 10.1016/j.bmc.2013.09.046.

Nam, N. (2003). Combretastatin A-4 analogues as antimitotic antitumor agents. *Current Medicinal Chemistry*, *10*(17), 1697-1722. doi: 10.2174/0929867033457151.

Nanocell drug delivery system - Patent CA-2558263-A1 - PubChem. (2005). Retrieved 29 January 2022, from https://pubchem.ncbi.nlm.nih.gov/patent/CA-2558263-A1.

Nik, M., Momtazi-Borojeni, A., Zamani, P., Navashenaq, J., Iranshahi, M., Jaafari, M., & Malaekeh-Nikouei, B. (2019). Targeted-nanoliposomal combretastatin A4 (CA-4) as an efficient antivascular candidate in the metastatic cancer treatment. *Journal Of Cellular Physiology*, *234*(9), 14721-14733. doi: 10.1002/jcp.28230.

Nogales, E., & Alushin, G. (2012). Tubulin and microtubule structure: Mechanistic insights into dynamic instability and its biological relevance. *Comprehensive Biophysics*, *4*, pp. 72-92.

No-Nitro- L -arginine = 98 TLC 2149-70-4. (2022). Retrieved 29 January 2022, from https://www.sigmaaldrich.com/US/en/product/sigma/n5501

Obach, R., & Kalgutkar, A. (2010). *Comprehensive toxicology* (2nd ed., pp. 309-347). Elsevier.

Oberg, H., Wesch, D., Kalyan, S., & Kabelitz, D. (2019). Regulatory interactions between neutrophils, tumour cells and T cells. *Frontiers In Immunology*, *10*, Article number 1690. doi: 10.3389/fimmu.2019.01690.

Parker, A., Kavallaris, M., & McCarroll, J. (2014). Microtubules and their role in cellular stress in cancer. *Frontiers In Oncology*, *4,* Article number 153. doi: 10.3389/fonc.2014.00153.

Pérez-Pérez, M., Priego, E., Bueno, O., Martins, M., Canela, M., & Liekens, S. (2016). Blocking blood flow to solid tumours by destabilizing tubulin: An approach to targeting tumour growth. *Journal Of Medicinal Chemistry*, *59*(19), 8685-8711.

Pettit, G., Singh, S., & Cragg, G. (1985). Synthesis of natural (-) - combretastatin. *Journal Of Organic Chemistry*, *50*(18), pp. 3404- 3406.

Pettit, G., Singh, S., Niven, M., Hamel, E., & Schmidt, J. (1987). Isolation, structure, and synthesis of combretastatins A-1 and B-1, potent new inhibitors of microtubule assembly,

derived from *Combretum caffrum*. *Journal Of Natural Products*, *50*(1), 119-131. doi: 10.1021/np50049a0161021/acs.jmedchem.6b00463.

Pettit, G., Singh, S., Boyd, M., Hamel, E., Pettit, R., Schmidt, J., & Hogan, F. (1995). Antineoplastic agents. 291. Isolation and synthesis of combretastatins A-4, A-5, and A-6. *Journal Of Medicinal Chemistry*, *38*(10), 1666-1672. doi: 10.1021/jm00010a011.

Piekuś-Słomka, N., Mikstacka, R., Ronowicz, J., & Sobiak, S. (2019). Hybrid cis-stilbene molecules: Novel anticancer agents. *International Journal Of Molecular Sciences*, *20*(6), Article number 1300. doi: 10.3390/ijms20061300.

Pyrzynska, K., & Pękal, A. (2013). Application of free radical diphenylpicrylhydrazyl (DPPH) to estimate the antioxidant capacity of food samples. *Analytical Methods*, *5*(17), 4288 -4295. doi: 10.1039/c3ay40367j.

Rambaud, M., Vecchio, A., & Villieras, J. (1984). Wittig-Horner reaction in heterogenous media: V1. An efficient synthesis of alkene-phosphonates and αL-hydroxymethyl-α-vinyl phosphonate in water in the presence of potassium carbonate. *Synthetic Communications*, *14*(9), 833-841. doi: 10.1080/00397918408075726.

Rameau, N., Russo, B., Mangematin, S., Pinel, C., & Djakovitch, L. (2018). Stilbene synthesis through decarboxylative cross-coupling of substituted cinnamic acids with aryl halides. *Applied Catalysis A: General*, *560*, 132-143. doi: 10.1016/j.apcata.2018.04.031.

Ray, P., Huang, B., & Tsuji, Y. (2012). Reactive oxygen species (ROS) homeostasis and redox regulation in cellular signalling. *Cellular Signalling*, *24*(5), 981-990. doi: 10.1016/j.cellsig.2012.01.008.

Robiette, R., Richardson, J., Aggarwal, V., & Harvey, J. (2006). Reactivity and Selectivity in the Wittig Reaction: A Computational Study. *Journal Of The American Chemical Society*, *128*(7), 2394-2409. doi: 10.1021/ja056650q

Roman, B., De Coen, L., Thérèse F.C. Mortier, S., De Ryck, T., Vanhoecke, B., & Katritzky, A. et al. (2013). Design, synthesis and structure–activity relationships of some novel, highly potent anti-invasive (E) - and (Z)-stilbenes. *Bioorganic & Medicinal Chemistry*, *21*(17), 5054-5063. doi: 10.1016/j.bmc.2013.06.048.

Seddigi, Z., Malik, M., Saraswati, A., Ahmed, S., Babalghith, A., Lamfon, H., & Kamal, A. (2017). Recent advances in combretastatin based derivatives and prodrugs as antimitotic agents. *Medchemcomm*, *8*(8), 1592-1603. doi: 10.1039/c7md00227k.

Seervi, M., & Xue, D. (2015). *Current Topics In Developmental Biology* (pp. 43-65). Academic Press.

Semenov, V., Kiselyov, A., Titov, I., Sagamanova, I., Ikizalp, N., & Chernysheva, N. et al. (2010). Synthesis of antimitotic polyalkoxyphenyl derivatives of combretastatin using plant allylpolyalkoxybenzenes (1). *Journal Of Natural Products*, *73*(11), 1796-1802. doi: 10.1021/np1004278.

Sherbet, G. (2017). Suppression of angiogenesis and tumour progression by combretastatin and derivatives. *Cancer Letters*, *403*, 289-295. doi: 10.1016/j.canlet.2017.06.032.

Shi, Y., Yuan, W., Wang, X., Gong, J., Zhu, S., & Chai, L. et al. (2016). Combretastatin A-4 efficiently inhibits angiogenesis and induces neuronal apoptosis in zebrafish. *Scientific Reports*, *6*(1), 1-11. doi: 10.1038/srep30189.

Siemann, D. (2011). The unique characteristics of tumour vasculature and preclinical evidence for its selective disruption by tumour-vascular disrupting agents. *Cancer Treatment Reviews*, *37*(1), 63-74. doi: 10.1016/j.ctrv.2010.05.001.

Sirerol, J., Rodríguez, M., Mena, S., Asensi, M., Estrela, J., & Ortega, A. (2016). Role of natural stilbenes in the prevention of cancer. *Oxidative Medicine And Cellular Longevity*, *2016*, 1-15. doi: 10.1155/2016/3128951.

Smolarczyk, R., Czapla, J., Jarosz-Biej, M., Czerwinski, K., & Cichoń, T. (2021). Vascular disrupting agents in cancer therapy. *European Journal Of Pharmacology*, *891*, Article number 173692. doi: 10.1016/j.ejphar.2020.173692.

Steinmetz, M., & Prota, A. (2018). Microtubule-targeting agents: Strategies to hijack the cytoskeleton. *Trends In Cell Biology*, *28*(10), 776-792. doi: 10.1016/j.tcb.2018.05.001.

Su, M., Huang, J., Liu, S., Xiao, Y., Qin, X., & Liu, J. et al. (2016). The anti-angiogenic effect and novel mechanisms of action of combretastatin A-4. *Scientific Reports*, *6*(1), 1-11. doi: 10.1038/srep28139.

Tangutur, A., Kumar, D., Krishna, K., & Kantevari, S. (2017). Microtubule targeting agents as cancer chemotherapeutics: An overview of molecular hybrids as stabilizing and destabilizing agents. *Current Topics In Medicinal Chemistry*, *17*(22), 2523-2537. doi: 10.2174/1568026617666170104145640.

Tarade, D., Pandey, S., & McNulty, J. (2017). Review of cytotoxic CA4 analogues that do not target microtubules: Implications for CA4 development. *Mini-Reviews In Medicinal Chemistry*, *17*(999), 1507-1514. doi: 10.2174/1389557517666170127115851.

Tremblay, M., & Sames, D. (2005). A new fluorogenic transformation: Development of an optical probe for coenzyme Q. *Organic Letters*, *7*(12), 2417-2420. doi: 10.1021/ol0507569.

Wang, B., Zhao, A., Sun, L., Zhong, X., Zhong, J., & Wang, H. et al. (2008). Protein phosphatase PP4 is overexpressed in human breast and lung tumours. *Cell Research*, *18*(9), 974-977. doi: 10.1038/cr.2008.274

What is cancer? (2022). Retrieved 27 January 2022, from https://www.cancerresearchuk.org/about-cancer/what-is-cancer

Yang, T., Wang, Y., Li, Z., Dai, W., Yin, J., & Liang, L. et al. (2012). Targeted delivery of a combination therapy consisting of combretastatin A4 and low-dose doxorubicin against tumour neovasculature. *Nanomedicine: Nanotechnology, Biology And Medicine*, *8*(1), 81-92. doi: 10.1016/j.nano.2011.05.003.

Yin, J., Lao, F., Fu, P., Wamer, W., Zhao, Y., & Wang, P. et al. (2009). The scavenging of reactive oxygen species and the potential for cell protection by functionalized fullerene materials. *Biomaterials*, *30*(4), 611-621. doi: 10.1016/j.biomaterials.2008.09.061

Zhang, Y., & Wang, X. (2020). Targeting the Wnt / beta - catenin signalling pathway in cancer. *Journal Of Hematology And Oncology*, *13*, article number 165.

Zong, Y., Shea, C., Maffucci, K., & Ojima, I. (2017). Computational design and synthesis of novel fluoro-analogs of combretastatins A-4 and A-1. *Journal Of Fluorine Chemistry*, *203*, 193-199. doi: 10.1016/j.jfluchem.2017.09.007.